

MSc thesis in Embedded Systems

**Towards Continuous Monitoring of Volatile  
Organic Compounds in the  
Gastrointestinal Tract**

David Alexander Emanuel de Gruijl

August 2023

A thesis submitted to the Delft University of Technology in  
partial fulfillment of the requirements for the degree of Master  
of Science in Embedded Systems

David Alexander Emanuel de Gruijl: *Towards Continuous Monitoring of Volatile Organic Compounds in the Gastrointestinal Tract* (2023)

© This work is licensed under a Creative Commons Attribution 4.0 International License. To view a copy of this license, visit <http://creativecommons.org/licenses/by/4.0/>.

The work in this thesis was carried out in the:



Embedded and Networked Systems Group  
Delft University of Technology

*The work in this thesis was supported by Brigham & Women's Hospital, Harvard Medical School and Massachusetts Institute of Technology. Their cooperation and guidance is hereby gratefully acknowledged.*



BRIGHAM AND  
WOMEN'S HOSPITAL



HARVARD  
MEDICAL SCHOOL



Massachusetts  
Institute of  
Technology

Supervisors: Prof. dr. Koen Langendoen  
dr. Carlo Giovanni Traverso, MD, PhD, MBBCH  
dr. Hen-Wei Huang

Graduation Date: 29th of August, 2023

Graduation Committee: Prof. dr. Koen Langendoen  
dr. Georgios Iosifidis  
dr. Hen-Wei Huang

# Abstract

Much like wearable devices today, ingestible devices have emerged as a promising platform for continuous health monitoring, and potentially even intervention. Recent research has demonstrated the feasibility of ingestible devices with a retention mechanism, enabling them to remain in the stomach for weeks. Equipping these devices with sensors capable of measuring complex biomarkers, would open up an entirely new era of continuous health monitoring.

This research focuses on the design of a gas sensor array for a retentive ingestible device, targeting the measurement of volatile organic compounds in the gastrointestinal tract. The research specifically addresses the outpatient treatment of alcoholism, in collaboration with the emergency medicine department at Brigham and Women's Hospital, Harvard Medical School. Current treatment relies on manual registration of drinking behavior, and the incorporation of an ingestible device that is able to continuously monitor drinking behavior enables more accurate behavioral assessment, and more targeted support and treatment.

Given the novelty of this approach, a sensor array capable of assessing ethanol concentrations in the air was gradually subjected to more complex tasks. Furthermore, a key aspect of the research was the design of an artificial gastric environment, that replicates the conditions and challenges that the sensor array would encounter within the human body. This experimental environment played a crucial role by providing a realistic testing platform without the need for a fully functional ingestible device, which can be incredibly challenging and resource-intensive to manufacture.

To ensure functionality in humid conditions, the sensors are encapsulated using parylene C and polycaprolactone (PCL) - biocompatible materials commonly used in the design of biomedical devices. The impact of these encapsulation methods on the sensors is thoroughly assessed, to determine their viability for in-vivo applications.

The findings of this study reveal that employing a convolutional neural network can enable the accurate measurement of ethanol in air, using off-the-shelf air quality sensors and algorithms with low computational complexity. It is worth highlighting that the neural network is capable of performing inference directly on the ingestible device. Furthermore, initial results show that a combination of parylene C and PCL, achieved through dip-coating in a PCL-dichloromethane solvent, yields a sensor capable of reliably distinguishing ethanol percentages from 4 to 11 volume percentages, while continually submerged in a self-designed artificial gastric environment.

Overall, this research contributes to the advancement of ingestible sensors and their potential for continuous health monitoring, with a use case in alcoholism treatment. The outcomes show the potential to produce a sensor array encapsulated in biocompatible materials, with a data-driven sensor fusion algorithm that is deployable on-device, which brings us closer to practical in-vivo applications. Additionally, the design and utilization of an artificial gastric environment establishes a solid foundation for future studies and the data generation that is vital for this technology.

# Acknowledgements

Embarking on my thesis research journey in the United States was both challenging and immensely rewarding. I am deeply grateful to my main supervisor, Professor Koen Langendoen, whose support and insightful feedback played a pivotal role in me finishing this research work at all. I would also like to extend my appreciation to Professor Giovanni Traverso for welcoming me to Boston and providing me with the opportunity to work alongside him, as well as to Henwei Huang for his supervision in the United States.

I am indebted to all those involved in this project, each of whom contributed to its realization. Niels Neidlein and Philipp Fritz offered their expertise in 3D printing and mechanical design, while David Werder shared his electronics know-how. I am also grateful to the technical staff, George Selsing, Ian Ballinger, and Injoo Moon, for their assistance and support, and for Emanuele Falli, who has helped me while being back in the Netherlands. Of course, I also want to thank Professor Peter Ray Chai, M.D. for being the medical advisor in this project.

Furthermore, I would like to acknowledge the valuable input and guidance of Alvin Chan and Ceara Byrne in the realm of machine learning. A special mention goes to Nabil Shalabi, with whom I had the privilege of crossing paths even before he joined the lab, at MIT Hacking Medicine and a lunch by the Gastroenterology Department. Nabil played an instrumental role in helping me overcome significant challenges encountered during my research.

Finally, I want to express my sincere gratitude to those who made my experience outside the lab all the more enriching. The friendships forged at the MIT entrepreneurship club and visiting student association, as well as the joy shared with my roommates Halithan Cetin, David Werder, and Gonzalo Arranz, have enhanced my life in immeasurable ways. I extend this appreciation to Jessica Bo, Michelle Chan, Jose Acitores for exploring the culinary heights of Boston together. Last but not least, I cherish the memories created with Eva Remlova, Julien Dosso, Jan Vukovic, Viktor Gaugg, Niels Neidlein, Amy Chiu, Jack Chen, Meishan Ross, Marcel Reimann, Sarvesh Karkhanis, Ciaran Brayboy, and many more amazing individuals who have left an incredible mark on my journey. To each of you, I offer my deepest gratitude—you know who you are!

# Contents

<b>1. Introduction</b>	<b>1</b>
1.1. Sensor Platform	2
1.1.1. Mechanical design	2
1.1.2. Electrical design	2
1.2. Clinical Context	3
1.3. Design Requirements	4
1.4. Contribution	5
1.5. Methodology	6
<b>2. Literature Review</b>	<b>7</b>
2.1. Measurement of Volatile Organic Compounds	7
2.1.1. Sensors	7
2.2. Electronic Pills for Biosensing	8
2.2.1. Gastric Residence	9
2.2.2. Biomaterials for Permeable Membrane	10
2.3. Research Gap	12
<b>3. Measuring Volatile Organic Compounds in Air</b>	<b>13</b>
3.1. Experimental Setup	13
3.1.1. Gas Sensors	13
3.1.2. Protocol	14
3.1.3. Hardware setup	15
3.2. Data Collection and Analysis	15
3.2.1. Classification of Acetone, Ethanol, and Methanol	16
3.2.2. Water and 0.2% Acetone	17
3.2.3. Alcoholic Drinks	17
3.2.4. Ethanol Regression	18
3.3. Regression Algorithm	19
3.3.1. Feature Extraction from Entire Experiment	19
3.3.2. Window-Based Slicing of the Raw Data	19
3.3.3. Feature Extraction from the Sliced Raw Data	19
3.3.4. Dummy Models	20
3.4. Methods	20
3.5. Results and Discussion	21
3.5.1. Window-Based Slicing of the Raw Data	21
3.5.2. Feature Extraction from Sliced Raw Data	23
3.6. Hardware Implementation	25
3.6.1. Edge Implementation	25
3.7. Limitations and Future Direction	27
3.8. Conclusion	27

<b>4. Measuring Volatile Organic Compounds in Liquid</b>	<b>28</b>
4.1. Encapsulation Materials	28
4.2. Experimental Approach	29
4.2.1. Production Methods	29
4.2.2. Experimental Protocol	31
4.3. Analysis of Sensor Response	32
4.3.1. Microscopic Analysis	32
4.3.2. Sensor Response	32
4.3.3. Temperature Sensitivity: Why the Parylene C with Heat-treated PCL Sensors Did Actually Not Sense VOCs.	35
4.4. Limitations and Future Direction	36
4.5. Conclusions	36
<b>5. Measuring Volatile Organic Compounds in an Artificial Gastric Environment</b>	<b>37</b>
5.1. Experimental Environment	37
5.1.1. System Overview	38
5.1.2. Sensors	39
5.1.3. Experimental Protocol	39
5.1.4. System Safety and Robustness	39
5.1.5. Experiment Queue	40
5.2. Experiments and Results	40
5.2.1. Epoxy Study	40
5.2.2. Lifetime and Consistency Study	41
5.2.3. PCL and Parylene C Study	43
5.3. Limitations and Future Directions	45
5.4. Conclusion	46
<b>6. Conclusion</b>	<b>47</b>
6.1. Research Question	47
6.2. Methods and Results	47
6.3. Limitations	49
6.4. Future Work	50
<b>A. Introduction</b>	<b>51</b>
A.1. Overview Sensor System	51
<b>B. Measuring Volatile Organic Compounds in Air</b>	<b>52</b>
B.1. Gas Sensor List	52
B.2. Data Streams Per Sensor	54
B.3. Features from Time Series	54
B.3.1. 15 Minute Experiment	54
B.3.2. Window-based features	55
B.4. Dummy Classifiers	60
B.4.1. Performance Metrics	61
B.5. Convolutional Neural Network Architectures	62
B.6. Edge Implementation	63
B.6.1. Energy Consumption Calculations	63
B.6.2. Microcontroller Units	66

<b>C. Measuring Volatile Organic Compounds in Liquid</b>	<b>67</b>
C.1. Previous Work . . . . .	67
C.2. Sensor Packaging . . . . .	68
C.3. Epoxy Protection . . . . .	69
C.4. Microscope Analysis . . . . .	70
C.5. Experimental Results . . . . .	71
C.5.1. Failed Experiments . . . . .	75
C.5.2. Temperature Correlation Plots . . . . .	76
<b>D. Artificial Gastric Environment</b>	<b>79</b>
D.1. Lid Production . . . . .	79
D.2. Schematics . . . . .	80
D.2.1. Sensor Readout . . . . .	80
D.2.2. Motor Control . . . . .	81
D.3. Finite State Machines . . . . .	82
D.4. Communication Protocol . . . . .	83
D.5. Experimental Procedure . . . . .	84
D.6. Experimental Results for Different Volumes of Ethanol . . . . .	85
D.7. Sensor Failure Analysis . . . . .	86

# List of Figures

1.1. (a) computer-aided design (CAD) design of the sensor platform’s electronics and (b) graphic of the pill’s deployment in the stomach . . . . .	3
1.2. The future of volatile organic compound (VOC) monitoring: breathalyzers are replaced by gastric resident electronics. Unique prints from the gas sensor arrays will enable the diagnosis and monitoring of diseases. . . . .	4
2.1. Sensor mechanics. a) metal oxide (MOX) sensors rely on a thin metal-oxide sheet, which has a high resistance when oxygen reacts with the sheet’s surface. volatile organic compounds (VOCs) react with this oxygen, hence lowering the resistance. b) optical sensors consist of a light source and detector. Gas molecules absorb some of the light frequencies, which is picked up by the detector. c) electrochemical sensors depend on two electrodes with an electrolyte in between. Upon contact with VOCs, a chemical reaction with the electrolyte will create free electrons to move between the electrodes. . . . .	9
2.2. a) Schematic diagram of pervaporation process: <i>pervaporation</i> = permeation + <i>Evaporation</i> and b) Vapor-Liquid Equilibrium (VLE) of ethanol mixed with water (data from [1]). . . . .	12
3.1. Experimental protocol for gas sensors in air. . . . .	14
3.2. Plot of the SGP40 MOX gas sensor response during the experiment visualized in Figure 3.1. The beginning and end of exposure to ethanol are denoted by vertical lines. . . . .	16
3.3. 5-minute average sensor values (H <sub>2</sub> and ethanol) of a collection of 71 experiments with 5 different SGP30 MOX gas sensors upon exposure to acetone, ethanol, and methanol. . . . .	16
3.4. The average sensor value when the SGP40 MOX gas sensors are exposed to 0.2% Acetone and Water over a 5-minute period. . . . .	17
3.5. Average sensor values when the SGP40 MOX gas sensors are exposed to water, wine, Irish cream, or gin for 5 minutes. A line is drawn through the median data point at every alcohol type. . . . .	18
3.6. The ethanol calibration curve of an individual BME680 MOX gas sensor. Individual data points are added as scatter, with a line through the median data point at every measured ethanol concentration. . . . .	18
3.7. Prediction versus actual ethanol percentage when a sensor array is exposed to an (a) 60 and (b) 80 percent ethanol mixture (root-mean-square error (RMSE) is (a) 3.14% vol. and (b) 8.83% vol. respectively). Model B, with a 60-second window and 30-second sampling time. . . . .	22
3.8. Relative feature importance for a Random Forest (RF) regressor trained on all extracted features of the BME680, BME688, SGP30, and SGP40 sensors, for a window size of 60 seconds. The sensors are color coded, while the features are denoted by “[datastream] feature”. . . . .	24



4.1.	The 3D-printed mold for heat-treated polycaprolactone (PCL) encapsulation. . . . .	30
4.2.	The SGP40 MOX gas sensor with <b>a</b> ) parylene C, <b>b</b> ) dip-coated PCL and <b>c</b> ) heat-molded PCL as outer layer. . . . .	31
4.3.	Different layers of the SGP40 sensor, visualized using the FlexSEM1000 scanning electron microscope. A larger close-up, including that of heat-molded PCL can be found in Figure C.4 . . . . .	33
4.4.	SGP40 with 4 different encapsulations exposed to a mixture of 50 mL Whiskey and 250 mL water (6.67% vol. ethanol) at a temperature of 37 degrees Celsius. The sensors are fully submerged in between the 15 and 45 minute marks. . . . .	34
4.5.	BME688 with 2 different encapsulations exposed to a mixture of 50 mL Whiskey and 250 mL water (6.67% vol. ethanol) between the "Ethanol" and "Empty" mark. As can be seen. the sensor coated with parylene C and dip-coated PCL has a strong and immediate response to ethanol. The sensor coated with parylene C and heat-treated PCL has an exactly opposite response to the temperature. . . . .	35
5.1.	Drawing of the experimental environment. . . . .	38
5.2.	Schematic overview of the system. . . . .	39
5.3.	The dynamic response of the sensors over 3 hours when <b>(1)</b> a VOC at room temperature is added to the solution, <b>(2)</b> the gastric environment is emptied and <b>(3)</b> the gastric environment is filled with fresh water at room temperature. <b>(a)</b> and <b>(c)</b> refer to the SGP40 raw sensor value response, while <b>(b)</b> and <b>(d)</b> are the BME688 temperature responses in degrees Celsius. . . . .	42
5.4.	<b>(a)</b> lifetime and <b>(b)</b> latency ( $t_{90\%}$ ) of selected sensors, obtained from at least three sensors for each coating thickness. . . . .	43
5.5.	Experimental results of the SGP40 encapsulated with parylene C and dip-coated PCL in the experimental environment. The graph shows the decrease in sensor value after 30 minutes of exposure to VOCs as a function of the percentage of ethanol in % vol. for 9 consecutive experiments. The experiments were not necessarily in increasing or decreasing order with respect to ethanol percentage. . . . .	44
A.1.	Block Schematic of the alcohol sensor system. The gas sensors that are considered in the sensor array in this thesis, but not on the current sensor platform are faded out. . . . .	51
B.1.	Power consumption and area of different microcontroller units. The green area represents the area footprint that fits on the sensor arm. The nRF52832 is the processor that is currently on the sensor platform. . . . .	66
C.1.	The encapsulation process using fast curing silicon around the electronics and polyvinylidene difluoride (PVDF), poly-tetrafluoroethylene (PTFE), and polydimethylsiloxane (PDMS) around the sensor membrane. . . . .	67
C.2.	The packaging of the three sensors that were extensively tested in liquid. <b>a)</b> plastic packaging with large permeable membrane (SGP40, SGP30, STC31), <b>b)</b> metal casing with pinhole (BME688, BME680, ENS160, MiCS5524, ZMOD4410) and <b>c)</b> plastic packaging with large air inlets (CCS811, CCS801). . . . .	68
C.3.	Visualization of the SGP40 sensor breakout board <b>a)</b> during the application of epoxy, and <b>b)</b> the result after curing. . . . .	69

List of Figures

C.4. Visualization of the different encapsulation layers, including the intrinsic sensor membrane of the SGP40. . . . .	70
C.5. SGP40 with 4 different encapsulations submerged in a 6.67% vol. ethanol solution at 37 degrees Celsius for 30 minutes. . . . .	71
C.6. BME688 with 4 different encapsulations submerged in a 6.67% vol. ethanol solution at 37 degrees Celsius for 30 minutes. . . . .	72
C.7. CCS811 with 4 different encapsulations submerged in a 6.67% vol. ethanol solution at 37 degrees Celsius for 30 minutes. . . . .	73
C.8. SGP40 with 4 different encapsulations submerged in a 6.67% vol. ethanol solution at 37 degrees Celsius for 30 minutes: a comparison of repetitions. . . . .	73
C.9. BME688 with 4 different encapsulations submerged in a 6.67% vol. ethanol solution at 37 degrees Celsius for 30 minutes: a comparison of repetitions. . . . .	74
C.10. SGP40 encapsulated with heat-treated PCL submerged in a 6.67% vol. ethanol solution at 37 degrees Celsius for 30 minutes (see gray areas) over a period of more than 24 hours. . . . .	75
C.11. SGP40 with 2 different encapsulations exposed to a mixture of 50 mL Whiskey and 250 mL water (6.67% vol. ethanol) between the "Ethanol" and "Empty" mark. As can be seen, the sensor coated with parylene C and dip-coated PCL responds to ethanol, characterized by a clear dip in the sensor response. The sensor coated with parylene C and heat-treated PCL has an exactly opposite response to the temperature. . . . .	76
C.12. Scatter Plot of the BME688 in a long-term experiment, encapsulated with a) parylene C and heat-treated PCL and b) parylene C and dip-coated PCL. The red scatter are the data points corresponding with the exposure to ethanol. As can be seen, there is almost a perfect correlation between the sensor values and the temperature (correlation factor of -0.95). . . . .	77
C.13. Scatter Plot of the SGP40 in a long-term experiment, encapsulated with a) parylene C and heat-treated PCL and b) parylene C and dip-coated PCL. The red scatter are the data points corresponding with the exposure to ethanol. . . . .	78
D.1. Schematic of the production process. . . . .	79
D.2. Pictures of a) the beaker with lid with wires and tubes, during a running experiment, b) the 3d-printed beaker holder and c) the 3d-printed mold for silicone. . . . .	79
D.3. Sensor Readout Circuit Schematic. . . . .	80
D.4. Motor Control Circuit Schematic. . . . .	81
D.5. Motor Control - Arduino side. a,b,c,d and e are commands from the PC over the serial port. . . . .	82
D.6. Motor Control - PC Side . . . . .	82
D.7. Experimental Process (SGF = Simulated Gastric Fluid) . . . . .	84
D.8. Experimental results of the BME688 encapsulated with parylene C and dip-coated PCL in the experimental environment. The graph shows the decrease in sensor value after 30 minutes of exposure to VOCs as a function of the percentage of ethanol in % vol. for 4 experiments. . . . .	85
D.9. Four different captions of logging prints, in which can be seen that between "water in state" and "motor off state", i.e. during the inflow of fresh water, the sensors fail, the COM port receives strange characters and the COM port connected to the sensors even disconnects. The microcontroller sends out a string called "sensor data" to specify that it is sending back sensor data. What the computer receives instead is an indecipherable string. . . . .	86

D.10. The different datastreams of the BME688 encapsulated in parylene C and heat-treated PCL during a single experiment. The periods at which more than 250 mL water is added to the experiment is marked in blue. As can be seen, the sensors break every time this happens. . . . . 87

# List of Tables

2.1. <u>Non-retentive</u> ingestible capsules for biosensing in the gastrointestinal (GI) tract: state-of-the-art. . . . .	10
2.2. <u>Retentive</u> ingestible (gastric resident electronic (GRE)) devices for continuous biosensing: state-of-the-art. . . . .	10
3.1. Details of the gas sensors used in the experiments. . . . .	14
3.2. Fluids used and their volume percentage of VOC. Pure VOCs were diluted using tap water. . . . .	15
3.3. Average RMSE of model A (in volume percentage), for different window sizes and sampling times, using all 10 sensors. . . . .	21
3.4. Average RMSE of model B (in volume percentage), for different window sizes and sampling times, using all 10 sensors. . . . .	21
3.5. Average mean absolute error (MAE) of model A (in volume percentage), for different window sizes and sampling times, using all 10 sensors. . . . .	22
3.6. Average MAE of model B (in volume percentage), for different window sizes and sampling times, using all 10 sensors. . . . .	22
3.7. The RMSE for model B, at a time window of 60 seconds and sampling time of 30 seconds for different combinations of sensors. . . . .	23
3.8. Average RMSE of model B (in volume percentage), for features extracted from all 10 sensors. . . . .	24
3.9. Average MAE of model B (in volume percentage), for features extracted from all 10 sensors. . . . .	24
3.10. The RMSE for model B, at a time window of 60 seconds and sampling time of 30 seconds for different combinations of sensors. . . . .	25
3.11. Comparison between the edge implementation of the convolutional neural network on raw data, and ensemble model on feature extracted data. Although the inference time of the ensemble method is lower, it does not include the processing of the feature extraction. . . . .	26
4.1. The thickness of heat-treated PCL after 3D molding, measured from the top of the sensor's membrane until the surface of the coating. . . . .	30
4.2. The sensor response of the SGP40 MOX gas sensor when exposed to water and a 6.67% vol. ethanol solution, for a sensor only protected by the SGP40s inherent sensor membrane, and encapsulated by 20 $\mu\text{m}$ parylene C (see Figure 4.3 for a breakdown of the layers). . . . .	32
4.3. The sensor response of the BME688 and SGP40 when being immersed in a 6.67% vol. ethanol solution. The sensor value before ethanol exposure ( $R_0$ ), the steady-state value after exposure ( $R_{SS}$ ), and the time it takes to reach 90% of the steady-state value ( $t_{90\%}$ ). Average taken of 1 to 3 experiments. . . . .	35

5.1. Average sensor value of SGP40 gas sensors without coating (electronics protected with epoxy) after 30 minutes in different volume percentages of a water-ethanol solution. . . . .	41
B.1. Details of the gas sensors used in the experiments. . . . .	53
B.2. Sensors and Data Streams available for Regression . . . . .	54
B.3. convolutional neural network (CNN) Model A Architecture . . . . .	62
B.4. CNN Model B Architecture . . . . .	62
B.5. Manually optimized hyperparameters used for training the convolutional neural network. . . . .	62
B.6. Estimated Power Consumption and Lifetime of the Sensor Platform with a Sampling Time of 30 seconds . . . . .	64
B.7. Estimated Power Consumption and Lifetime of the Sensor Platform with a Sampling Time of 5 seconds . . . . .	65
C.1. The lifetime of different MOX gas sensor encapsulations, given the process visualized in Figure C.1. . . . .	67

# List of Algorithms

D.1. Data Exchange Between Python and Arduino . . . . . 83

# Acronyms

RMSE	root-mean-square error	x
VOCs	volatile organic compounds	x
VOC	volatile organic compound	x
MOX	metal oxide	x
VLE	Vapor-Liquid Equilibrium	x
RF	Random Forest	x
CAD	computer-aided design	x
PCL	polycaprolactone	xi
PDMS	polydimethylsiloxane	xi
PTFE	poly-tetrafluoroethylene	xi
PVDF	polyvinylidene difluoride	xi
GRE	gastric resident electronic	xiv
MAE	mean absolute error	xiv
GI	gastrointestinal	xiv
CNN	convolutional neural network	xv
HMS	Harvard Medical School	1
MIT	Massachusetts Institute of Technology	1
FDA	Food and Drug Administration	1
ML	machine learning	1
PCB	printed circuit board	2
MCU	microcontroller unit	2
BLE	Bluetooth Low Energy	2
RAM	random-access memory	5
GC-MS	gas chromatography–mass spectrometry	7
NG	nasogastric	7
I <sup>2</sup> C	Inter-Integrated Circuit	15
MUX	multiplexer	15
ANOVA	analysis of variance	20
DCM	dichloromethane	31
SEM	scanning electron microscope	32





# 1. Introduction

The gastrointestinal (GI) tract offers the opportunity to detect and monitor physiological signals in the human body in a minimally invasive way. Examples include the Food and Drug Administration (FDA)-approved MedTech PillCam, which introduced camera technology that replaces complex endoscopic procedures, such as double-balloon enteroscopy [2, 3].

The development of ingestible electronics is not exactly new. Its first recorded innovation dates back to the 1950s, when Mackay et al. proposed a Radiosonde [4, 5]. Over the years, subsequent studies have shown that pressure [6], pH [7], temperature [8] and GI motility [9] can be monitored throughout the GI tract.

More recently, breakthroughs in sensor fabrication, low-powered electronics [10], and material science [11, 12] have enabled the monitoring of more complex biomarkers, such as gaseous molecules. Steiger et al. confirmed in 2021 that 94% out of 125 small molecule analytes in blood can also be detected in the gastric fluid [13]. Monitoring these biomarkers through the gastric fluid would open up alternatives to more invasive, discontinuous methods of monitoring.

Volatile organic compounds (VOCs) are an important class of molecules that can be used as biomarkers for a variety of diseases. Measuring VOCs in exhaled breath is already a non-invasive and cost-effective way to diagnose and monitor diseases, and has been the subject of much research in recent years. Measuring the presence of VOCs in breath has already enabled the long-term monitoring and diagnosis of inflammatory gastrointestinal diseases [14], colon and gastric cancer [15], asthma [16] and obesity [17]. Moreover, a combination of VOC sensors with machine learning (ML) methods has been shown to offer a huge potential in the monitoring and detection of diseases, such as multiple sclerosis [18], breast cancer [19] and lung cancer [20, 21].

Traditional methods can however only provide information of VOC levels at a specific time. This is where electronic pills, otherwise known as smart pills, show a lot of promise. By continuously monitoring VOCs in the digestive tract, and transmitting the data wirelessly, electronic pills offer a more convenient, and possibly more accurate way to diagnose and monitor diseases [22].

A promising use case is the outpatient treatment of alcohol abuse disorders. Alcohol abuse accounts for 20% of all deaths in the United States among adults aged 20 to 49 years old [23]. As with the management of many substance abuse disorders, treatment relies on long-term monitoring of alcohol intake. The current standard of care often requires self-report by patients, which can be unreliable, and therefore limits opportunities for intervention and treatment [24].

A main challenge for continuous monitoring in the GI tract is that the current solutions are either tethered or have a low retention time within the gastric environment. Very recently, researchers at Massachusetts Institute of Technology (MIT) and Harvard Medical School (HMS) have developed smart pills that can stay in the gastrointestinal tract for a longer duration,

## 1. Introduction

by leveraging gastric resident structures [8, 25]. These pills could be equipped with sensors that can measure various physiological and pathological indicators, and transmit the data to an external device.

In this master's thesis, we will present the design of a sensor array that can continuously monitor VOCs in the GI tract. The array is deployed on an ingestible device, which is described in Section 1.1. The clinical relevance of this project will be discussed in Section 1.2. The design requirements of the ingestible device are discussed in Section 1.3 after which the research question is summarized in Section 1.4. The structure of the thesis is subsequently laid out in Section 1.5.

### 1.1. Sensor Platform

A group of researchers at MIT and HMS have been developing a gastric residence electronic (GRE) device, with a unique mechanical structure that allows for entry into the stomach but prevents egress. This allows the sensor to effectively monitor stomach conditions long-term. The device fits in a 000 capsule, which is the largest standardized FDA-approved capsule size, with a length of 26.1 millimeters and a diameter of 9.9 millimeters. This device has the capability to support a gas sensor array, which could measure VOCs.

#### 1.1.1. Mechanical design

A computer-aided design (CAD) of the sensor platform can be seen in Figure 1.1a. It exists of a battery pack with six electronic arms that are connected to a flexible printed circuit board (PCB). The flexible PCB allows the electronic arms to fold into a triple 0 capsule. Once the capsule dissolves, three of the six arms will unfold, while the other three stay attached to the battery pack. Its expansion makes it impossible for the device to pass through the pylorus, until the arms separate from the main body. This happens naturally, as the elastomer that keeps the arms together breaks down over time. The three stages of the sensor's deployment mechanism are shown in Figure 1.1b. The residence mechanism was tested in-vivo, on a pill without electronics. The pill remained resident until the terminal study of this individual animal model, which was after 35 days.

#### 1.1.2. Electrical design

The sensor platform exists of four different components, which are purposefully isolated by respective PCB arms. The microcontroller unit (MCU) arm exists of an nRF52832 microcontroller. Three arms are dedicated to power management, which includes the use of 8 super capacitors. One arm is dedicated to Bluetooth Low Energy (BLE) communication, and one arm is reserved for the sensor array. A schematic overview of the system, including power management, can be seen in Figure A.1.

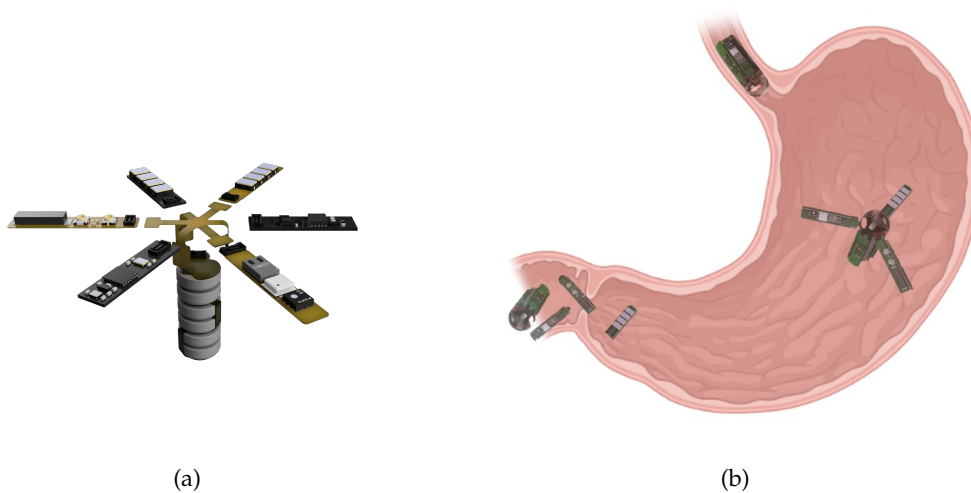


Figure 1.1.: **(a)** CAD design of the sensor platform's electronics and **(b)** graphic of the pill's deployment in the stomach

## 1.2. Clinical Context

In clinical practice, analysis of VOCs is commonly done with the use of electronic noses, which provide so-called "breath prints". Research has shown that these individual fingerprints of the VOCs in breath are related to a variety of pathological states [26].

However, breath analysis has its limitations. It usually requires a patient to blow into a breath analyzer, which is not suitable for continuous monitoring. This is where ingestible devices could open up a new paradigm for VOC monitoring. Through the utilization of gastroretentive devices, continuous real-time "stomach prints" can be obtained without any action needed from the patients (see Figure 1.2).

One prospective use case for continuous VOC detection in the stomach is the detection of alcohol consumption. This use case is specifically suitable for the early development of an ingestible gas sensor platform since we hypothesize that the high ethanol concentrations in the stomach are relatively easy to detect and distinguish, in comparison to complex and subtle VOC footprints that are related to other diseases. In the field of alcoholism treatment, ingestible electronics could be used to monitor a patient's drinking behavior in real-time, and potentially with much greater accuracy than current state-of-the-art technology. Currently, most registration of alcohol consumption is still done manually, by the patient itself. state-of-the-art measurement techniques rely on secondary biomarkers that are directly related to a person's blood alcohol level but do not actually provide any direct indication of a patient's consumption. Moreover, most of these techniques do not offer a method to monitor continuously.

In this research, we collaborate with Peter R Chai, MD, MMS, Associate Professor of Emergency Medicine at HMS, and a trained toxicologist. We expect to prescribe the ingestible sensor to outpatients, who are treated for alcoholism. During a period of 7 days, the sensor

## 1. Introduction

will gather information, which will be communicated to the healthcare professional during a weekly check-up.

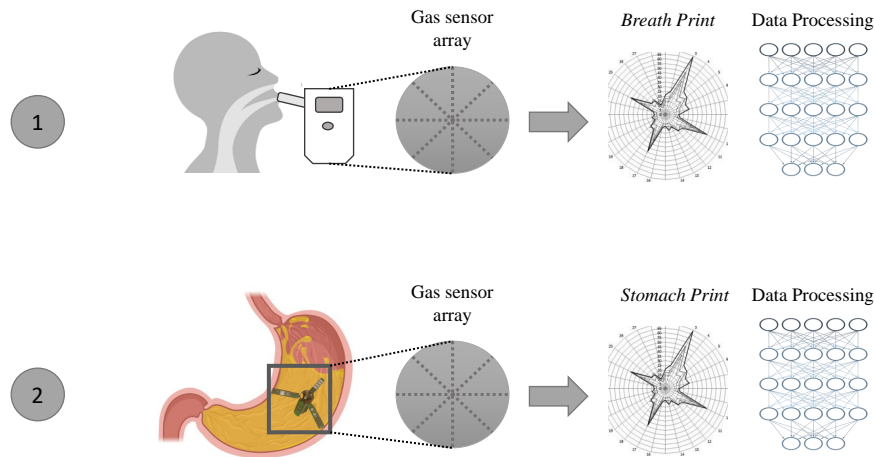


Figure 1.2.: The future of VOC monitoring: breathalyzers are replaced by gastric resident electronics. Unique prints from the gas sensor arrays will enable the diagnosis and monitoring of diseases.

## 1.3. Design Requirements

For the design of the gastric residence device with a gas sensor array, the following limitations need to be taken into account:

1. **Size:** The PCB sensor arm has a surface of 18.5 x 3.3 millimeters. This is all the space that is available for gas sensors.
2. **Energy Capacity:** The sensor's battery pack consists of six Renata 376 batteries, with a capacity of 27 mAh at 1.55 V. The total capacity is therefore 0.2511 Wh.
3. **Computational:** The sensor fusion algorithms should either be done off-the-chip or be runnable on an nRF52832 processor.
4. **Sensitivity:** The sensor should at least be able to sense the intake of ethanol equivalent to a beer. Preferably, it can distinguish different ethanol concentrations and different volumes of drinks.
5. **Economical:** The device should be translational, meaning that it is made of off-the-shelf electronics and is economically viable. Similar products on the market include the Medtronic PillCam, which costs about \$500, replacing a \$4000 procedure [27]. In the context of alcohol monitoring, a standard breathalyzer costs at most \$130 [28]. Although breathalyzers are more durable, a GRE device would offer more information.
6. **Mechanical:** The sensor should ideally be built using biocompatible, FDA-approved materials. This means that there is a limitation to the materials that can be used to encapsulate the electronics.

Given the design limitations, we can establish the following requirements list:

- The sensor array should fit within the 18.5 x 3.3 millimeter dimensions of the PCB sensor arm.
- The battery should last at least 7 days with the sensors running.
  - The average power consumption cannot exceed 1.5 mW.
  - The electronics should not break.
- The system needs to run on an nRF52832 processor, with 512 kB flash memory and 64 kB random-access memory (RAM).
- The materials used to protect the sensors should preferably be FDA-approved and bio-compatible.
- The total cost of the device should not exceed \$130.

## 1.4. Contribution

Although the foundations of a sensor platform have been laid, numerous obstacles still need to be addressed before it can be used as a VOC monitoring platform as envisioned in Figure 1.2. Conventional sensors have difficulty surviving in the harsh environment of the GI tract, which includes low pH levels, being fully immersed in liquid, and continuous collisions with food and the stomach lining. Protecting the sensors and electronics from this harsh environment often impacts the sensor's performance, as it will limit the diffusion of analytes through the protective layers.

Furthermore, research and development are heavily stagnated by the lack of realistic experimental environments, which makes it challenging to iterate over design cycles and identify causes of failures. Building and validating a sensor array with as many design variables as in this problem requires an experimental environment with as few unknowns as possible, in which data sets can be created without building a full device as in Figure 1.1a, as the production of such a device is incredibly labor intensive and often prone to manufacturing variations and errors. This brings us to the following problem statement:

### Problem Statement

How can we build a sensor array that is capable of continuous VOC monitoring in the stomach, considering the harsh environment in the GI tract and the lack of realistic experimental environments?

**This master's thesis will address this problem by adopting the following approach:**

1. Designing and evaluating a sensor array capable of detecting volatile organic compounds (VOCs) in the gastric environment for an extended time period.
2. Developing an experimental environment that facilitates efficient design cycles and generates significant ex-vivo data.

## 1.5. Methodology

An overview of previous research can be found in [Chapter 2](#). In this review, we can conclude that the idea of building a gas sensor for continuous VOC monitoring in the stomach is so novel, that it is vital to start designing from first principles. First, a sensor array that works with the hardware available for an ingestible device is designed to perform VOC detection tasks in the air. This is detailed in [Chapter 3](#). This is a critical milestone in determining the feasibility of this project, and narrowing down on the design variables.

Subsequently, in [Chapter 4](#), initial steps are taken to make a sensor array that works in a liquid environment, by experimenting with different sensor encapsulations in water for short periods.

The final step in this thesis is to evaluate an encapsulated sensor's long-term performance in a clinical setting. To this end, an artificial gastric environment is made, emulating many of the conditions in the human body, including body temperature and constant humidity. The design of this environment and experimental results are discussed in [Chapter 5](#).

## 2. Literature Review

This literature review aims to provide a comprehensive overview of the scientific literature related to sensors used for measurement of VOCs, electronic pills, gastric resident devices, and materials for permeable membranes.

### 2.1. Measurement of Volatile Organic Compounds

#### 2.1.1. Sensors

There are a large variety of sensing techniques for the detection of VOCs. gas chromatography–mass spectrometry (GC-MS), for example, is acclaimed for its extremely precise detection [29, 30]. Performance on a micro scale has yet to be achieved, however, and therefore this technology is not yet deployable on an ingestible device. Advances in nanotechnology have allowed for miniaturization and commercialization of chemiresistive, optical and electrochemical sensors [31]. This section will focus on these three types, and shortly touch upon some other state-of-the-art technologies available. The working principles of each sensor is visualized in Figure 2.1.

#### Chemiresistive Sensors

Chemiresistors are materials that change in resistance, given a particular chemical environment [32]. The most commonly used chemiresistive VOC sensors use metal oxide semiconductor technology to detect and quantify gaseous molecules in the air. These sensors are popular for their relatively small size, their low-power requirements and their price [33].

Within this category, there are a variety of companies that supply gas sensors that fit the requirements of the sensor platform, including those of manufacturers such as Bosch [34], Sensirion [35] and Sciosense [36]. All of these sensors are used in research on VOC monitoring in air, and have showed promising results. Sciosense's CCS811 was used to detect Parkinson's disease [37], while Bosch's BME680 was shown to be able to detect ketoacidosis through a nasogastric (NG) tube in the stomach [13].

#### Optical sensors

Compared to chemiresistive and electrochemical gas sensors, optical sensors are usually highly selective in nature [31]. Although some optical sensors can be made using micro-fabrication techniques, the light source and optical pathlength are much harder to miniaturize [38]. Because of this the miniaturization of state of the art optical sensors is often limited to handheld devices [39]. One of the smallest commercially available optical sensors in the

## 2. Literature Review

PMSA003I, which has a size of 38 by 35 millimeter [40]. This sensor is used as an air quality sensor, but unlike its indoor air quality counterparts, this one is only responsive to particles that are 10  $\mu\text{m}$  or less in width, and cannot measure VOCs.

### Electrochemical Sensors

Electrochemical sensors detect gaseous molecules by measuring changes in electric properties due to adsorption or chemical reactions between the VOCs and a gas-sensitive material. Sensors such as these are commonly used in breathalyzers and have also been used to measure blood alcohol levels through skin perspiration [41, 42].

The smallest electrochemical sensor that is currently available on the market is 11 by 11 millimeters [43], and is therefore not suitable for the design requirements laid out in Section 1.3. Since its working principle relies on a chemical reaction that produces a current, its energy consumption is literally zero, which makes it a promising sensor type for this use case in the future.

### Promising technologies

This review prioritizes commercialized VOC gas sensor technologies with miniaturization potential, and cannot provide an exhaustive analysis of all technologies. One example of a technology that is not covered is heat conductivity-based gas sensors. Although they have reached commercialization and sufficient miniaturization [44], they are currently deemed unsuitable for medical VOC detection, because of their low sensitivity. In breath prints for disease diagnosis, for example, VOCs present themselves in parts per billion or parts per trillion [45, 46]. However, when presented in volume percentages, such as in alcoholic beverages, these sensors could possibly be very useful. Moreover, unlike MOX sensors, these sensors do not require oxygen to work, hence are less vulnerable to losing sensitivity in relatively low oxygen environments, such as the GI tract [47].

Other state-of-the-art solutions have often only proven to work in laboratories. An example is a hydrogel-based sensor by Erfkamp et al. [48]. This sensor relies on the swelling of hydrogel upon contact with VOCs, and the measurement of pressure build-up due to this. Furthermore, there are numerous acoustic [49] and carbon nanotube [50, 51] gas sensors that have shown interesting developments in recent years.

## 2.2. Electronic Pills for Biosensing

The GI tract is still a relatively unexplored medium of long-term physiological sensing, despite offering the opportunity to detect and monitor physiological signals in a minimally invasive way [22]. The first ingestible device dates back to the 1950s when Mackay and Jacobson proposed a Radio Pill in Nature [4, 5]. Fifty years later, in the early 2000s, technology had finally matured enough to use ingestible electronic devices in practice. In 2001, the FDA approved the SmartPill, which could measure pH, pressure and temperature to diagnose slow gastric emptying [52]. That same year, the FDA also approved the first version of the Medtronic PillCam, which introduced camera technology that replaced complex endoscopic procedures, such as double-balloon enteroscopy [2, 53].



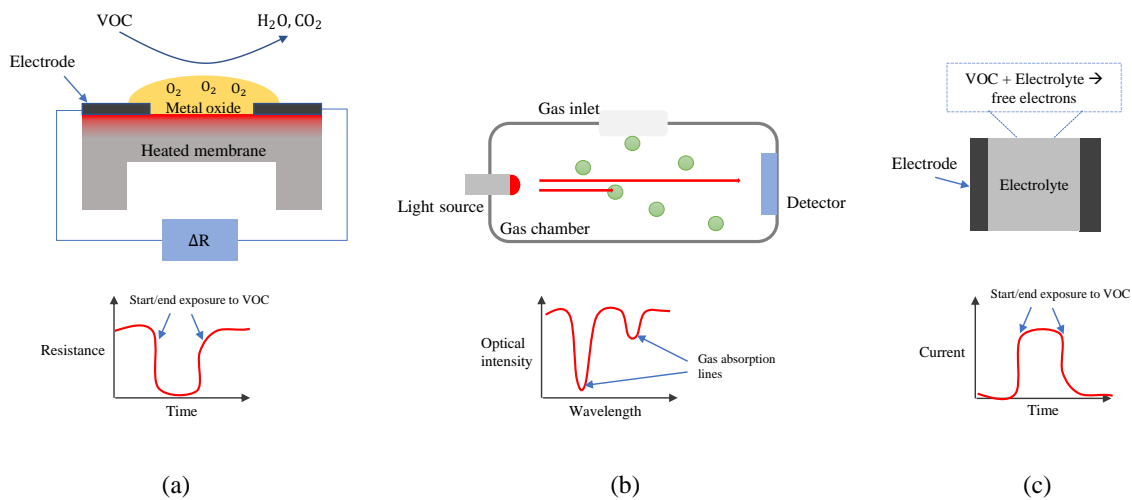


Figure 2.1.: Sensor mechanics. **a) MOX sensors** rely on a thin metal-oxide sheet, which has a high resistance when oxygen reacts with the sheet's surface. **VOCs** react with this oxygen, hence lowering the resistance. **b) optical sensors** consist of a light source and detector. Gas molecules absorb some of the light frequencies, which is picked up by the detector. **c) electrochemical sensors** depend on two electrodes with an electrolyte in between. Upon contact with **VOCs**, a chemical reaction with the electrolyte will create free electrons to move between the electrodes.

Over the next years, breakthroughs in low-powered electronics [10] and materials science [11, 12] have enabled the monitoring of increasingly complex biomarkers. A large number of biomarkers, such as small molecules, electrolytes, gases, proteins, and DNA can all be leveraged to monitor a patient's wellbeing in real-time. Steiger et al. confirmed in 2021 that 94% out of 125 small molecule analytes in the blood can also be detected in the gastric fluid [13]. Monitoring these biomarkers through the gastric fluid would open up alternatives to more invasive, discontinuous methods of monitoring.

Monitoring some of these molecules in a gaseous state has already been proven to be possible in humans and pigs [54, 55, 56]. In these experiments, capsules with a gas-permeable membrane were swallowed, which shield the sensitive gas sensors from the harsh GI environment. These ingestible sensors have no way of retaining in the GI tract, however, and will usually leave the body within 48 hours. An overview of the state-of-the-art, non-retentive ingestible capsules for biosensing can be found in Table 2.1.

### 2.2.1. Gastric Residence

A major limiting factor in achieving the continuous monitoring of biomarkers in the GI tract is the short residency period of the devices mentioned in Table 2.1. The median transit time of a Medtronic Pillcam through the stomach is typically around 25 minutes, although it can range from 1 minute to 3 hours [71]. As for the gas-sensing electronic capsule, it resided in the stomach for 4.5 to 12 hours, depending on the patient's diet [54]. This is significantly higher than that of the PillCam, despite its similar size, but no explanation is given.

## 2. Literature Review

Biomarkers Measured	Development Stage	Note	Reference
Gas ( $O_2$ , $H_2$ , $CO_2$ ), Temperature	In-Vivo (Human)	MOX gas sensor	[54, 57]
Endoscopy	In-Vivo (Human)	-	[2]
pH, Temperature, Pressure (GI Motility)	In-Vivo (Human)	-	[58]
Location (Medicine Adherence)	In-Vivo (Human)	-	[59, 60]
Gas ( $NO_x$ , $H_2S$ , $TT^1$ and $ROS^2$ )	In-Vivo (Porcine)	Bacterial gas sensor	[55]
Gas (NO)	In-Vivo (Porcine)	Electrochemical Gas Sensor	[56]
Gastric Bleeding	In-Vivo (Porcine)	Bacterial sensor	[61]
Glucose	In-Vivo (Porcine)	Battery-free	[62]
Sound (Heart Rate)	In-Vivo (Porcine)	-	[63]
pH	In-Vivo (Porcine)	-	[64]
Location (GI Dynamics)	In-Vivo (Porcine)	-	[65]
Gastric Bleeding	In-Vitro	Optical sensor	[66]
Enzymes (Lipase)	In-Vitro	-	[67]
Endoscopy	In-Vitro	X-ray	[68]
Endoscopy	In-Vitro	Ultrasound	[69]
Molecules (not specified)	In-Vitro	E-tongue (Electrochemical Sensor)	[70]

Table 2.1.: Non-retentive ingestible capsules for biosensing in the GI tract: state-of-the-art.

<sup>1</sup> tetrathionate

<sup>2</sup> reactive oxygen species

Researchers have developed a number of ingestible electronic devices that prolong the gastric residency periods of ingestible capsules to over 24 hours, with the goals of drug delivery, biosensing, and treatment of obesity. There are only a few devices in the literature that have managed to achieve continuous monitoring of biomarkers in the stomach. An overview of these devices, including their residence mechanism can be seen in Table 2.2.

Residence Mechanism	Biomarkers Measured	Development Stage	Reference
Hydrogel	Temperature	In-Vivo (Porcine)	[25]
Unfolding structure	Temperature	In-Vivo (Porcine)	[8]
Inflatable system	<i>Not specified</i>	In-Vitro	[72]

Table 2.2.: Retentive ingestible (GRE) devices for continuous biosensing: state-of-the-art.

### 2.2.2. Biomaterials for Permeable Membrane

While gas sensing in the GI tract has been achieved and even commercialized, none of these sensors focused on detecting VOCs [54, 55, 56, 57]. One specific reason is that it is hard to allow these molecules access to the sensing element while protecting the element from the harsh environment of the GI tract. Separation often relies on leveraging the difference in chemical properties between molecules, but VOCs have a lot of properties in common with the water and hydrochloric acid that is damaging to the sensing element.

VOCs such as methanol, ethanol and acetone contain an -OH bond, making them polar. Hydrophobic membranes would therefore be ineffective in separating these molecules from water. Since both HCl and  $H_2O$  are smaller in size, it is also easier for these molecules to permeate through small pores or gaps in materials.

### Pervaporation fundamentals

Pervaporation is a membrane-based separation process that could be used to isolate volatile organic compounds from gastric fluid. This method is mainly used in industrial processes, such as the production of alcohol-based biofuels. Other processes, such as distillation, adsorption, and liquid extraction are not applicable to sensing VOCs in the GI tract.

Any membrane without pervaporation characteristics will separate ethanol and the harmful liquids in the GI tract according to the Vapor-Liquid Equilibrium (VLE), plotted in Figure 2.2b. This means that for low ethanol concentrations in the gastric fluid, the ethanol concentration on the sensor side will be relatively high. However, the amount of water and hydrochloric acid molecules that will permeate through the membrane would likely still influence the sensor in a harmful way. Especially during a sudden change of temperature, due to drinking cold fluids, the water vapor on the sensor side could condensate and cause electrical short-circuits.

The mechanism of pervaporation is visualized in Figure 2.2a. The pervaporation membrane exploits different affinities towards the membrane and diffusion rates through the membrane to enhance the concentration of a certain component in comparison to the VLE. There are two driving forces that make this happen: the flux and separation factor of the membrane. The flux is how fast different liquids permeate through the membrane, in kilogram per meter square per hour [ $kg \cdot m^{-2}h^{-1}$ ]. The separation factor is defined as the ratios of the molecules in liquid in comparison to that in vapor (see Equation 2.1, where  $C_i^V$  and  $C_i^L$  are the concentrations of molecule  $i$  in vapor and liquid respectively). An ideal pervaporation membrane would allow for a high flux of ethanol through the membrane, which would allow a fast response time for the sensors while having an infinitely high separation factor. An infinitely high separation factor would mean that it would not allow through any water and HCl but does let through ethanol.

$$\alpha_{12} = \frac{C_1^V/C_2^V}{C_1^L/C_2^L} \quad (2.1)$$

### Materials

Although it is much easier to find membranes that are selective for H<sub>2</sub>O, there are materials that preferentially let ethanol pass through, while blocking water and hydrochloric acid. One polymer that has been used in gastric resident electronics and has shown these properties is PDMS [8]. PDMS has shown to have separation factors up to 14 [73], and fluxes of 5.4 kg·m<sup>-2</sup>h<sup>-1</sup> [74].

Another commonly used polymer that could be used is PTFE. PTFE has shown to be able to reach a separation factor of 8.63 with a flux of 24.145 kg·m<sup>-2</sup>h<sup>-1</sup>, given specific formulations [75]. In literature, there has been only one example of a VOC membrane being used in the stomach, through a NG tube [13]. This was a J050A025A Advantec PTFE membrane, which was able to detect acetone, and protect the BME680 MOX gas sensor behind it [34]. The acetone flux of this membrane is 0.00869 kg·m<sup>-2</sup>h<sup>-1</sup>, and it claims to block water entirely until a pressure of 1040 mmHg [76]. This pressure is 10 times higher than the maximum pressure in the stomach [9].

## 2. Literature Review

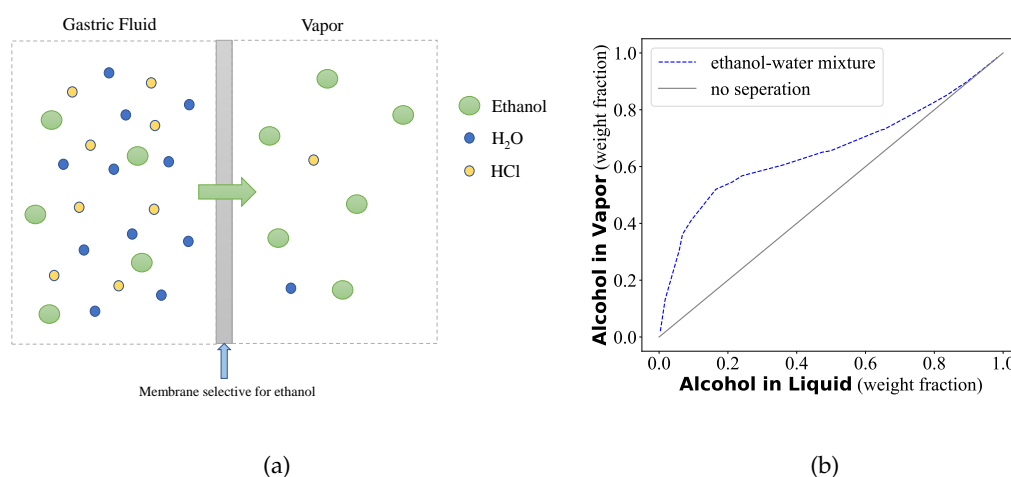


Figure 2.2.: **a)** Schematic diagram of pervaporation process: **pervaporation** = **permeation** + **Evaporation** and **b)** VLE of ethanol mixed with water (data from [1]).

State-of-the-art research in materials science has shown other materials, such as graphene and dopamine zeolites to show separation factors and flux that are even higher than the aforementioned materials [77, 78]. Production and biocompatibility make these materials however difficult to integrate in a medical device. Furthermore, many of these membranes lose their separation capabilities over time [77].

It is important to note that the separation factor and flux are dependent on conditions such as temperature, pressure, and the thickness of the membrane. For this reason, it is vital to conduct our own experiments.

### 2.3. Research Gap

Current state-of-the-art shows that although the measurement of VOCs for healthcare purposes has been employed in diagnosis and health monitoring, it has never truly been miniaturized to fit on a pill, while using off-the-shelf sensors. Developing an affordable VOC detection system within a pill's size already surpasses current research limits.

Besides miniaturization, the harsh environment of the stomach requires the creation of a biocompatible membrane that protects VOC gas sensors while maintaining sensitivity to analytes. This has only been achieved by measuring acetone through a NG tube, and never through a pill, let alone one that can stay resident in the GI tract. The development of a gas sensor platform that reliably measures ethanol over extended periods of time in the GI tract would mark a notable scientific advancement.

## 3. Measuring Volatile Organic Compounds in Air

Measuring VOCs in the GI tract is an incredibly difficult task with an enormous amount of design decisions in both hardware and software design. To prove its viability and narrow down on design choices, a sensor array was created in air first.

Another reason to design a sensor array in air, is that in order to build data-driven detection models, a large amount of data is required. The sensor dynamics are significantly slowed once they are encapsulated, because the materials limit the flux of VOCs towards the gas sensor, and therefore building up a large dataset requires much more time. Furthermore, doing experiments on a large scale is much harder to realize when each sensor requires an extensive manufacturing process and must be placed in a more complex experimental environment.

In this chapter, we discuss the experimental setup in air in [Section 3.1](#). Subsequently, we look at the qualitative results of the experiments in air in [Section 3.2](#). After this, we discuss the different types of regression techniques that could be used to determine the percentage of ethanol in a liquid in [Section 3.3](#), with further elaboration on the methods in [Section 3.4](#). After this, the regression techniques are implemented and compared in [Section 3.5](#). Finally, the resulting implementations are built to fit the hardware of the sensor platform in [Section 3.6](#). The chapter ends with a discussion of future directions and a conclusion in [Section 3.7](#) and [Section 3.8](#) respectively.

### 3.1. Experimental Setup

#### 3.1.1. Gas Sensors

Ten off-the-shelf sensors were chosen based on price, size, and power consumption, and evaluated on their ability to measure VOCs. Relevant details are summarized in [Table 3.1](#). A more extensive table can be found in [Table B.1](#). Each sensor, except for the MiCS5524, fits on a 18.5 by 3.3 millimeter sensor arm. 9 sensors are MOX sensors, except for the STC31, which is heat conductivity based. 8 sensors are digital, while 2 sensors are analog.

#### Power consumption

The power consumption at 1 Hertz for each sensor's standard settings was measured using a Nordic Semiconductor Power Profiler Kit II (PPK2). 1 Hertz was used in some datasheets, and the measured power consumption could therefore be validated. As can be seen in [Table 3.1](#), none of these sensors can run at 1 Hertz, given the energy requirements given in

### 3. Measuring Volatile Organic Compounds in Air

**Section 1.3.** The average power consumption should not exceed 1.5 mW if the battery should last for 7 days.

For this reason, all sensors should eventually be optimized for power consumption, by reducing the sampling frequency and putting the sensors in sleep mode in between samples. This however is only of later concern, as we analyze the sensor's performance under optimal conditions first.

	parameters					area [mm x mm]	power <sup>1</sup> [mW]
	digital	gas	temperature	humidity	pressure		
<b>BME688</b> [79]	✓	✓	✓	✓	✓	3.00 x 3.00	10.89
<b>BME680</b> [34]	✓	✓	✓	✓	✓	3.00 x 3.00	9.70
<b>SGP40</b> [35]	✓	✓	x	x	x	2.40 x 2.40	10.76
<b>SGP30</b> [80]	✓	✓	x	x	x	2.45 x 2.45	165.99
<b>CCS811</b> [36]	✓	✓	x	x	x	2.70 x 4.00	62.24
<b>ZMOD4410</b> [81]	✓	✓	x	x	x	3.00 x 3.00	5.95
<b>ENS160</b> [82]	✓	✓	x	x	x	3.00 x 3.00	96.00
<b>STC31</b> [44]	✓	✓	✓	x	x	3.00 x 3.50	6.11
<b>CCS801</b> [83]	x	✓	x	x	x	2.70 x 4.00	46.20
<b>MiCS5524</b> [84]	x	✓	x	x	x	5.00 x 7.00	163.40

Table 3.1.: Details of the gas sensors used in the experiments.

<sup>1</sup> Measured using Nordic Power Profiler Kit II (PPK2) at 1 Hz sampling rate, no sleep mode.

#### 3.1.2. Protocol

The experimental protocol is summarized in [Figure 3.1](#). A group of sensors was held for 5 minutes in the open air. Subsequently, it would be exposed to 25 mL of a given fluid in a 600 mL beaker. Each sensor would be held approximately at the 300 mL line. An overview of all fluids tested can be found in [Table 3.2](#).

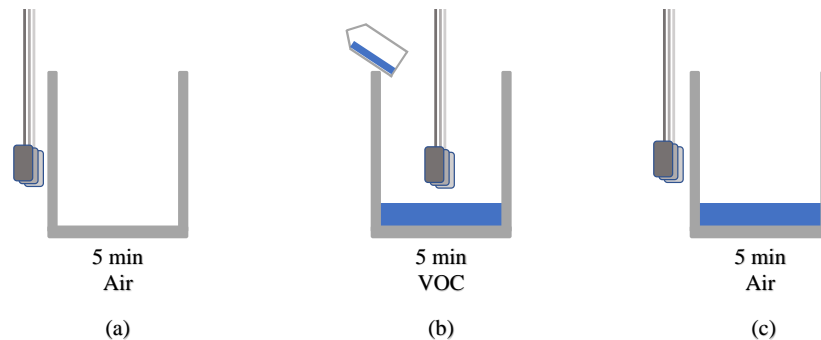


Figure 3.1.: Experimental protocol for gas sensors in air.

Fluid	Concentration [% vol.]
Ethanol (pure)	10, 20, 40, 60, 80, 100
Acetone (pure)	0.2, 100
Methanol (pure)	100
Vodka	40
Gin	40
Irish Cream	17
Wine	12
Water	0

Table 3.2.: Fluids used and their volume percentage of VOC. Pure VOCs were diluted using tap water.

### 3.1.3. Hardware setup

The overall system has a computer as the main station, which is connected to a microcontroller unit (MCU). The MCU is connected to the sensors through an Inter-Integrated Circuit (I<sup>2</sup>C) multiplexer (MUX). The MUX allows multiple sensors with the same I<sup>2</sup>C address to be connected to the I<sup>2</sup>C bus of the MCU at the same time. The computer requests the data from the sensors every sampling time, which is set to be five seconds, as it takes time to sample one sensor, and lower sampling times cannot be satisfied when 8 sensors are connected.

## 3.2. Data Collection and Analysis

In total, 1001 individual sensor experiments were performed. Some of the sensors used had more than one data stream. For example, the BME680 and BME688 measured a gas resistance value, temperature, pressure, and humidity. The SGP30 measured both an ethanol and H<sub>2</sub> value. An overview of all these data streams can be found in Table B.2. Given the multiplicity of data streams, there is a total **2510 data points**, each structured as a time series with 15 minutes of data. An example of such a data point can be seen in Figure 3.2. The sensor response is instant: within one sample (5 seconds), the sensor reaches 90% of its steady-state value. Generally, the response is analyzed by taking the average sensor value during the time of exposure to the vapor.

In this section, we will discuss the qualitative performance of gas sensors across four different experiments. First, we will investigate the ability to detect and classify ethanol, methanol, and acetone - three molecules that can all be present in the body, through for example methanol poisoning and ketoacidosis. Secondly, we will assess the sensor's capability to distinguish water from 0.2% acetone, a concentration that approaches a realistic ketoacidosis scenario. Further elaboration on ketoacidosis will be given in that section. Thirdly, we will delve into the sensor's effectiveness in classifying different alcoholic drinks. Finally, we will examine the sensor's performance in classifying ethanol-water mixtures over a wider volume percentage range - which is the type of experiment that will be used in developing a regression algorithm.

### 3. Measuring Volatile Organic Compounds in Air

SGP40 (ID: S034) Exposed to Ethanol Vapor (Concentration: 100%), Repetition 2

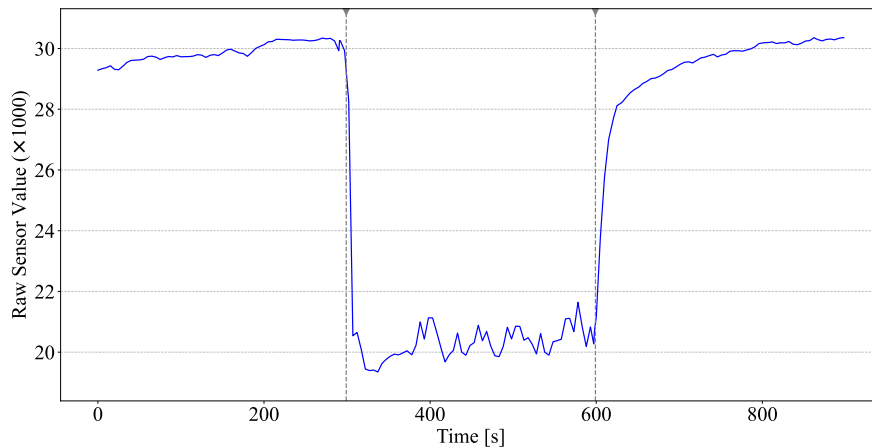


Figure 3.2.: Plot of the SGP40 MOX gas sensor response during the experiment visualized in Figure 3.1. The beginning and end of exposure to ethanol are denoted by vertical lines.

#### 3.2.1. Classification of Acetone, Ethanol, and Methanol

Based on the average sensor value during vapor exposure, certain sensors can effectively classify pure acetone, ethanol, and methanol. However, unidimensional data could be of concern - a lower concentration of one compound could be identified as the other compound. Sensor confusion offers the solution. A great illustration is the SGP30s mean sensor values of the SGP30s data streams in Figure 3.3. In a multidimensional space, compounds are covered by distinct areas, preventing overlap that occurs when projected to one dimension.

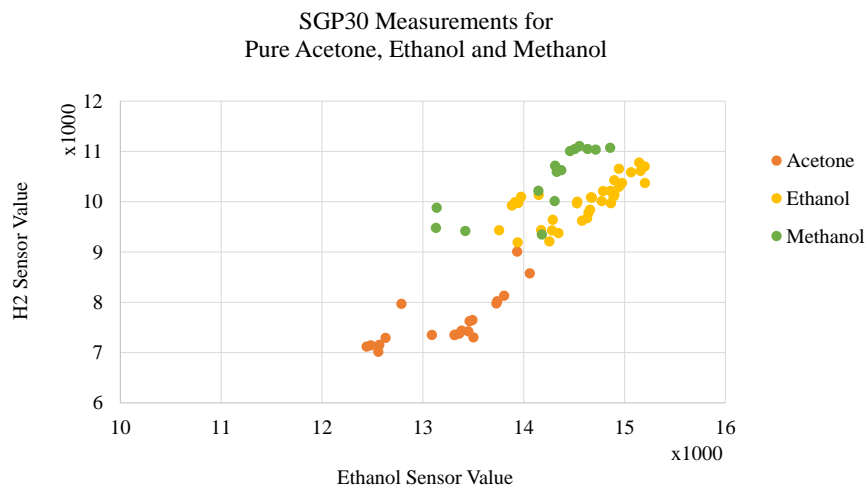


Figure 3.3.: 5-minute average sensor values ( $H_2$  and ethanol) of a collection of 71 experiments with 5 different SGP30 MOX gas sensors upon exposure to acetone, ethanol, and methanol.



### 3.2.2. Water and 0.2% Acetone

Acetone in the blood is correlated to a condition known as ketoacidosis. Ketoacidosis is a serious medical condition that occurs when the body produces high levels of ketones, including acetone, as a result of insufficient insulin and increased fat metabolism. It commonly affects individuals with uncontrolled diabetes, particularly type 1 diabetes. Ketoacidosis can lead to an accumulation of acidic ketone bodies in the bloodstream, causing symptoms such as excessive thirst, frequent urination, abdominal pain, nausea, and even potentially life-threatening complications if left untreated.

The levels of acetone in the blood that correlate with ketoacidosis are however extremely low: 3 mmol per liter [85], which corresponds with 0.022 volume percentage. Steiger et al. already showed that these levels can be measured in the stomach using the BME680 in an NG tube [13].

Since one drop of acetone in 25 mL of water already corresponds to 0.2% of ethanol, we performed an experiment that checked if one drop of acetone was detectable in 25 mL of water, in comparison to 25 mL of pure water. The results can be seen in Figure 3.4. As can be seen, a simple threshold is enough to decide with 100% accuracy whether 25 mL contains a drop of acetone, when considering the SGP40 sensor alone.

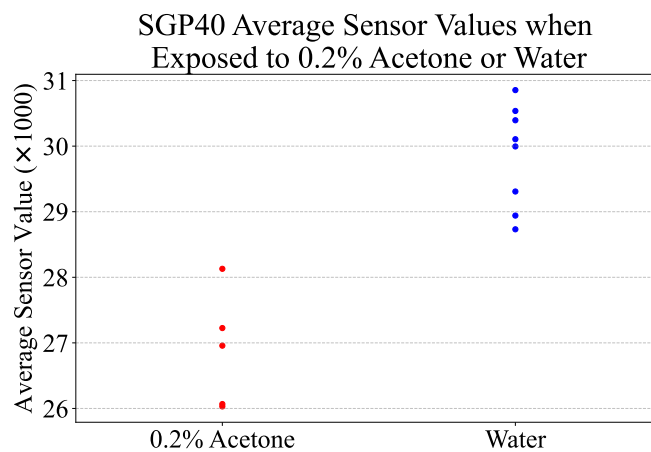


Figure 3.4.: The average sensor value when the SGP40 MOX gas sensors are exposed to 0.2% Acetone and Water over a 5-minute period.

### 3.2.3. Alcoholic Drinks

In this experiment, we exposed the gas sensors to water, wine, Irish cream, and gin. The results can be seen in Figure 3.5, where the average sensor value of the SGP40 during exposure is plotted. A median line is drawn through the individual experimental results. We can observe that the results do align with both the VLE curve and the calibration curve in Figure 3.6. We can also see that with the SGP40 alone, these drinks could be distinguished with a 100% accuracy.

### 3. Measuring Volatile Organic Compounds in Air

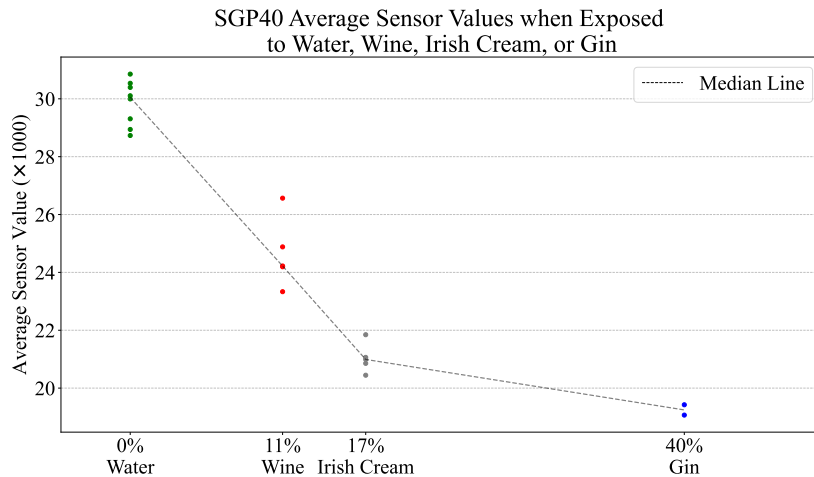


Figure 3.5.: Average sensor values when the SGP40 **MOX** gas sensors are exposed to water, wine, Irish cream, or gin for 5 minutes. A line is drawn through the median data point at every alcohol type.

#### 3.2.4. Ethanol Regression

The sensors were exposed to ethanol at 10, 20, 40, 60, 80, and 100 percent respectively. Not all sensors were exposed to 10 percent ethanol. The individual average sensor values of the BME680 are plotted in [Figure 3.6](#), with a line drawn through the median result at each ethanol percentage. It can be observed that the line follows the [VLE](#) plotted at [Figure 2.2b](#). The response is steep around 0 to 20 percent. It flattens out between 20 and 60, and then starts to decrease again. At the 100% line, the sensor starts to reach its minimum value for a number of repetitions.

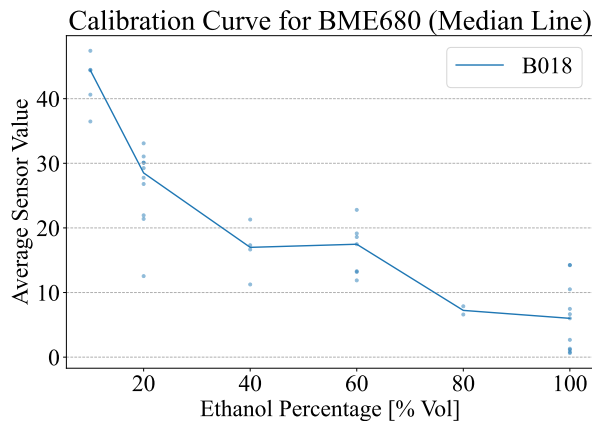


Figure 3.6.: The ethanol calibration curve of an individual BME680 **MOX** gas sensor. Individual data points are added as scatter, with a line through the median data point at every measured ethanol concentration.

### 3.3. Regression Algorithm

In developing a regression and detection algorithm for measuring VOCs using off-the-shelf gas sensors, three distinct approaches were considered for feature extraction. Feature extraction plays a crucial role in transforming raw sensor data into meaningful representations that can be used for accurate analysis and prediction. The three options explored in this study include: (1) feature extraction from the entire 15-minute experiment, (2) window-based slicing of the raw data, and (3) feature extraction from the sliced raw data.

#### 3.3.1. Feature Extraction from Entire Experiment

This approach involves extracting features directly from the entire duration of each experiment. By considering the complete experiment as a single data instance, this method captures the overall behavior and trends of the gas sensors over time. The features extracted from this approach provide a holistic representation of the sensor response, encompassing any variations or patterns that may arise throughout the entire 15-minute period.

A total of four different features were chosen. Two features capture the steady-state behavior of the sensor, as it is exposed to the gas. The other two encompass transient behavior. The formulas of these features can be found in [Section B.3](#). Although extensive regression experiments were done with these features, they were left out of the results because the data as presented by an entire experiment does not represent a realistic medical scenario. Furthermore, the dataset was too small. Some notable results were that, as [Figure 3.5](#) suggests, wine, Irish cream, and gin can be distinguished with 100% accuracy, using the SGP40 alone, in combination with a simple decision tree. Feature importance showed that the mean sensor value over the 15-minute period was by far the most important feature.

#### 3.3.2. Window-Based Slicing of the Raw Data

A main concern of considering the entire experiment is that the dataset size is way too small. When considering all sensors, and a regression problem, there are often only 2 or 3 data points per class. A solution for this is to slice up the data into windows that are of a shorter duration. Each window represents a snapshot of the sensor readings within a specific time interval.

This is also a more realistic approach when looking at implementation because, in real life, there will not be exact 15-minute windows, with a dramatic switch between “no VOCs” and “presence of VOCs” at the 5 and 10-minute mark.

#### 3.3.3. Feature Extraction from the Sliced Raw Data

Building upon the window-based slicing approach, this option involves extracting features from the sliced raw data within each window. By focusing on the segmented portions of the experiment, this method aims to capture the specific characteristics of the sensor response during shorter intervals. The extracted features from the sliced raw data can uncover nuanced details and dynamics within each window, potentially enhancing the algorithm’s ability to detect and predict VOC concentrations accurately.

### 3. Measuring Volatile Organic Compounds in Air

We extracted a total of 22 features, which were divided into 6 different categories. The details for each feature along with their equations are provided in [Section B.3.2](#).

1. **Statistical:** Statistical features are derived from analyzing the statistical properties of a signal. Some commonly used statistical features include mean, variance, skewness, and kurtosis. These features provide information about the distribution and shape of the signal and are commonly used for gas sensor applications [86, 87].
2. **Spectral:** Spectral features involve analyzing the frequency content of a signal using the Fourier transform. These features provide insights into the energy distribution across different frequencies and have been for example used alongside wavelet features to detect common pathogens on wounds, using a MOX gas sensor array [88].
3. **Peak-based:** Peak-based features focus on identifying prominent peaks or local maxima in a signal. These features are often used in applications related to audio or vibration analysis.
4. **Time Domain:** Time domain features are computed directly from the raw signal or a segment of it. These features capture various characteristics of the signal in the time domain. Time domain features such as the autocorrelation have been shown to even enable the classification of three different beers, using 8 MOX gas sensors and a Raspberry Pi [89].
5. **Wavelet:** Wavelet features involve decomposing a signal using wavelet transforms and analyzing the resulting wavelet coefficients. Wavelet analysis provides information about the signal at different scales and resolutions.

#### 3.3.4. Dummy Models

For both regression and classification, the performance of models is always compared with a random classifier. For regression, this is the median regressor (see [Equation B.20](#)), while for classification, it is the most frequent class classifier (see [Equation B.21](#)).

## 3.4. Methods

The experiments were performed on the MIT engaging open on-demand cluster. Data points, including windows and extracted features, were processed and labeled beforehand, as this was a computationally heavy task. In order to keep the computation time under the maximum of 12 hours, the feature extraction process had to be split into one sensor and one experiment per node. The features and labels would later then be merged into comma-separated value files that were between 0.5 and 1 GB in size. Each line of this file consists of a sensor, experiment number, label, and features.

Datasets were made by overlaying the data of several sensors together, in order to create experiments that replicate a sensor array. The data was then split into a train, test, and validation set, using leave-one-out cross-validation. Each evaluation was repeated at least 8 times to rule out randomness in the results, which were analyzed using analysis of variance (ANOVA).

## Performance Metrics

In this study, we employed both root mean square error (RMSE) and mean average error (MAE) as evaluation metrics for the regression algorithm. RMSE measures the average magnitude of the errors, giving more weight to larger deviations. It provides a robust assessment of the typical magnitude of the errors, making it sensitive to outliers. MAE, on the other hand, calculates the average absolute difference between the predicted and actual values, disregarding their direction. It provides a straightforward measure of how close the predictions are to the actual values, without penalizing large errors as heavily as RMSE.

Both metrics are easily interpretable, as their units are the same as the actual predicted unit. By using both MAE and RMSE, you can gain a more comprehensive understanding of the algorithm's performance. If the MAE and RMSE values are similar, it suggests that the errors are evenly distributed and not skewed by outliers. However, if there is a significant difference between the two metrics, it indicates the presence of outliers or a skewed error distribution.

## 3.5. Results and Discussion

### 3.5.1. Window-Based Slicing of the Raw Data

For the window-based slicing of the raw data, there was chosen for 2 different CNN models, for which the hyperparameters were first optimized to the settings found in Table B.5. Model A had layers with a kernel size of 2, allowing for the capturing of more global details in the data. Model B had layers with a kernel size of 1, meaning that it considers one data point at a time, without its relation to data points close to it. Due to its kernel size, Model A requires time series with a length of more than 8 data points.

The outcomes for different window sizes and sampling times can be seen in Table 3.3, Table 3.4, Table 3.5, and Table 3.6. The approach involved taking the average error values (in volume percentage) of repeated leave-one-out cross-validation.

Sampling Time [s]	Window Size [s]			
	60	120	240	480
5	<b>11.64</b>	12.33	13.61	16.74
10	-	13.02	12.12	15.41
15	-	-	12.98	15.77
30	-	-	-	17.79

Table 3.3.: Average RMSE of model A (in volume percentage), for different window sizes and sampling times, using all 10 sensors.

Sampling Time [s]	Window Size [s]			
	60	120	240	480
5	12.80	13.18	14.43	14.82
10	11.44	13.34	15.04	13.72
15	11.86	12.98	13.80	15.47
30	<b>11.02</b>	12.55	12.45	15.34

Table 3.4.: Average RMSE of model B (in volume percentage), for different window sizes and sampling times, using all 10 sensors.

As can be observed from the results, a lower window time is more beneficial for both model A and model B. This could be explained by the fact that there would be more windows in which the gas sensor data is stable, instead of windows where there is both a fragment of where the gas sensor is still in air and a fragment of where the data is exposed to the VOC.

### 3. Measuring Volatile Organic Compounds in Air

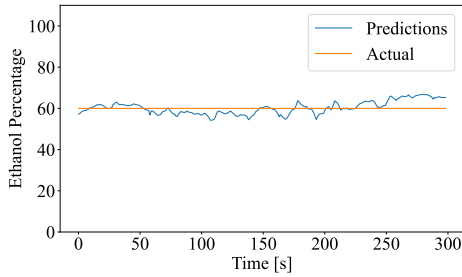
Sampling Time [s]	Window Size [s]			
	60	120	240	480
5	<b>10.37</b>	11.21	12.77	16.63
10	-	11.70	11.37	15.30
15	-	-	12.04	15.64
30	-	-	-	17.62

Table 3.5.: Average MAE of **model A** (in volume percentage), for different window sizes and sampling times, using all 10 sensors.

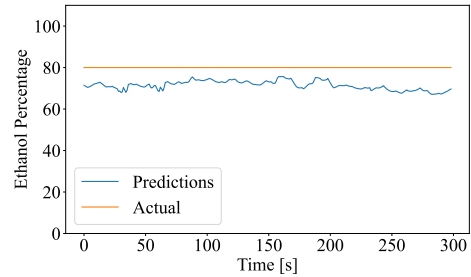
Sampling Time [s]	Window Size [s]			
	60	120	240	480
5	11.50	12.03	13.27	14.67
10	10.23	12.20	13.77	13.59
15	10.38	11.66	12.71	15.36
30	<b>9.45</b>	11.33	11.40	15.21

Table 3.6.: Average MAE of **model B** (in volume percentage), for different window sizes and sampling times, using all 10 sensors.

For **model A**, some of the window size and sampling time combinations were not compatible with the kernel size of the model. In **model B**, there was no statistically significant difference between the results of a window time of 60 seconds and a sampling time of 10, 15, and 30 seconds when using ANOVA ( $p > 0.05$ ). This shows that the information in the data likely comes from the combination of the information in a combination of different sensors, but not from the sensor values over time. Choosing a model that samples the least is preferable because a low sampling rate will save energy in a practical application.



(a)



(b)

Figure 3.7.: Prediction versus actual ethanol percentage when a sensor array is exposed to an (a) 60 and (b) 80 percent ethanol mixture (RMSE is (a) 3.14% vol. and (b) 8.83% vol. respectively). **Model B**, with a 60-second window and 30-second sampling time.

#### Further Optimization

After choosing for **model B** with a window size of 60 and sampling time of 30 seconds, further optimization was done. If we limit ourselves to all combinations of the 10 sensors from [Table 3.1](#), with no possibility for duplicate sensors in the array, we still have options according to the combinatorics equation in [Equation 3.1](#), which is  $2^{10}-1 = 1023$ .

$$\sum_{k=1}^n \binom{n}{k} = 2^n - 1 \quad (3.1)$$

Sensor Array	RMSE [% vol]	MAE [% vol]
BME688    SGP40	11.61	8.36
BME688    SGP40    CCS801	16.54	13.65
BME688    SGP40    CCS811	17.85	14.58
BME688    SGP40    STC31	16.85	14.44
<b>BME680    BME688    SGP30    SGP40</b>	<b>9.77</b>	<b>6.78</b>
Median Classifier	28.09	28.50

Table 3.7.: The RMSE for model B, at a time window of 60 seconds and sampling time of 30 seconds for different combinations of sensors.

Realistically, using 10 sensors will not be possible, as there is limited area to place the sensors on the ingestible device, and because there are power consumption limitations. In the current design as proposed in Section 1.1, the SGP40 and BME688 are deployed on the pill. Using model B for a 60-second window with 30-second sample time, we find an average RMSE of 11.61% and an MAE of 8.36%. Comparing this with Table 3.4 and Table 3.6, we can see that the difference between the RMSE and MAE is much higher when using fewer sensors. This indicates that there are still outliers that perform badly on the regression task, but that the regression of tasks that were already relatively close to the real value performed even better, even though most sensors are removed from the regression task.

A few tested combinations can be found in Table 3.7. It shows that choosing the right sensors is a non-trivial task. It is proven that a variable (in this case a sensor) that is completely useless by itself, can improve the model’s performance when taken with others [90]. Furthermore, the experiments in Table 3.7 show that adding extra information can result in confusing the model, hence decreasing its prediction accuracy.

A combination of BME680, BME688, SGP30, and the SGP40 was found to be better performing than when using the current setup or all the sensors ( $p < 0.05$ ), while still fitting on an 18 by 3.3 millimeters sensor arm.

### 3.5.2. Feature Extraction from Sliced Raw Data

With respect to the features extracted from sliced raw data, a naive regression approach was implemented first. Model B was trained on all features for all 10 sensors. Model A was not used this time, as using kernel sizes of higher order are used to blend information of nearby features. This makes sense when using spatial data, such as a picture or time series, but not when features are already extracted from the time series.

The results can be seen in Table 3.8 and Table 3.9. We can conclude that also for this sensor, increasing the window size does not seem to have a significant influence on the regression capabilities. Both for a window size of 60 and 240 seconds, the model performed better than using the raw data.

The trade-off is however that extracting features from the raw data is computationally heavy. Furthermore, it results in a significantly larger amount of features than when using the raw data. Where the raw data required only 2 data points per window per data stream, the feature data required 22.

### 3. Measuring Volatile Organic Compounds in Air

Sampling Time [s]	Window Size [s]		
	60	120	240
5	9.76*	11.00	9.02*

Table 3.8.: Average **RMSE** of **model B** (in volume percentage), for features extracted from all 10 sensors.

Sampling Time [s]	Window Size [s]		
	60	120	240
5	9.00*	10.25	8.51*

Table 3.9.: Average **MAE** of **model B** (in volume percentage), for features extracted from all 10 sensors.

\* The difference is not statistically significant, when analyzed using **ANOVA**.

#### Further Optimization

Just as with the models trained on raw data, we can reduce the dimensionality of the data by reducing the number of sensors used in training. Another way to reduce dimensionality is by eliminating features. A popular method for accomplishing this is through the use of ensemble models, with random forests (RFs) standing out as particularly effective in achieving this goal [91].

For this reason, a **RF Regressor**<sup>1</sup> was trained for using leave-one-out cross-validation, using the sensor array obtained in **Table 3.7**, and the accumulative feature importance was plotted in **Figure 3.8**. Cutting off at 10 features, we can find that the BME680 is actually not storing important feature information, and all information is stored in statistical and peak-based features.

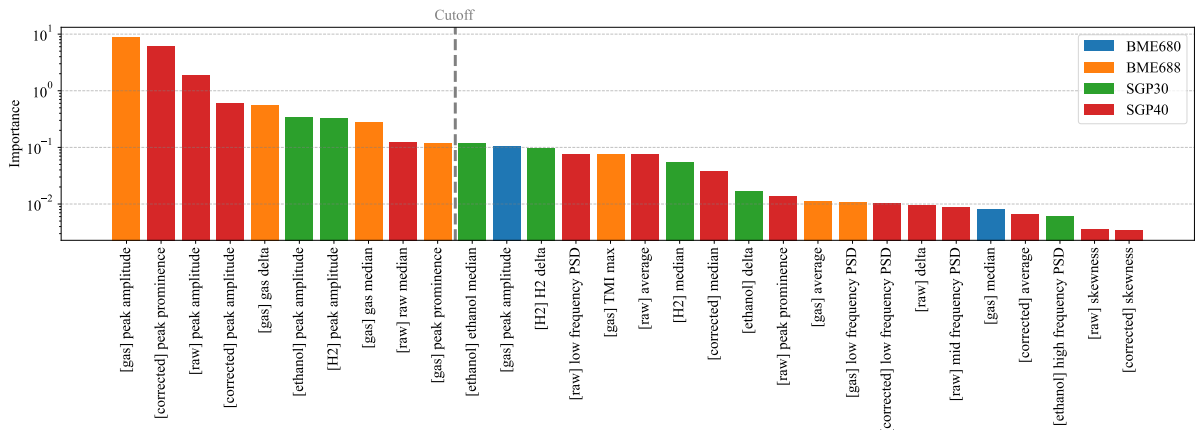


Figure 3.8.: Relative feature importance for a **RF** regressor trained on all extracted features of the BME680, BME688, SGP30, and SGP40 sensors, for a window size of 60 seconds. The sensors are color coded, while the features are denoted by “[datastream] feature”.

<sup>1</sup>number of estimators: 2000, maximum depth: 7.



As seen in Table 3.10, using only the BME688, SGP30, and SGP40 to train the RF improves the model's performance. Eliminating the features below the cut-off improves the model's performance even more. The difference is statistically significant, using ANOVA ( $p < 0.05$ ). Retraining the CNN on the reduced features gives an RMSE of 10.14% vol. and MAE of 9.57% vol. We can see that this is worse than the results of Table 3.8, but it comes with an enormous reduction of complexity.

It can also be concluded that a RF is a better-performing model than a CNN when using feature extraction. This might be partially because the RF gives a stable prediction, that is similar to the volume percentages in the training set. In some of its predictions during the cross-validation, it would have an error of 0% vol. It is not sure if this model will still predict better for volume percentages that are not part of the training set.

Finally, it can be seen that even with optimizations, the model trained on features does not outperform the models trained on raw data based on the MAE. This suggests that feature extraction improves the performance of outliers in specific.

Features	RMSE [% vol]	MAE [% vol]
All	9.15	8.09
Sensor selection	8.40	7.96
<b>Sensor and feature selection</b>	<b>7.50</b>	<b>7.13</b>
Median Classifier	28.09	28.50

Table 3.10.: The RMSE for model B, at a time window of 60 seconds and sampling time of 30 seconds for different combinations of sensors.

## 3.6. Hardware Implementation

Given the datasheets of all the components on the sensor platform, a back-of-the-envelope estimation of the sensor platform's lifetime could be made, assuming on and off times. The calculations can be found in Section B.6.1. We can find that the RF implementation has an estimated lifetime of 6.3 days, while the CNN with a sampling time of 30 seconds has a lifetime of 25.3 days. The major difference is due to the higher sampling rate. This can be solved by:

- Only measuring the temperature, and activating the gas sensors once a change in temperature is detected.
- Sampling the gas sensors at a lower frequency until a significant and sudden change is detected.

### 3.6.1. Edge Implementation

A large bottleneck in the implementation of the sensor platform is communication with the outside world. Bluetooth signals have a significant attenuation through tissue, and therefore, a patient would have to hold a receiver close to their body continuously [92]. A possible solution would be to run the detection algorithm on the pill and only send out the processed data with a receiver at a doctor's visit.

### 3. Measuring Volatile Organic Compounds in Air

To test this possibility, the CNN and RF were both converted to models deployable on an MCU, using the Tensorflow Lite Micro [93] and Python’s micromlgen library [94] respectively. With full quantization, the model’s 18,145 parameters are all converted from 32-bit floating point numbers to 8-bit integers. Using the edge impulse EON optimizer [95], a model of 48.9 KB was left, including all library functions. The RF had a size of 5MB, which is way too large for implementation on the MCU, which only has 512 KB flash memory. For this reason, the parameters were tuned down to 100 estimators with a maximum depth of 7, resulting in a model of 271 KB. This had little effect on the performance of the model, which is a common occurrence for RFs, which are relatively insensitive to hyperparameter tuning [96]. The RAM consumption was measured by Edge Impulse [97], and was found to be 3.3 KB - well below the 64 KB available. The RAM requirements for a RF are essentially 0.

#### Microcontroller Deployment

The model was deployed on an Arduino Nano 33 BLE, which has an nRF52840, which is from the same product family as the chip currently used on the sensor platform, but has slightly more memory. A test set was stored on the microcontroller, and inference was performed on each data point. The inference time for the CNN was 6 ms.

Previous research by ETH Zürich has found that the nRF52832’s power consumption is 14.94 mW during inference [98]. Given a 6-millisecond inference time, we can add the local inference to the energy consumption model of Table B.6, and find that this would only contribute as 1.4% of the total power consumption, with most (91.4%) still coming from the gas sensors.

A comparison between the two implementations can be seen in Table 3.11. The CNN implementation has a higher lifetime and significantly lower flash memory footprint. It has to be taken into account that while the inference time of the random forest is lower than that of the convolutional neural network, the RF requires feature extraction, which will take a significant amount of processing time.

An analysis was done to find other possible MCUs that could deploy neural networks, which fit the requirements of the pill. This would possibly reduce the energy consumption and latency of running the algorithms locally if more complex networks are deployed. An overview of this analysis can be found in Figure B.1, which is dated from early 2022.

	CNN	RF
Sampling Time [s]	30	5
Lifetime [days]	25.3	6.3
Flash [KB]	49	271
RAM [KB]	3.3	0
Inference Time [ms]	6	1

Table 3.11.: Comparison between the edge implementation of the convolutional neural network on raw data, and ensemble model on feature extracted data. Although the inference time of the ensemble method is lower, it does not include the processing of the feature extraction.

### 3.7. Limitations and Future Direction

Although the results in [Table 3.4](#) show that the sampling time of the sensors could possibly be lowered, sampling time could influence on [MOX](#) gas sensor's performance characteristics, such as response time and sensitivity. Metal-oxide sensors rely on periodic heating of the sensor material, which causes gas adsorption and desorption, as explained in [Chapter 2](#). A lower sampling rate might influence these dynamics, and the effects of switching to a 30-second sampling time should therefore be researched further.

The protocol in [Figure 3.1](#) also has an important flaw. Because the air above the beaker is not closed off, there will never really be a full equilibrium between the ethanol in liquid and in vapor, as described by the [VLE](#) curve of [Figure 2.2b](#). The noise introduced will inevitably influence the results of the regression models.

### 3.8. Conclusion

In this chapter, we looked at the development of a [VOC](#) gas sensor array in air. We first selected 10 different gas sensors and gathered a total of 2510 15-minute time series from these sensors. Then we analyzed the data qualitatively and constructed a [CNN](#) that could predict the ethanol percentage that a sensor array was exposed to. After optimization, we can conclude that using the [BME680](#), [BME688](#), [SGP30](#), and [SGP40](#) with a sampling time of 30 seconds, over a window of 60 seconds is the most optimal configuration when considering the [RMSE](#), [MAE](#), and design constraints laid out in [Section 1.3](#). The [RMSE](#) of this design is 9.77, and its footprint fits on an 18.5 by 3.3 millimeters sensor arm. When sampling only once every 30 seconds, its expected lifetime is approximately 25 days.

The network was successfully deployed and tested on an embedded system. Deploying and continuously running this network on an [nRF52832](#) only takes up 1% of the power consumption, and fits well within the flash memory and [RAM](#) requirements.

Sampling every 5 seconds over a 60-second window, and extracting features from this window to a [RMSE](#) of 7.50%, when training an [RF](#), but does not improve the [MAE](#). Furthermore, it reduces the lifetime to 6.3 days, which is below the design requirements.

Hereby, a fully functional ethanol detection system using off-the-shelf [MOX](#) gas sensors are built, with a footprint small enough to fit on the sensor platform described in [Section 1.1](#). We have shown that we can identify different ethanol-water mixtures from 0 to 100% ethanol, and even distinguish water, wine, Irish cream, and gin with 100% accuracy in air using just the [SGP40](#). Achieving this using edge machine learning, such a small footprint and off-the-shelf electronics already exceeds state-of-the-art research [[99](#), [100](#), [101](#)].

The next step is to transfer these findings to a gas sensor array that works in the [GI](#) tract. This requires an encapsulation that protects the sensors but does not compromise their sensitivity to ethanol. The design and effects on sensor sensitivity of such an encapsulation will be explored in the next chapters.

## 4. Measuring Volatile Organic Compounds in Liquid

In order to effectively sense gaseous biomarkers in the GI tract, the electronics must survive in its harsh environment, which is highly acidic and humid. While resident in the stomach, the ingestible device will be exposed to chemical corrosion, the risk of short-circuits due to the humidity, and chemical collisions with food and the stomach lining. At the same time, the gas sensors must be sufficiently exposed to the environment, to allow the inflow of VOCs.

In the literature review, we have shown a number of research efforts that prove that sensing gaseous molecules in the stomach is possible, yet none have shown any long-term capacity, since without a gastric residence mechanism, these devices pass through the stomach relatively quickly. Furthermore, sensing VOCs is especially difficult, since it is hard to separate from molecules such as H<sub>2</sub>O and HCl, which are damaging to the sensors and electronics.

In this chapter, we explore a number of encapsulation techniques and their effect on the sensor response. This is done by dipping the encapsulated sensors into water-ethanol mixtures at 37 degrees Celsius for periods of 30 minutes and evaluating their response. An initial assessment will be made, whether the gas sensors discussed in Chapter 3 can be deployed in a humid environment and still be functional.

In Section 4.1, we will discuss the possible encapsulation materials that could be used to protect the sensors. Subsequently, we will discuss the setup of the experiments in Section 4.2. This section includes an overview of the production methods of different encapsulation layers, followed by the experimental protocols. The results are discussed in Section 4.3, followed by a discussion and conclusion in Section 4.4 and Section 4.5 respectively.

### 4.1. Encapsulation Materials

As discussed in Chapter 2, there is a variety of materials that potentially could be used to protect electronics from the harsh environment of the GI tract, such as PDMS, PTFE or graphene. In previous experiments, PDMS, PTFE, and PVDF membranes were tested on an SGPC3 MOX gas sensor, in 37 degrees water. In these experiments, the sensor was first coated with fast-curing silicon (Elite® Double 22 [102]), on which a hole was made for the permeable membrane (see Section C.1 for the experimental summary). All coating methods showed a relatively fast response for ethanol (100-200 seconds), but their lifetime was between half and two and a half days. This is why a novel method with a longer lifetime is needed.

Parylene C and polycaprolactone (PCL) are two commonly used materials for encapsulating electronics [103, 104, 105], offering unique properties and benefits. Parylene C, a conformal polymer coating, is highly regarded for its exceptional barrier properties, biocompatibility,

and resistance to chemicals. Its ultra-thin coating provides excellent protection against moisture, acids, and other environmental factors, making it ideal for encapsulating electronics in harsh conditions, and a popular choice in medical device development. On the other hand, PCL, a biodegradable polyester, offers ease of manufacturing due to its low melting point (60 degrees Celsius), thicker layer of mechanical protection, and controlled degradation properties. It could allow for a more robust physical barrier, which is relatively porous to the molecules in the stomach environment. Additionally, the gradual degradation of PCL over time presents an advantageous feature, enabling the controlled detachment of the sensor arms and natural disposal of the pill once its intended purpose has been fulfilled.

## 4.2. Experimental Approach

In this section, the experimental approach of this chapter is laid out. The first subsection will focus on the production methods of the sensors, including their encapsulations in parylene C and PCL. Subsequently, the exact experimental protocol is discussed, including the combinations of encapsulations that were tested.

### 4.2.1. Production Methods

A large number of sensor breakout boards were first carefully soldered using flexible wires. Subsequently, the contact points of the solder were protected with a thin layer of UV-curing epoxy, which is used for extra protection of this vulnerable region. Since there are small spaces where the wires are stripped, and these wires move as you carry the sensor breakout boards, the epoxy can make sure that the ultra-thin layer of parylene C does not easily break in this region.

#### Epoxy (No Coating)

We also tested whether a sensor could survive with no coating at all, given that the rest of the electronics would be protected with epoxy. A highly viscous epoxy from McMaster [106] was applied carefully around the sensor using a needle. Subsequently, the epoxy was cured under a constantly running ventilator, as the gases that are released during the curing, were found to be damaging to the MOX gas sensor. The application process and resulting breakout board can be seen in Figure C.3.

#### Parylene C Conformal Coating

Sensors were loaded into a SCS Labcoter® 2 Parylene Deposition System [107]. An aluminum foil structure was used to expose the breakout board from all directions within the vacuum chamber during the deposition process. This ensured that the parylene C covers all the electrical areas of the breakout board uniformly.

Parylene C dimer was loaded into the SCS Labcoter's furnace, with the assumption that one gram of parylene C dimer would result in 2  $\mu\text{m}$  of deposition, in accordance with previous calibration. In order to achieve a near-perfect vacuum, the deposition chamber can host up to approximately 5 sensors. One deposition run, including cleaning and maintenance of the machine, takes about one full workday.

#### 4. Measuring Volatile Organic Compounds in Liquid

##### Heat-treated PCL

Custom 3D-printed molds were utilized for the encapsulation of the sensors with PCL by use of heat. These molds were based on molds used for the arms of the sensor platform design laid out in Section 1.1, and customized to fit PCB breakout boards of the different sensors.

PCL pellets ( $M_n^1=50,000$ ) were placed into the mold cavity. The mold with the PCL pellets was subsequently placed in an oven set to a temperature of 60 degrees Celsius, which corresponded to the melting point of PCL. During the heating process, the PCL pellets liquefied, eliminating any air gaps within the mold. Subsequently, a PCB containing the sensors was carefully pressed into the molten PCL within the mold cavity, and both sides of the mold were pressed together. Due to the variable sizes of the sensors along the z-axis, the resulting PCL thickness between the mold and the sensor membrane exhibited significant variability (see Table 4.1).

Sensor	Thickness [ $\mu\text{m}$ ]
SGP40	521
BME688	355
CCS811	213

Table 4.1.: The thickness of heat-treated PCL after 3D molding, measured from the top of the sensor's membrane until the surface of the coating.



(a) Without sensor

(b) With sensor

Figure 4.1.: The 3D-printed mold for heat-treated PCL encapsulation.

---

<sup>1</sup>Average molecular weight [gram/mol]

### Dip-coated PCL

The coating process involved dissolving PCL pellets in dichloromethane (DCM). To ensure safety, the process was carried out in a well-ventilated hood with safety equipment. PCL pellets were added to a beaker containing DCM and a magnetic stirrer. The PCL is evenly dissolved in the solvent, forming a homogenous PCL-DCM solution. The sensors were then dipped in the solution where a thin layer of the solution adhered to their surfaces. After leaving the coated sensors to dry, the DCM evaporated and a thin layer of PCL covered the sensor breakout boards. The dip-coated PCL had visibly different properties than the heat-treated PCL. Whereas the heat-treated PCL is white in color, the dip-coated PCL was clearly more transparent (see Figure 4.2).

Experimentally, it was found that using 1 gram of PCL pellets per 100 mL DCM created a conformal layer of 100  $\mu\text{m}$  after two dipping cycles. 10 grams per 100 mL resulted in a more gel-like solution. Two dipping cycles here resulted in a thickness of approximately 300  $\mu\text{m}$ . A more extensive evaluation needs to be done to create a precise protocol.

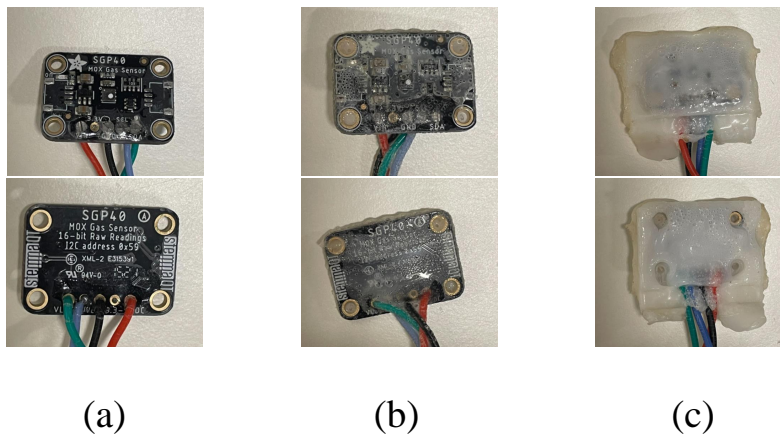


Figure 4.2.: The SGP40 MOX gas sensor with a) parylene C, b) dip-coated PCL and c) heat-molded PCL as outer layer.

#### 4.2.2. Experimental Protocol

It was chosen to test the CCS811, BME688, and SGP40 sensors with different encapsulation methods, as they cover the three different packaging methods that were observed in the 10 sensors (see Figure C.2). The sensors were each coated in 5 different ways:

1. 20  $\mu\text{m}$  Parylene C
2. Heat-treated PCL
3. Dip-coated PCL
4. 20  $\mu\text{m}$  Parylene C + 300  $\mu\text{m}$  Dip-coated PCL
5. 20  $\mu\text{m}$  Parylene C + Heat-treated PCL

#### 4. Measuring Volatile Organic Compounds in Liquid

The epoxy coating is initially only tested for the SGP40 MOX gas sensor since we know that this sensor already has an intrinsic membrane. Pictures of the outer layers of the coated sensors can be seen in Figure 4.2.

A single experiment was set to take 1 hour, where the sensor would hang in the air for 15 minutes. After 15 minutes, the sensors would be submerged into a 6.67% ethanol solution, consisting of 250 mL Water and 50 mL Whiskey (40% vol) at 37 degrees Celsius. The beaker would be covered to minimize ethanol evaporation. The sensors would stay there for 30 minutes and then would be left out for 15 minutes again.

### 4.3. Analysis of Sensor Response

In this section, the experimental results are analyzed in Section 4.3.1. First, a qualitative analysis of the sensor's coating is done. Subsequently, the sensor response of the different gas sensors is assessed in Section 4.3.2. Finally, an explanation of why the sensors capsulated with parylene C and heat-treated PCL were non-functional is given in Section 4.3.3.

#### 4.3.1. Microscopic Analysis

The different encapsulations were studied using a scanning electron microscope (SEM). Since the SGP40 gas sensor has an intrinsic sensor membrane, the layers of each material, including the intrinsic membrane can be seen in Figure 4.3. Larger SEM images, including that of heat-treated PCL can be seen in Figure C.4. In this figure, dip-coated PCL and heat-treated PCL have a totally different structure. The dip-coated PCL has visible pores at a scale of 200  $\mu\text{m}$ , while heat-treated PCL has none, even at a scale of 50  $\mu\text{m}$ .

#### 4.3.2. Sensor Response

##### Parylene Coating and Epoxy (No Coating)

First, it was tested if the SGP40 sensors could survive with no coating over the sensor membrane at all. The experiment according to Section 4.2.2 was repeated three times for a parylene C coated sensor and a sensor without any coating, for a submersion in water and in a 6.67% vol. ethanol solution. Table 4.2 shows the sensor value before the exposure ( $R_0$ ), the steady-state sensor value ( $R_{SS}$ ), and the time to reach 90% of the steady-state value ( $t_{90\%}$ ).

Encapsulation	Water			Ethanol (6.67% vol)		
	$R_0$	$R_{SS}$	$t_{90\%}$ [s]	$R_0$	$R_{SS}$	$t_{90\%}$ [s]
No Coating (Epoxy)	36,169	32,607	14	32,181	18,241	18
20 $\mu\text{m}$ Parylene C	30,733	29,146	199	32,000	27,745	125

Table 4.2.: The sensor response of the SGP40 MOX gas sensor when exposed to water and a 6.67% vol. ethanol solution, for a sensor only protected by the SGP40s inherent sensor membrane, and encapsulated by 20  $\mu\text{m}$  parylene C (see Figure 4.3 for a breakdown of the layers).



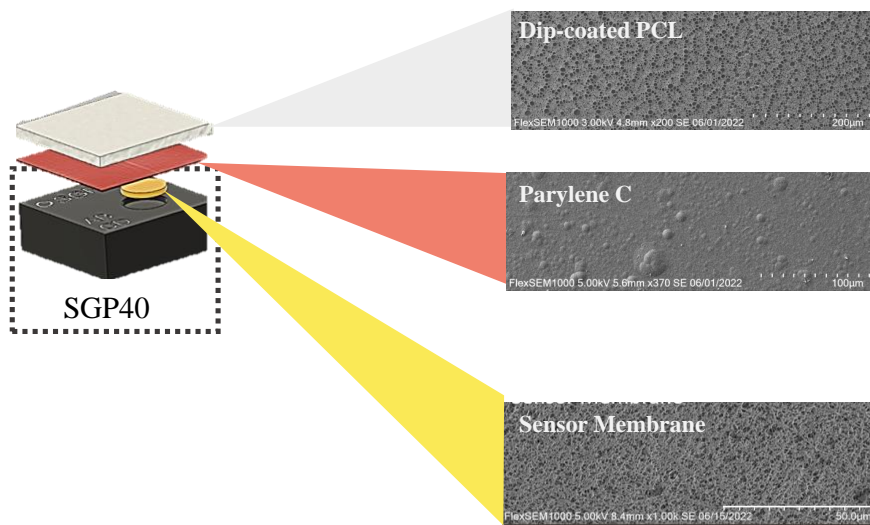


Figure 4.3.: Different layers of the SGP40 sensor, visualized using the FlexSEM1000 scanning electron microscope. A larger close-up, including that of heat-molded PCL can be found in Figure C.4

Interestingly enough, the sensor without encapsulation had no problem surviving in the solution for periods of 30 minutes. In comparison, the parylene C coated sensor stopped communicating halfway through one of the experiments, most likely due to an electrical short-circuit.

One can also observe that the range of the sensor values between 0 and 6.67% vol. is heavily impacted by the sensor coating. It was expected that coatings would impact the transient response of the sensor, as it limits the flow of gaseous molecules towards the gas sensor, and therefore it takes longer for the sensor to reach a steady-state value. A different steady-state value was however somewhat surprising. There could be two possible reasons for this:

1. **Barrier effect:** parylene C creates a significant barrier, which physically impedes the interaction between VOCs and the MOX gas sensor, and thus leads to a difference in the steady-state sensor reading.
2. **Chemical interaction:** the SGP40 has its own proprietary surface membrane. An interaction between parylene C could alter this membrane's affinity to VOCs, hence leading to a different resistance value.

These effects have not earlier been described in scientific literature, so further investigation is necessary. If the barrier effect hypothesis holds true, the parylene C coating should affect other MOX gas sensors in a similar way. Furthermore, a thinner layer of parylene C should result in a higher sensitivity of the sensor. If the chemical interaction hypothesis holds true, the parylene C coating could impact the SGP40 sensor's sensitivity significantly more than that of other sensors.

#### 4. Measuring Volatile Organic Compounds in Liquid

##### Other encapsulation methods

The experiment laid out in Section 4.2.2 was performed for all sensors. The raw experimental data of such an experiment for the SGP40 MOX gas sensor can be seen in Figure 4.4. All figures of these experiments, including ones that compare the same experiment at different repetitions, can be seen in Section C.5.

For all sensors, the sensors solely coated with DCM-PCL instantly broke upon contact with liquid. This means, that such a protective layer is not enough. Furthermore, the heat-PCL coated sensors experienced a low yield rate. The ones that still functioned after the manufacturing process often did not function well. For all three sensors solely encapsulated with heat-treated PCL, the sensors broke did not properly recover (see Figure C.10, Figure C.9b and Figure C.7). A combination of heat-treated PCL and parylene C did not break the sensors electrically, but made them entirely insensitive to ethanol. This was not immediately visible for the SGP40 and BME688, for which a signal response seemed present. An explanation of that is given in Section 4.3.3.

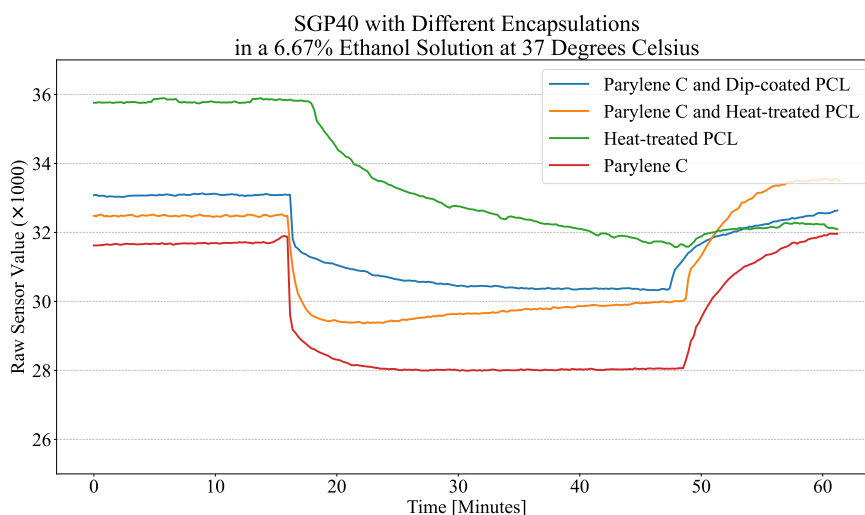


Figure 4.4.: SGP40 with 4 different encapsulations exposed to a mixture of 50 mL Whiskey and 250 mL water (6.67% vol. ethanol) at a temperature of 37 degrees Celsius. The sensors are fully submerged in between the 15 and 45 minute marks.

As one can see from the figures, different coatings do seem to influence the MOX gas sensor response. For the SGP40 and BME688 gas sensors, the response time ( $t_{90\%}$ ) and absolute value before ( $R_0$ ) and after exposure ( $R_{55}$ ) were analyzed. Their results are laid out in Table 4.3. One thing that can be observed is the enormous fluctuation in baseline sensor values. The BME688 coated with parylene C alone and the one with parylene C and dip-coated PCL both dropped to their saturated  $R_{55}$  (5.7), but their  $R_0$  was massively different. We can also observe that for the BME688 and CCS811, the dip-coated PCL does not seem to influence the flux of the ethanol through the protective layers, whereas, for the SGP40, it does.

Encapsulation	BME688			SGP40		
	$R_0$	$R_{SS}$	$t_{90\%}$ [s]	$R_0$	$R_{SS}$	$t_{90\%}$ [s]
20 $\mu$ m Parylene C	31.0	5.7	14.0	32,068	27,745	125.0
Heat-treated PCL	291.0	58.0	291.0	35,797	32,470	465.0
20 $\mu$ m Parylene C and Heat-treated PCL	1163.0	75.1	333.5	32,523	30,124	65.0
20 $\mu$ m Parylene C and Dip-coated PCL	549.4	5.7	7.5	32,902	30,729	369.0

Table 4.3.: The sensor response of the BME688 and SGP40 when being immersed in a 6.67% vol. ethanol solution. The sensor value before ethanol exposure ( $R_0$ ), the steady-state value after exposure ( $R_{SS}$ ), and the time it takes to reach 90% of the steady-state value ( $t_{90\%}$ ). Average taken of 1 to 3 experiments.

### 4.3.3. Temperature Sensitivity: Why the Parylene C with Heat-treated PCL Sensors Did Actually Not Sense VOCs.

After the submersion experiments laid out in Section 4.2.2, the sensors were placed in a long-term experimental environment. In these experiments, it became clear that the SGP40 and BME688 with parylene C with Heat-treated PCL as encapsulation seemed to be solely dependent on the temperature fluctuations of the experiment, with a correlation coefficient of -0.87 and -0.95 respectively. In Figure 4.5, it is clear that the sensor with heat-treated PCL solely responds to the temperature difference, causing an upward peak in the signal. The sensor encapsulated in dip-coated PCL has a significant dip in its response instead. Similar response can be seen for the SGP40 in Figure C.11. In Figure C.12 and Figure C.13, the data points of the entire experiment are plotted against the temperature at that exact point. The red scatter indicates the time when ethanol was present in the experimental setup. It shows clearly how the dip-coated PCL causes outliers, whereas the sensors coated with heat-treated PCL do not respond differently to water and ethanol.

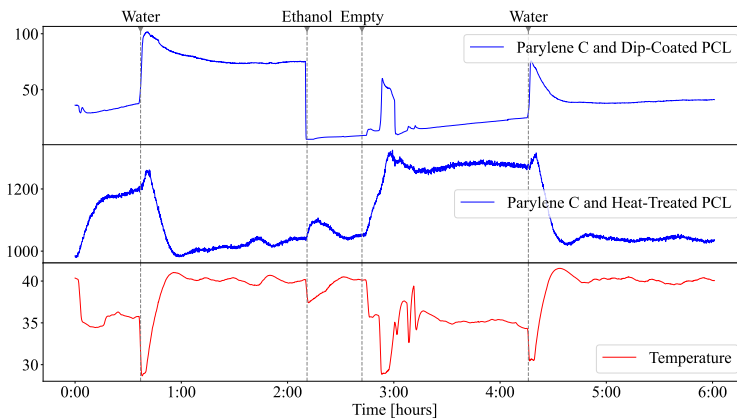


Figure 4.5.: BME688 with 2 different encapsulations exposed to a mixture of 50 mL Whiskey and 250 mL water (6.67% vol. ethanol) between the “Ethanol” and “Empty” mark. As can be seen, the sensor coated with parylene C and dip-coated PCL has a strong and immediate response to ethanol. The sensor coated with parylene C and heat-treated PCL has an exactly opposite response to the temperature.

## 4.4. Limitations and Future Direction

Although some of the results of the experiments were surprising, one cannot draw definite conclusions from them yet. Due to the significant amount of resources it costs to produce these sensors, including the fact that there is not a perfect yield rate in the production methods, it was only possible to do these experiments for one sensor per coating method, and for 1 to 3 repetitions. More experiments would need to be done to get conclusive data.

Furthermore, it is common practice in manufacturing to evaluate each sample after every step in the manufacturing process. That means, that a sensor is extensively tested before a parylene C coating, and subsequently after, before adding an extra layer, such as parylene C on top of the sensor. In that way, it is easier to understand where in the design process certain failures and changes happen. This should be taken into account in further experiments.

One should also take into account that the actual thicknesses of the PCL and parylene C are actually not as certain as is projected in this research. First of all, the 3D-printed mold is produced using a Prusa I3 Mk3 printer, which has a resolution of 50 microns [108]. Errors on both sides of the cavities could easily result in a 100-micron difference in coating thickness. That would not include the fact that the molds are not pressed very tightly during the molding process.

The parylene C thickness should be taken into question because the deposition machine needs maintenance and calibration to maintain its performance, which was not ensured. An attempt was done to assess the real thickness of the parylene C coating, after loading in 10 grams of the dimer, using a light microscope. The results were however inconclusive, as the SEM relies on light, and parylene C is transparent.

## 4.5. Conclusions

In this chapter, we analyzed how the response of three different gas sensors change, based on their encapsulation. These gas sensors were chosen based on their different gas inlet architecture, namely the SGP40's membrane, the BME688's metal casing, and the CCS811's air gap (see Figure C.2).

The results have shown that even without coating and just protection of the electronics, the SGP40 MOX gas sensor can survive in an ethanol-water mixture at 37 degrees Celsius, and remains highly sensitive to ethanol.

Coating the sensors through molding PCL at 60 degrees Celsius turned out to be destructive to all three of the sensors and their sensing mechanisms, regardless of whether a layer of parylene C was deposited first. Furthermore, a PCL encapsulation through dipping the sensor in a PCL-DCM solution seemed to be not sufficient to protect the sensor breakout boards from immediate short-circuits in water.

The sensors encapsulated with either parylene C alone, or parylene C with dip-coated PCL were both still sensitive to the ethanol solution. For the CCS811 and BME688, the sensitivity did not seem to be impacted by the DCM-PCL or parylene C, as their sensing values both saturated upon exposure to the VOC solution. For the SGP40, however, the sensing range was 10 times smaller than that of uncoated sensors. In the next chapter, we will do experiments to see if this decrease is detrimental to its performance.

## 5. Measuring Volatile Organic Compounds in an Artificial Gastric Environment

After showing that [MOX](#) gas sensors can survive and measure [VOCs](#) when dipped into an ethanol-water mixture in [Chapter 4](#), it is vital to show that they will still perform well in long-term experiments, which are more representative of the real use case. Switching immediately to in-vivo experiments is challenging at this stage since a lot of design parameters are not decided on yet. Producing sensors that work in an in-vivo experiment is much more resource intensive, and generating sufficient data to build models as were built in [Chapter 3](#) will be almost impossible in that environment. Furthermore, the large amount of noise will make it hard to trace cause and effect in animal studies.

For the reasons mentioned above, a realistic experimental environment is designed for long-term studies of the encapsulated gas sensors. The design of this environment is discussed in [Section 5.1](#). Then, we will discuss the experiments that were done in this environment in [Section 5.1](#). The chapter closes with a discussion and conclusion in [Section 5.3](#) and [Section 5.4](#).

### 5.1. Experimental Environment

To study the behaviour of gas sensors and their electronics in an experimental environment, it was vital to make a design out of the following principle: the experimental model is supposed to be as simple as possible, but at the same time provide all information that is relevant to a real-life environment. It was, therefore, important to consider the factors that were most likely to influence the gas sensors, and only include these in the experiments.

Relevant literature describes numerous examples of experimental environments that simulate the [GI](#) tract [[109](#), [110](#), [111](#), [112](#), [113](#)]. Generally, these can be divided into two categories: static and dynamic models [[114](#)]. In the context of studying gas sensors in the [GI](#) tract, a dynamic model, which simulates inflow and outflow of fluids is most relevant.

Although the existing models can serve as an inspiration, there are important limitations for the sake of this thesis:

1. The dynamic models mostly aim to understand digestion. It is heavily focused on the chemical components of the simulated gastric fluids, which is not relevant to sensing volatile organic compounds unless these interfere with the signal.
2. The dynamic models use the gastric emptying times relevant to food (more than 2 hours [[115](#)]), whereas fluids have been shown to pass through the stomach much faster (approximately 30 minutes for clear liquids [[116](#)]).

## 5. Measuring Volatile Organic Compounds in an Artificial Gastric Environment

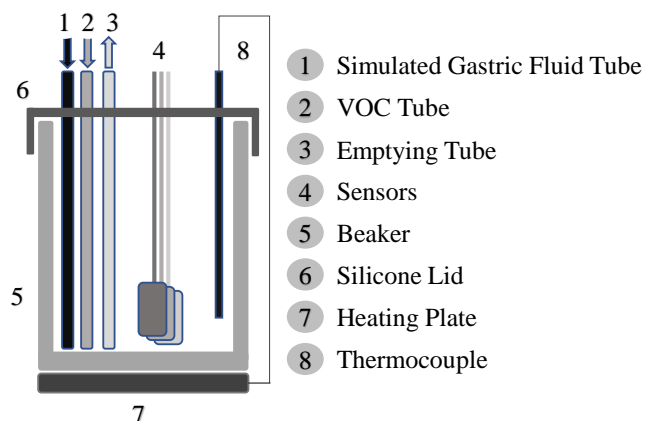


Figure 5.1.: Drawing of the experimental environment.

Looking at the different experimental environments and the possible environmental factors which impact the gas sensors, the following design parameters were proposed.

- Fully autonomous experimentation, minimizing the impact of human-introduced noise.
- Maintenance of 100 percent humidity and body temperature (37 °C).
- Dynamics simulating GI tract characteristics.

The final design of the experimental setup is visualized in Figure 5.1. It consists of a 600-milliliter beaker on a heating plate. The heating plate ensures a 37 degrees Celsius environment throughout the experiment. The beaker is closed with a custom-designed silicone lid, which keeps the environment at a constant humidity, and does not allow for evaporation of the chemicals that enter the environment. How the lid is made is shown in Section D.1. A magnetic stirrer enables quick diffusion of ethanol when pumped into the beaker.

The sensors are lifted into the environment through wires, and the lid has three openings for tubes that control the inflow and outflow of simulated gastric fluid and the VOCs. Since the setup was realized on a bench with a drain directly connected to the sink, it was chosen to use water instead of realistic simulated gastric fluid. It was believed that if a sensor would break or be unable to sense ethanol in such an environment, it would definitely not be capable of these things in an environment with a low pH. Experiments with real simulated gastric fluid could be done once more is known about the sensor's response in water.

### 5.1.1. System Overview

The overall system has a computer as the main station, which is connected to the experimental environment through two separate MCUs. An overview can be seen in Figure 5.2. The first MCU is connected in the same way as in Section 3.1.3, with a sampling time of five seconds. The second MCU is connected to three pumps, which control the inflow and outflow of fluids. The exact protocol and electrical system can also be found in Appendix D. Communication with the MCUs both run as threads in Python 3, while with every sampling time, data is written to a comma-separated values file.

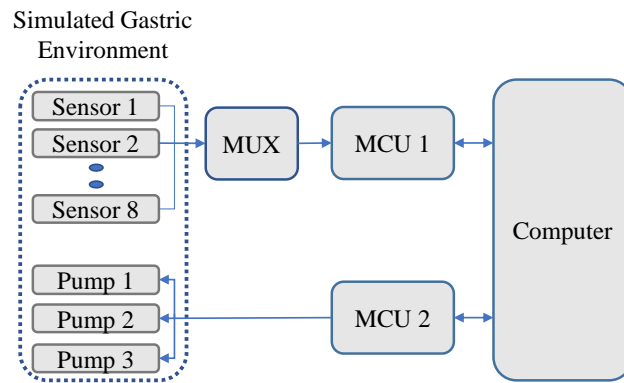


Figure 5.2.: Schematic overview of the system.

### 5.1.2. Sensors

The main environmental parameters that need to be monitored are a measure of **VOC** output, temperature, and humidity. **MOX** gas sensors are highly dependent on temperature and humidity, and their response to temperature fluctuations which change due to the inflow and outflow of fluids should be corrected for.

### 5.1.3. Experimental Protocol

The experimental procedure is outlined in [Figure D.7](#). Initially, the empty beaker would be filled with 250 mL of fresh water, which made sure the gas sensors were fully submerged and stayed in a 100% humid environment at all times. The duration of the experiment was set to 6 hours by default but was an adjustable parameter. After 1.5 hours in water, a specified volume of **VOC** was pumped into the environment and diffused quickly and evenly with the magnetic stirrer. In order to simulate the gastric emptying frequency, the environment was emptied after 30 minutes of exposure, as 30 minutes is the lower limit of the gastric emptying time according to the scientific literature [116].

The emptying process involved a series of in and outflow of water, to fully clean out the gastric environment of any **VOC** that was left. The experimental environment was then left empty for 1 hour before being filled again with 250 mL of water.

### 5.1.4. System Safety and Robustness

Putting electronics in liquids obviously brings risks. This could be seen when the sensors would break: the **MCU** would get stuck requesting data from a broken sensor, and the sampling of all 8 sensors connected to the setup would discontinue. To counter this, a system was put in place where the main station would request the data from a specific sensor, and wait for the microcontroller to respond back. If there would be no response within a certain amount of time, it would reset the entire **MCU**, remember that the sensor is broken

## 5. Measuring Volatile Organic Compounds in an Artificial Gastric Environment

and would not request data from this sensor again, permanently isolating the broken sensor from the system. Later, it would only isolate the broken sensor for 15 minutes, after which another attempt was made to read from the sensor again. The basis of the algorithm for the Python to Arduino communication thread can be found in [Algorithm D.1](#).

Another hazard was the communication discontinuing between the main station and the [MCU](#) controlling the pumps. If this would happen at the moment that water is being pumped into the system, it could happen that the entire beaker would overflow, spilling water over all the electronics. For this reason, safety timers were installed on the [MCU](#), which are visualized in [Figure D.5](#).

### 5.1.5. Experiment Queue

The main station of the experimental setup could be remotely accessed using AnyDesk, and experiments could be added to a queue through the command line. At the end of an experiment, a new experiment would immediately start if there was an experiment in the queue.

## 5.2. Experiments and Results

First, the SGP40 sensor without any coating was tested on its sensitivity, latency, and lifetime. This experiment would serve as a control group for the encapsulated sensors. Subsequently, the SGP40 and BME688 sensors were coated in two different thicknesses parylene C, and tested on their sensitivity, lifetime, and signal latency when continuously performing the same experiment. This experiment was performed to understand at which thickness the SGP40 sensors would survive for more than 7 days, and what effect this thickness would have on the sensor performance. Finally, sensors with parylene C and [PCL](#) were exposed to different volume percentages of ethanol, to see if the proposed encapsulations of [Chapter 4](#) would be able to measure and distinguish ethanol percentages while being constantly submerged. In this way, an initial assessment of their regression capabilities could be done.

### 5.2.1. Epoxy Study

In this experiment, the sensors that had no coating, except for the protection of the electronics by viscous epoxy, were tested in the experimental environment. In accordance with the experimental protocol, the sensors were submerged in 250 mL of water, and exposed to 25, 50, and 75 mL of Whiskey respectively, with a total experiment time of 6 hours per experiment.

#### Results and Discussion

The epoxy-coated sensor was immersed in the gastric environment and performed reliably for 42 hours. The steady-state sensor values after 30 minutes in different percentages of an ethanol solution can be seen in [Table 5.1](#).



It is observable that the SGP40 sensor values already saturate at an ethanol percentage of 7%, hence it would be unable to distinguish between hard liquor and wine on an empty stomach. Furthermore, the uncoated sensors seemed to be greatly affected by drift, with a baseline value reaching 38,000 instead of approximately 29,000 for its parylene C-coated counterparts.

4%	7%	9%
$25,590 \pm 2,206$	$20,080 \pm 1,321$	$20,036 \pm 845$

Table 5.1.: Average sensor value of SGP40 gas sensors without coating (electronics protected with epoxy) after 30 minutes in different volume percentages of a water-ethanol solution.

### 5.2.2. Lifetime and Consistency Study

The second experiment with encapsulation was focused on looking at the lifetime and consistency of the different sensors. The SGP40 and BME688 were coated with parylene C, using 5 and 10 grams of dimer respectively, which ought to correspond with a deposition of 2  $\mu\text{m}$  of parylene C per gram of dimer.

Every 12 hours, 50 mL of Whiskey was pumped into the experimental environment, resulting in a 6.67% vol. ethanol solution. This volume percentage is consistent with the exploratory experiments done in [Chapter 4](#).

For each sensor, the latency ( $t_{90\%}$ ) and steady state value ( $R_{SS}$ ) when exposed to the VOC are analyzed. The time in fluid up until the sensor started malfunctioning was recorded as well. There are generally two types of malfunctions that can happen:

1. **Sensor Malfunction:** The I<sup>2</sup>C communication with the sensor can still be established, but the sensor returns unusual values, or is only responsive to temperature changes.
2. **Electrical Short Circuit:** In this case, the sensor does not respond when the MCU makes a measurement attempt. This usually causes the entire communication to stop, and sometimes even the laptop, which powers the MCU to eject the USB serial port.

The lifetime is defined as the time until the sensor experienced one of the malfunctions above.

## Results and Discussion

The effect of parylene C on the dynamic response can be seen in [Figure 5.3](#). This figure shows the response of the SGP40 and BME688 encapsulated in different thicknesses of parylene C. The vertical lines indicate events within the experimental environment, namely 1) the inflow of 50 mL of whiskey, 2) the cleaning and emptying of the environment, and 3) the inflow of 250 mL of water.

The results show that the sensitivity is significantly impacted by the parylene C coating. The sensitivity was impacted so much, that the y-axis in [Figure 5.3\(c\)](#) needed to be rescaled to see any sensor response at all. For the SGP40 coated with 10  $\mu\text{m}$  of parylene C, the sensor values dropped nearly 10,000, to a value close to that of the sensor without coating. Meanwhile,

## 5. Measuring Volatile Organic Compounds in an Artificial Gastric Environment

the drop for the 20  $\mu\text{m}$ -coated sensors was closer to 1,500. The average sensor drop for the SGP40 with different coatings was 9,422 and 1,739 respectively.

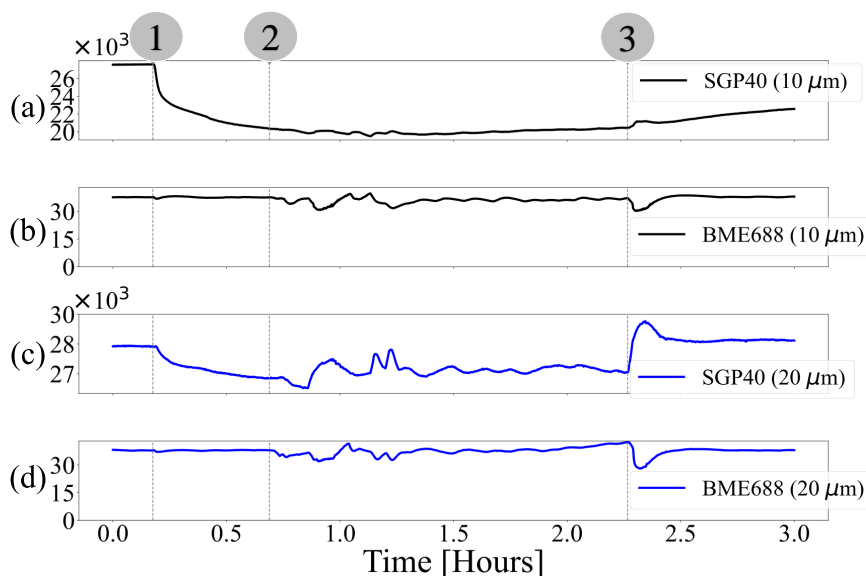


Figure 5.3.: The dynamic response of the sensors over 3 hours when (1) a VOC at room temperature is added to the solution, (2) the gastric environment is emptied and (3) the gastric environment is filled with fresh water at room temperature. (a) and (c) refer to the SGP40 raw sensor value response, while (b) and (d) are the BME688 temperature responses in degrees Celsius.

The effect of coating thickness on lifetime and latency can be seen in Figure 5.4. The average latency is increased by 38.3%, when comparing 10 and 20  $\mu\text{m}$  encapsulations. The  $t_{90\%}$  in the gastric environment is much higher in comparison to the experiments done in Chapter 4, rising from 2 to over 20 minutes on average for the sensors with 20  $\mu\text{m}$  coating thickness. There are two possible reasons for this:

- The pumps only pump at 1 mL per second. Therefore, it already takes 50 seconds to pump in 50 mL of whiskey.
- The response time is impacted by temperature sensitivity. When the temperature goes down due to an influx of fluids, the sensor value goes up. The thermocouple then slowly warms up the gastric environment again. For the experiments in Table 4.2, however, the temperature drop is instant, from room temperature to 37 degrees Celsius. Since the temperature goes up, the sensor response to the temperature is instant and downwards, which will be taken into account when calculating the  $t_{90\%}$ .

The sensor's lifetime was also investigated, using a minimum of 3 sensors per coating thickness. The results can be seen in Figure 5.4. The BME688's lifetime is especially impacted by the coating thickness. For the SGP40, the average lifetime of 2 out of 3 sensors was lower than that of the uncoated SGP40 gas sensor. In order to reach a required lifetime of 7 days, as is required for the design of the sensor array, a parylene thickness of 20  $\mu\text{m}$  is needed. At this thickness, the lifetime is 10.0 and 12.2 days for the SGP40 and BME688 respectively.

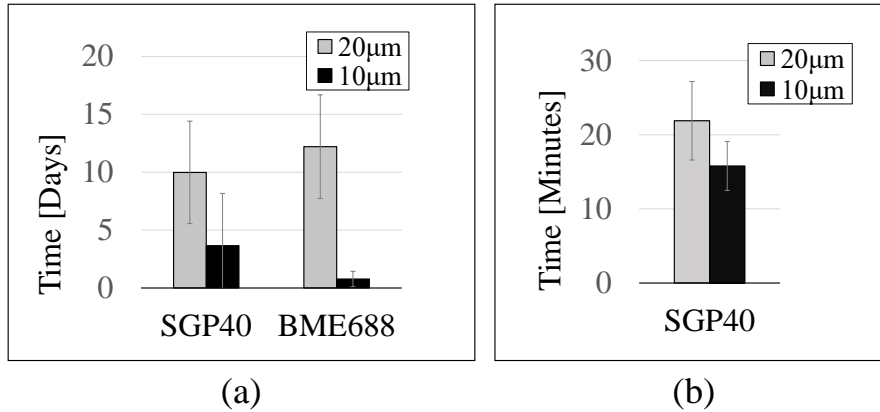


Figure 5.4.: (a) lifetime and (b) latency ( $t_{90\%}$ ) of selected sensors, obtained from at least three sensors for each coating thickness.

### 5.2.3. PCL and Parylene C Study

After the experiments laid out in [Chapter 4](#), the SGP40 and BME688 sensors with PCL and parylene C were analyzed in the experimental environment. The duration of one experiment was set to 6 hours, and the sensors were exposed to 25, 50, 75, and 100 mL of whiskey, and 25, 50, and 75 mL of pure ethanol. This subsection will first discuss the results of the sensors coated with heat-treated PCL. Afterward, we will discuss the results of the sensors encapsulated in dip-coated PCL.

#### Parylene C and Heat-treated PCL

From the experiments, it was found that the gas sensors that were encapsulated with heat-treated PCL had a direct correlation with the temperature deviations in the experimental environment. Most of the analysis regarding this is already discussed in [Section 4.3.3](#) since this was relevant for the interpretation of the experimental results in this chapter.

After 2 days in the experimental environment, the BME688 sensor experienced a short circuit right at the point that 250 mL water was added to the environment. The signal flatlined, meaning that the computer in [Figure 5.2](#) stopped requesting the sensor value after a failed attempt at communication.

A software update one week later introduced a 15-minute waiting period after a short circuit, after which data from that same sensor was requested again. The results were astounding. Upon an influx of 250 mL water or more, which happened 3 times throughout the experiment, the BME688 and SGP40 that were coated with heat-treated PCL would flatline, but when data was requested 15 minutes later, the sensor would be electrically functional again. The other sensors in the same setup would not experience this behavior. An example of this phenomenon can be seen in [Figure D.10](#). A further observation was that, as the short circuit happened, the main station of the system started receiving indecipherable symbols over the COM port. A picture of this phenomenon can be seen in [Figure D.9](#). It is clear from the terminal that the COM port was ejected and reconnected, even though the sensors were powered through an external voltage supply. A possible explanation was that

## 5. Measuring Volatile Organic Compounds in an Artificial Gastric Environment

the large temperature difference created by the influx of water at room temperature causes water molecules behind the encapsulation to condense, creating electrical malfunctions. As temperature rises again to 37 degrees Celsius, the condensation evaporates again.

For other SGP40 sensors, gas readings showed a value of 0 for one sample around moments of malfunction. It is unclear if this was due to invalid data over the COM port or electrical issues caused by the short circuit. Notably, the BME688 sensor encapsulated with dip-coated PCL continued to function without interruptions throughout these experiments.

### Parylene C and Dip-coated PCL

For the sensors with a parylene C and dip-coated PCL layer, the sensor performed reliably for 9 consecutive experiments, which is equal to 2 days and 6 hours. After this, the sensor still communicated over I<sup>2</sup>C for 3.5 days, after which a short circuit interrupted communication.

Analysis showed a serious variation in sensor values before the sensors are exposed to VOC (the  $R_0$ ) and the steady-state value after 30 minutes (the  $R_{SS}$ ). However, when subtracting the  $R_{SS}$  and the  $R_0$ , one can find an almost perfect correlation between the amount of ethanol, and the drop of the sensor. A visualization of this can be seen in Figure 5.5. Interpolating a linear formula, shows a correlation factor of 0.93 with an almost exact intersection with the origin, meaning that the sensor drop would be 0 when exposed to 0% ethanol. The linear relationship could possibly be explained by the fact that the vapor-liquid equilibrium (VLE) can be estimated as a linear curve between 0 and 11% on this scale.

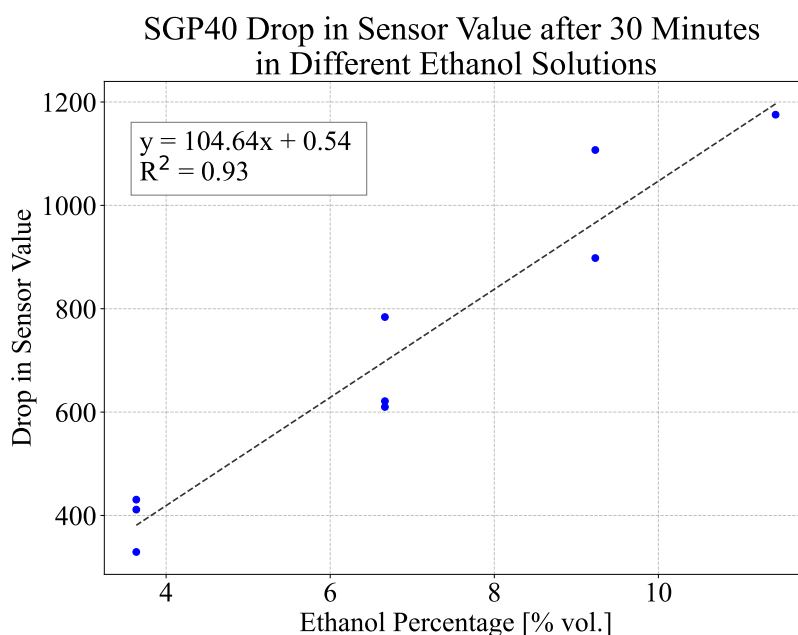


Figure 5.5.: Experimental results of the SGP40 encapsulated with parylene C and dip-coated PCL in the experimental environment. The graph shows the decrease in sensor value after 30 minutes of exposure to VOCs as a function of the percentage of ethanol in % vol. for 9 consecutive experiments. The experiments were not necessarily in increasing or decreasing order with respect to ethanol percentage.

For the BME688 with the same coating, there was a drop in the sensor response for 31 experiments over a duration of 11.5 days. After this, experiments stopped, since this sensor was the only sensor in the setup that was still responsive. When looking at its results, there seems to be no correlation between the amount of ethanol and any of the indicators discussed above. An attempt was made to correlate the difference between the  $R_{55}$  and the  $R_0$  with the ethanol percentage, just as for the SGP40. This however only worked when done for the first 4 experiments, with a correlation coefficient (linear interpolation) of 0.86 (see [Figure D.8](#)). The reason for this is unknown. We know from the first experiment that the sensor is capable of saturating, yet it never reaches this saturation point again after the first experiment. It is difficult to infer why this is the case.

## 5.3. Limitations and Future Directions

The experiments in this chapter were mostly exploratory. To fully understand the dynamics of the sensors in the long-term gastric environment, more data needs to be generated. This can easily be done using the experimental environment, as at the end of the research period, there were three fully functioning environments, each with a capacity of 8 sensors and 4 experiments per day. This would mean that this environment could generate 96 data points per day. Unfortunately, towards the end of the research period, there were problems with the parylene C deposition machine, limiting the number of sensors that could be produced at once, and thus limiting the amount of data that could be gathered. This was especially a bottleneck in the analysis of sensors coated with a combination of parylene C and PCL in [Section 5.2.3](#).

Furthermore, as with the results in [Chapter 4](#), the sensors were produced in a way, where the actual thickness of the parylene C and PCL might differ from what is expected. More measurements should be done to really ensure the exact coating thicknesses and their variation.

Another point of attention is that water was used in the experiments, instead of fluids with a pH that is similar to that in the stomach. This decision was taken such that the experiments could be done entirely autonomously, with an outlet of the fluids into the sink. The amount of acid needed to do these experiments would also be very large with the current setup. It will be important to see if low pH values drastically decrease the lifetime and performance of the sensors.

Lastly, only a small range of ethanol percentages were tested, because of the 250 mL baseline of water, which ensured submersion of all the sensors. In a real environment, there will be only very low amounts of gastric fluids, especially on a fasted stomach. For this reason, if one drinks a spirit like whiskey, the actual ethanol percentage surrounding the sensors will be higher than measured in this experiment (close to 40%). A possible solution would be to use only one sensor in a beaker with a small diameter but a larger height. Adding the same amount of ethanol in this beaker will have a larger effect on the ethanol percentage because the baseline of water is smaller. It will however impact the amount of data that can be gathered at once.

## 5.4. Conclusion

In this chapter, an experimental environment was designed, which replicated relevant conditions of long-term in-vivo studies, such as constant 100% humidity at 37 degrees Celsius. The environment was easily replicable, and could perform multiple experiments a day, with the capacity to read out 8 sensors at once.

The designed environment is subsequently used to test the long-term behavior of different sensors. First, the long-term behavior of an uncoated SGP40 sensor was tested. The sensor showed a lifetime of almost 2 days, in constant 100% humidity at 37 degrees Celsius. The sensor was highly sensitive to ethanol and saturated at a percentage of 7%.

Subsequently, the consistency and lifetime of sensors encapsulated in 10 and 20  $\mu\text{m}$  were tested in the experimental environment, repeating the same experiment where 50 mL of whiskey was added to the environment every 12 hours. It was found that doubling the coating thickness had a significant impact on the sensor lifetime, and a 20  $\mu\text{m}$  coating thickness is needed to reach the minimum requirements laid out in [Section 1.3](#). Doubling the coating thickness comes however with a significant cost. For the SGP40, the signal latency ( $t_{90\%}$ ) was increased by almost 40%, and the sensitivity was decreased from an average sensor value drop of approximately 9,500 to a drop of 1,500 after 30 minutes of exposure.

Finally, the coating variations discussed in [Chapter 4](#) were tested in the experimental environment. We concluded that the sensors coated in heat-treated PCL were not sensitive to ethanol from the start of the experiment. The sensors coated in parylene C and DCM-PCL were sensitive to ethanol and also showed to differentiate within a range of 4 and 12% vol. Experiments with more sensors need to be done to confirm this relationship and see if the sensor value drop keeps increasing as the percentage of ethanol increases.

## 6. Conclusion

This chapter breaks down the core aspects of this research project. It will first summarize the research questions. Then, a description of the methods used to answer these questions, followed by a discussion of the results will be given. In the final sections, the limitations of this research are acknowledged, and future research directions are suggested.

### 6.1. Research Question

Researchers at [MIT](#) and [HMS](#) have developed a sensor platform, which folds out in the stomach, and opens up the opportunity for continuous monitoring of specific biomarkers. Together with a toxicologist at [HMS](#), we identified the use case of alcohol intake monitoring, which could help recovering alcoholics in their treatment. Measuring [VOCs](#) such as ethanol in the stomach is however not a trivial task. The analytes - in this case ethanol - should be able to reach the sensor, while the rest of the electronics are still protected against the harsh environment of the [GI](#) tract. Furthermore, developing a robust sensor array will cost a large number of development cycles and a significant amount of data, which is stagnated by the lack of a realistic and controlled experimental environment.

This resulted in the following research question: *how can we build a sensor array that is capable of continuous [VOC](#) monitoring in the stomach, considering the harsh environment in the [GI](#) tract and the lack of realistic experimental environments?* The question was broken down into two individual tasks:

1. Build the initial iteration of a [VOC](#) monitoring platform, which can be deployed in the stomach.
2. Develop a realistic and controlled gastric experimental environment.

### 6.2. Methods and Results

The research is divided into three separate phases. In the first phase, a sensor array was developed to measure [VOCs](#) in air, taking into account the stringent hardware limitations of the sensor platform. In the second phase, the sensors were encapsulated in different [FDA](#)-approved materials, and exposed to ethanol-water mixtures for short durations. After showing that these sensors could detect ethanol in 100% humidity for short durations of time, a realistic experimental environment for long-term studies was designed in the third phase, and the sensors with different encapsulations were tested on their performance and lifetime.

## 6. Conclusion

### Measuring Volatile Organic Compounds in Air

In the first phase of this research project, a gas sensor array was built, that can detect and classify alcoholic beverages in the air. This was done to prove that it was viable to build this technology on the hardware available for the sensor platform of [Section 1.1](#), and to narrow down the search space of possible sensors, features, and regression models that could be used in further development.

The research found that a combination of 4 [MOX](#) gas sensors - the BME680, BME688, SGP30, and SGP40 - contained the most valuable information when being used to quantify volume percentages in ethanol-water mixtures. It was found that the information came mostly from the combination of different sensor values at one specific point in time, and not from the information in the time series. With a sampling time of 30 seconds over a window of 60 seconds, a [CNN](#) measures ethanol-water mixtures with an [RMSE](#) of 9.77% vol. and [MAE](#) of 6.78% vol. Deploying this model on a microcontroller unit similar to that of the sensor platform yielded an expected lifetime of 25.3 days, with only 1% of the power consumption used for inference. The inference time was 6 ms, and memory footprint was 48.9 KB of flash memory, and 3.3 KB of [RAM](#). Extracting features from the time series data was considered, with regression using a [RF](#). It was found that this reduced the lifetime of the platform to 6.3 days due to a higher sampling rate, required significantly more flash memory, and did not improve the [MAE](#). Furthermore, it would require more processing of the gas sensor data. For this reason, it is not worth switching to feature extraction.

### Measuring Volatile Organic Compounds in Liquid

In the second phase of this research, an attempt was made to make the sensors tested in air work when submersed in an ethanol-water mixture for short durations of time. It was chosen to work with the SGP40, BME688, and CCS811 sensors because these covered all the different packaging variations of the sensors tested in the air. Sensors were encapsulated in combinations of parylene C and [PCL](#), two [FDA](#)-approved polymers that are commonly used for encapsulating electronics. The SGP40 gas sensor was also tested without any encapsulation, having epoxy as protection for its electronics.

Experiments showed that the SGP40 sensor was functional without any coating on its sensor membrane at all. Coating sensors with heat-treated [PCL](#) showed to be harmful to all sensors, while a combination of dip-coated [PCL](#) and parylene C resulted in functional sensors. With this coating, the BME688 and CCS811 reached their maximum sensor values when exposed to a 6.67% vol. ethanol solution. The SGP40, however, showed a reduction in its sensitivity, with a value drop that was 10 times smaller than the SGP40 without any coating.

### Measuring Volatile Organic Compounds in an Artificial Gastric Environment

Finally, a realistic and fully autonomous experimental environment was created to test the long-term performance of the encapsulated gas sensors. The environment allowed to measure 8 sensors in the same environment at once, while simultaneously controlling and logging the state of the experiment. The environment was robust against electrical malfunctions of the sensors, which are caused by the diffusion of water through the encapsulation.



The uncoated SGP40 sensor survived in this environment for 42 hours and showed to saturate at 7% vol. already, making it too sensitive to measure the entire range of ethanol volume percentages that could be present in the GI tract. The SGP40 was tested with a 10 and 20  $\mu\text{m}$  parylene C coating, and it was found that with 20  $\mu\text{m}$  parylene C, the SGP40 survives an average of 10 days in the experimental environment, in comparison to approximately 3.5 days for its 10  $\mu\text{m}$  counterpart. The differences for the BME688 were even more apparent. This comes however with a cost of 40% latency and a sensor value drop that is more than times smaller. Finally, it was found that a combination of parylene C and dip-coated PCL does seem to enable the distinction between different ethanol percentages in a range from beer to wine. More experiments have to be done to confirm this finding.

#### Research Contributions

As a recap of the design requirements in [Section 1.3](#), we can draw the following conclusions.

We built a sensor array that can:

- **Size:** fit on a 18.5 x 3.3 millimeters sensor arm
- **Energy Capacity:** has a hypothetical battery life of more than a week (25 days).
- **Economical:** uses sensors with a combined worth of less than 130 US dollars.
- **Storage:** only uses 48.9 KB of flash memory and 3.3 KB of RAM
- **Sensitivity:** can estimate ethanol percentages between 0 and 100 percent with up to 6.8% vol. accuracy (MAE).

Subsequently, we were able to encapsulate the SGP40 and BME688 gas sensors - which are present in the current design of the gas sensor platform - in a combination of parylene C and dip-coated PCL and showed that:

- **Sensitivity:** the sensors can potentially distinguish ethanol percentages between 0 and 12 % (e.g. beer and wine) in a long-term experimental environment.
- **Lifetime:** the sensors have an average lifetime that is higher than 7 days in an experimental environment at 100% humidity and 37 degrees Celsius.
- **Mechanical:** the sensors show consistent performance while being encapsulated using only FDA-approved materials.

## 6.3. Limitations

Some assumptions have been made during this research project which will be addressed below. The main limitation of this work is that design decisions have been made in air, which are then assumed to be transferable to the optimal decisions in another medium, i.e. liquid. It might be that some of the sensors tested in [Chapter 3](#) are actually more suitable for the alcohol detection task in water, after encapsulation.

## 6. Conclusion

Furthermore, the long-term experimental environment currently exclusively uses water. This is partially because one experiment requires almost a liter of fluids, to clean out the beaker of ethanol residual, and to maintain full submersion of the sensors in fluids at all times. Furthermore, the liquids from the artificial stomach are pumped directly into the sink, which is acceptable when using fluids like whiskey, but not with strong acids. Smaller beakers and neutralization of the acid before disposal could be a future design option.

Finally, the encapsulation methods are currently very time-consuming, and not well-calibrated. This resulted in too little data for the sensors in liquid, and possible variation in results when the experiments are repeated.

## 6.4. Future Work

Overall, future research should aim to pursue the following three directions:

**Data and Regression Model in Liquid.** More data should be gathered on the sensor's response when coated in parylene C and dip-coated PCL, especially with a variation of ethanol percentages. Preferably, these percentages should be in a larger range than what currently has been done, up to at least 40 or even 60% vol. This data should be used to verify the results found in this research and to possibly build a robust regression model as was developed for sensing in air.

**Lifetime Improvement and Robustness in Low pH.** Verification is needed whether the suggested coating method is robust against low pH. A combination of epoxy coating, parylene C and dip-coated PCL should be tested, to see whether the epoxy coating can increase the protection of the electronics in specific, thereby increasing the lifetime of the sensors.

**Embedded System Deployment.** The algorithms proposed should be deployed on the actual pill, and validation of the lifetime and sensitivity while on the embedded system needs to be evaluated.

# A. Introduction

## A.1. Overview Sensor System

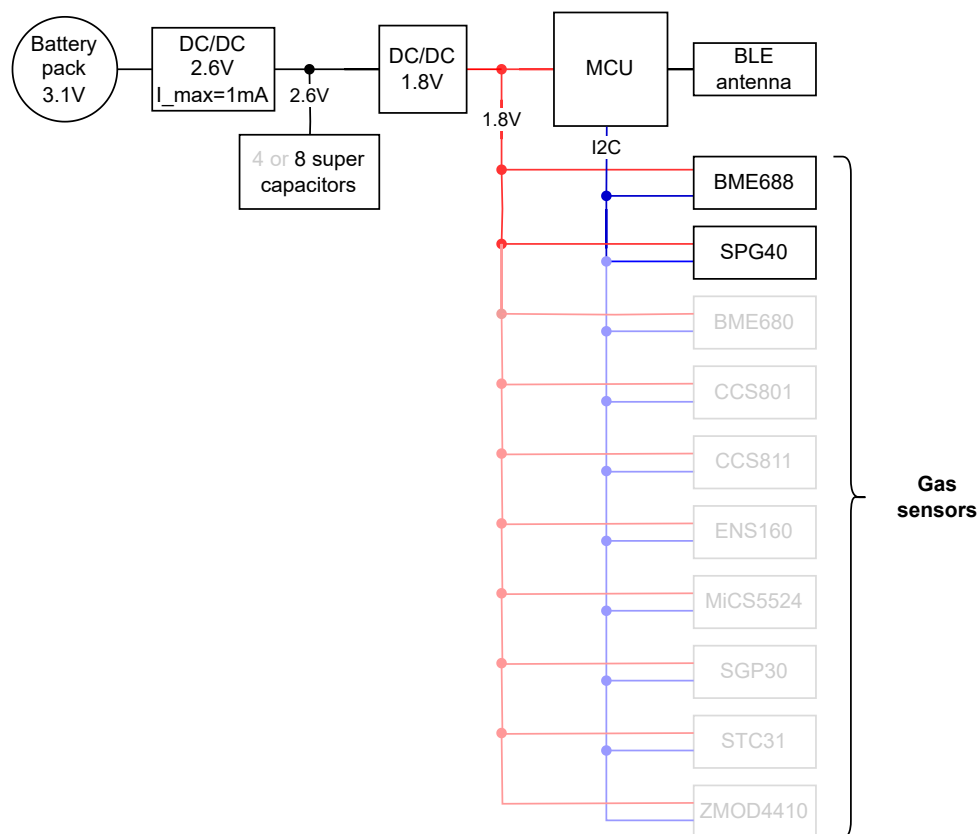


Figure A.1.: Block Schematic of the alcohol sensor system. The gas sensors that are considered in the sensor array in this thesis, but not on the current sensor platform are faded out.

## **B. Measuring Volatile Organic Compounds in Air**

### **B.1. Gas Sensor List**

	Type	parameters							
		digital	gas	temperature	humidity	pressure	area [mm x mm]	power <sup>1</sup> [mW]	price <sup>2</sup> [\$]
<b>BME688</b> [79]	MOX	✓	✓	✓	✓	✓	3.00 x 3.00	10.89	11.48
<b>BME680</b> [34]	MOX	✓	✓	✓	✓	✓	3.00 x 3.00	9.70	10.76
<b>SGP40</b> [35]	MOX	✓	✓	x	x	x	2.40 x 2.40	10.76	8.71
<b>SGP30</b> [80]	MOX	✓	✓	x	x	x	2.45 x 2.45	165.99	10.95
<b>CCS811</b> [36]	MOX	✓	✓	x	x	x	2.70 x 4.00	62.24	12.94
<b>ZMOD4410</b> [81]	MOX	✓	✓	x	x	x	3.00 x 3.00	5.95	5.37
<b>ENS160</b> [82]	MOX	✓	✓	x	x	x	3.00 x 3.00	96.00	12.03
<b>STC31</b> [44]	heat conductivity	✓	✓	✓	x	x	3.00 x 3.50	6.11	61.27
<b>CCS801</b> [83]	MOX	x	✓	x	x	x	2.70 x 4.00	46.20	7.26
<b>MiCS5524</b> [84]	MOX	x	✓	x	x	x	5.00 x 7.00	163.40	10.41

Table B.1.: Details of the gas sensors used in the experiments.

<sup>1</sup> Measured using Nordic Power Profiler Kit II (PPK2) at 1 Hz sampling rate, no sleep mode. See Appendix A for measurement setup.<sup>2</sup> Unit price at Mouser or DigiKey.

## B.2. Data Streams Per Sensor

Sensors	Data Streams
BME680	Gas, Pressure, Temperature, Humidity
BME688	Gas, Pressure, Temperature, Humidity
SGP30	Ethanol, H2
SGP40	Raw, Temperature Corrected
CCS811	eCO2, TVOC
CCS801	Raw
MiCS5524	Raw
STC31	CO2
ZMOD4410	rnox0-12 ,iaq, ethanol, TVOC

Table B.2.: Sensors and Data Streams available for Regression

## B.3. Features from Time Series

### B.3.1. 15 Minute Experiment

#### Steady-state Features

##### 1. Sensitivity

$$S = \frac{R_0 - R_{\text{gas}}}{R_0} \quad (\text{B.1})$$

where:

- The sensitivity  $S$  quantifies the magnitude of the sensor's response relative to its baseline value
- $R_0$  is the baseline value of the sensor in the absence of gas.
- $R_{\text{gas}}$  is the value of the sensor when exposed to a specific gas.

##### 2. Average Sensor Value

$$\bar{R}_{\text{gas}} = \frac{1}{N} \sum_{i=1}^N R_{\text{gas},i} \quad (\text{B.2})$$

where:

- $\bar{R}_{\text{gas}}$  represents the steady-state value of the sensor's resistance when exposed to gas.
- $N$  denotes the total number of measurements or samples taken over time.
- $R_{\text{gas},i}$  represents the  $i$ th measurement or sample of the sensor's resistance when exposed to gas.

## Transient Features

### 1. Time to Reach 90% of Final Value

$$t_{90\%} = t_0 + 0.9 \times (t_n - t_0) \quad (\text{B.3})$$

where:

- $t_{90\%}$  represents the time at which the gas sensor reaches 90% of its final value.
- $t_0$  represents the gas sensor value before exposure to the VOC.
- $t_n$  represents the final time when exposed to the VOC.

### 2. 90% Recovery Time

$$t_{90\%\text{recovery}} = t_0 + 0.9 \times (t_{\text{baseline}} - t_0) \quad (\text{B.4})$$

where:

- $t_{90\%\text{ recovery}}$  represents the 90% recovery time of the gas sensor after exposure to a VOC.
- $t_0$  denotes the time at which the sensor stops being exposed to the VOC
- $t_{\text{baseline}}$  denotes the time at which the sensor returns to its baseline reading in the air.

## B.3.2. Window-based features

### 1. Statistical Features

#### 1.1 Mean

$$\text{Mean} = \frac{1}{N} \sum_{i=1}^N x_i \quad (\text{B.5})$$

where:

- $N$  is the total number of observations in the time window.
- $x_i$  represents the value of the  $i$ -th observation in the time window.

#### 1.2 Median

$$\text{Median} = \begin{cases} x_{\frac{N}{2}} & \text{if } N \text{ is odd,} \\ \frac{1}{2}(x_{\frac{N}{2}} + x_{\frac{N}{2}+1}) & \text{if } N \text{ is even,} \end{cases} \quad (\text{B.6})$$

where:

- $N$  is the total number of observations in the time window.

## B. Measuring Volatile Organic Compounds in Air

- $x_{\frac{N}{2}}$  represents the value of the middle observation when  $N$  is odd.
- $x_{\frac{N}{2}}$  and  $x_{\frac{N}{2}+1}$  represent the values of the two middle observations when  $N$  is even.

### 1.3 Variance

$$\text{Variance} = \frac{1}{N-1} \sum_{i=1}^N (x_i - \bar{x})^2 \quad (\text{B.7})$$

where:

- $N$  is the total number of observations in the time window.
- $x_i$  represents the value of the  $i$ -th observation in the time window.
- $\bar{x}$  is the mean (average) of the observations in the time window.

### 1.4 Delta

$$\text{Delta} = x_N - x_1 \quad (\text{B.8})$$

where:

- $x_N$  is the value of the last observation in the time window.
- $x_1$  is the value of the first observation in the time window.

### 1.5 Kurtosis

$$\text{Kurtosis} = \frac{\frac{1}{N} \sum_{i=1}^N (x_i - \bar{x})^4}{\left( \frac{1}{N} \sum_{i=1}^N (x_i - \bar{x})^2 \right)^2} \quad (\text{B.9})$$

where:

- $N$  is the total number of samples or observations in the time window.
- $x_i$  is the value of the  $i$ -th sample.
- $\bar{x}$  is the mean of the samples.

### 1.6 Skewness

$$\text{Skewness} = \frac{\frac{1}{N} \sum_{i=1}^N (x_i - \bar{x})^3}{\left( \frac{1}{N} \sum_{i=1}^N (x_i - \bar{x})^2 \right)^{\frac{3}{2}}} \quad (\text{B.10})$$

where:



- $N$  is the total number of observations in the time window.
- $x_i$  represents the value of the  $i$ -th observation in the time window.
- $\bar{x}$  is the mean of the observations in the time window.

## 2. Spectral Features

### 2.1 Average Power Spectral Density

$$\text{PSD}(f) = \frac{1}{N} |\text{FFT}(x)|^2 \quad (\text{B.11})$$

where:

- $\text{PSD}(f)$  represents the Power Spectral Density at frequency  $f$ .
- $N$  is the total number of samples in the time window.
- $\text{FFT}(x)$  denotes the Fast Fourier Transform of the time window  $x$ , which provides the complex-valued spectrum.
- $|\text{FFT}(x)|^2$  calculates the magnitude squared of each spectral component, representing the power spectrum.

The PSD was divided into three different frequency bands given the sampling frequency. For each frequency band, the average PSD was used as a feature.

### 2.2 Spectral Centroid

$$\text{Centroid} = \frac{\sum_{k=1}^N f(k) \cdot P(k)}{\sum_{k=1}^N P(k)} \quad (\text{B.12})$$

where:

- Centroid represents the spectral centroid value.
- $N$  is the total number of frequency bins or spectral components.
- $f(k)$  is the frequency value associated with the  $k$ -th frequency bin.
- $P(k)$  is the power or magnitude of the  $k$ -th frequency bin.

### 2.3 Spectral Flatness

$$\text{Flatness} = \frac{\exp\left(\frac{1}{N} \sum_{k=1}^N \ln(P(k))\right)}{\frac{1}{N} \sum_{k=1}^N P(k)} \quad (\text{B.13})$$

where:

## B. Measuring Volatile Organic Compounds in Air

- Flatness represents the spectral flatness value.
- $N$  is the total number of frequency bins or spectral components.
- $P(k)$  is the power or magnitude of the  $k$ -th frequency bin.

### 3. Peak Based Features

#### 3.1 Peak Amplitude

$$\text{Peak Amplitude} = \max(|x_1|, |x_2|, \dots, |x_N|) \quad (\text{B.14})$$

where:

- Peak Amplitude represents the maximum absolute value within the time window.
- $x_1, x_2, \dots, x_N$  are the samples within the time window.
- $N$  is the total number of samples in the time window.

3.2 *Peak Width* The peak width is derived from the peak found by calculating the peak amplitude.

$$\text{Peak Width} = t_{\text{end}} - t_{\text{start}} \quad (\text{B.15})$$

where:

- Peak Width represents the duration or width of the peak within the time window.
- $t_{\text{start}}$  is the starting time of the peak (0.5 times the amplitude).
- $t_{\text{end}}$  is the ending time of the peak (0.5 times the amplitude).

## 4. Time Domain Features

### 4.1 Hurst Component

$$H = \lim_{n \rightarrow \infty} E \left[ \frac{R(n)}{S(n)} \right] = \lim_{n \rightarrow \infty} \frac{1}{n} \log_2 \left( \frac{S(n)}{S(1)} \right) \quad (\text{B.16})$$

where:

- $R(n)$  is the range (maximum minus minimum) of the cumulative sum of deviations from the mean over  $n$  observations.
- $S(n)$  is the standard deviation of the cumulative sum of deviations from the mean over  $n$  observations.
- $S(1)$  is the standard deviation of the time series.

The Hurst component is a value between 0 and 1, where

- $H=0.5$  indicates no correlation between current observations and future observations
- $H>0.5$  indicates that in the short term, the values within the window are following their existent trend.
- $H<0.5$  indicates that in the short term, the values will go against their existing trends.

### 4.2 Time Lagged Mutual Information

$$I(X_{t_i}; Y_{t_j}) = \sum_{x_{t_i} \in X, y_{t_j} \in Y} p(x_{t_i}, y_{t_j}) \log \left( \frac{p(x_{t_i}, y_{t_j})}{p(x_{t_i}) \cdot p(y_{t_j})} \right) \quad (\text{B.17})$$

where:

- $I(X_{t_i}; Y_{t_j})$  represents the time lagged mutual information between variable  $X$  at time  $t_i$  and variable  $Y$  at time  $t_j$  within the time window.
- $X_{t_i}$  denotes the value of variable  $X$  at time  $t_i$  within the window.
- $Y_{t_j}$  denotes the value of variable  $Y$  at time  $t_j$  within the window.
- $p(x_{t_i}, y_{t_j})$  is the joint probability mass function (PMF) of  $X$  and  $Y$  within the time window, representing the probability of observing the pair  $(X_{t_i} = x_{t_i}, Y_{t_j} = y_{t_j})$ .
- $p(x_{t_i})$  and  $p(y_{t_j})$  are the marginal PMFs of  $X$  and  $Y$  within the time window, respectively, representing the probabilities of observing  $X_{t_i} = x_{t_i}$  and  $Y_{t_j} = y_{t_j}$ .

## B. Measuring Volatile Organic Compounds in Air

From the resulting time series, the mean, maximum, and variance are extracted.

### 4.3 Autocorrelation

$$\rho_k = \frac{\sum_{i=k+1}^N (x_i - \bar{x})(x_{i-k} - \bar{x})}{\sum_{i=1}^N (x_i - \bar{x})^2} \quad (\text{B.18})$$

where:

- $\rho_k$  represents the autocorrelation coefficient at lag  $k$ .
- $N$  is the total number of observations in the time window.
- $x_i$  represents the value of the time series at index  $i$  within the window.
- $\bar{x}$  is the mean of the time series values within the window.

From the resulting time series, the mean, maximum, and variance are extracted.

## 5. Wavelet Features

### 5.1 Wavelet Entropy

$$H = - \sum_{i=1}^n p_i \log_2(p_i) \quad (\text{B.19})$$

where:

- $H$  represents the wavelet entropy.
- $p_i$  is the normalized probability of the  $i$ -th wavelet coefficient.
- $n$  is the total number of wavelet coefficients.

## B.4. Dummy Classifiers

### 1. Median Regressor

$$\hat{y} = \text{median}(\{y_1, y_2, \dots, y_k\}) \quad (\text{B.20})$$

where:

- $\{y_1, y_2, \dots, y_k\}$  are the labels of the training set, with  $\hat{y}$  representing the median of this set.

## 2. Most Frequent Class Classifier

$$\hat{y} = \operatorname{argmax}_{y_i \in \{y_1, y_2, \dots, y_k\}} \left( \sum_{i=1}^k \mathbb{I}(y_i = y) \right) \quad (\text{B.21})$$

- $\{y_1, y_2, \dots, y_k\}$  are the set of labels in the training set.
- The indicator function  $\mathbb{I}(y_i = y)$  is equal to 1 if  $y_i$  is equal to  $y$ , and 0 otherwise.
- $\hat{y}$  represents the value of  $y$  that maximizes the expression.

**B.4.1. Performance Metrics**

## 1. Root Mean Square Error (RMSE)

$$\text{RMSE} = \sqrt{\frac{1}{N} \sum_{i=1}^N (y_i - \hat{y}_i)^2} \quad (\text{B.22})$$

where:

- $N$  is the total number of samples or observations.
- $y_i$  is the true value of the target variable for the  $i$ -th sample.
- $\hat{y}_i$  is the predicted or estimated value of the target variable for the  $i$ -th sample.

## 2. Mean Absolute Error (MAE)

$$\text{MAE} = \frac{1}{N} \sum_{i=1}^N |y_i - \hat{y}_i| \quad (\text{B.23})$$

- $N$  is the total number of samples or observations.
- $y_i$  is the true value of the target variable for the  $i$ -th sample.
- $\hat{y}_i$  is the predicted or estimated value of the target variable for the  $i$ -th sample.

## B.5. Convolutional Neural Network Architectures

Table B.3.: CNN Model A Architecture

Layer	Hyperparameter	Value
Conv1D	Filters	32
	Kernel Size	2
	Activation	ReLu
MaxPooling1D	Pool Size	2
Dropout	Rate	0.1
Conv1D	Filters	64
	Kernel Size	2
	Activation	ReLu
MaxPooling1D	Pool Size	2
Conv1D	Filters	64
	Kernel Size	2
	Activation	ReLu
Flatten	-	-
Dense	Units	64
Dense	Units	1

**Total # Params**<sup>1</sup> 17,473

<sup>1</sup> For the best performing model (60 second window size, 5 second sampling time)

Table B.4.: CNN Model B Architecture

Layer	Hyperparameter	Value
Conv1D	Filters	32
	Kernel Size	1
	Activation	ReLu
Conv1D	Filters	128
	Kernel Size	1
	Activation	ReLu
MaxPooling1D	Pool Size	2
Dropout	Rate	0.1
Conv1D	Filters	64
	Kernel Size	1
	Activation	ReLu
Flatten	-	-
Dense	Units	64
Dense	Units	1

**Total # Params**<sup>1</sup> 18,145

<sup>1</sup> For the best-performing model (60-second window size, 30-second sampling time)

Hyperparameter	Setting
Number of Epochs	600
Learning Rate	0.0005
$\beta_1$	0.9
$\beta_2$	0.999
Batch Size	128
Optimizer	Adam
Loss Function	Mean Squared Error
Early Stopping	Patience = 10, Restore Best Weights = True

Table B.5.: Manually optimized hyperparameters used for training the convolutional neural network.

## **B.6. Edge Implementation**

### **B.6.1. Energy Consumption Calculations**

B. Measuring Volatile Organic Compounds in Air

#	Component	Description	$P_{ON}$	$P_{SLEEP}$	Time On [per 30s]	$P_{Average}$
6	Renata 376	Battery	N/A	N/A	30	N/A
6	CPX3225A752D	Super Capacitor	156 nW	156 nW	30	156 nW
1	nRF52832	Microcontroller	7.83 mW	2.70 $\mu$ W	0.11	29.8 $\mu$ W
1	TPS63900DSKR	Buck-boost converter 2.6V	233 nW	233 nW	30	233 nW
1	TPS62840YBGR	Buck-boost converter 1.8V	156 nW	156 nW	30	233 nW
1	BME680 <sup>1</sup>	Gas sensor	21.6 mW	270 nW	0.109	78.6 $\mu$ W
1	BME688 <sup>1</sup>	Gas sensor	21.6 mW	270 nW	0.109	78.6 $\mu$ W
1	SGP30	Gas sensor	86.4 mW	3.6 $\mu$ W	0.052	153 $\mu$ W
1	SGP40	Gas sensor	6.3 mW	61.2 $\mu$ W	0.052	72.0 $\mu$ W
<b>Total:</b>						413 $\mu$ W
<b>Lifetime [Days]:</b>						25.3

Table B.6.: Estimated Power Consumption and Lifetime of the Sensor Platform with a Sampling Time of 30 seconds  
<sup>1</sup> These sensors also measure temperature, humidity and pressure.



#	Component	Description	$P_{ON}$	$P_{SLEEP}$	Time On [per 5s]	$P_{Average}$
6	Renata 376	Battery	N/A	N/A	30	N/A
6	CPX3225A752D	Super Capacitor	156 nW	156 nW	30	156 nW
1	nRF52832	Microcontroller	7.83 mW	2.70 $\mu$ W	0.11	165 $\mu$ W
1	TPS63900DSKR	Buck-boost converter 2.6V	233 nW	233 nW	30	233 nW
1	TPS62840YBGR	Buck-boost converter 1.8V	156 nW	156 nW	30	233 nW
1	BME688 <sup>1</sup>	Gas sensor	21.6 mW	270 nW	0.109	126 $\mu$ W
1	SGP30	Gas sensor	86.4 mW	3.6 $\mu$ W	0.052	902 $\mu$ W
1	SGP40	Gas sensor	6.3 mW	61.2 $\mu$ W	0.052	126 $\mu$ W
<b>Total:</b>						1.66 mW
<b>Lifetime [Days]:</b>						6.28

Table B.7.: Estimated Power Consumption and Lifetime of the Sensor Platform with a Sampling Time of 5 seconds

<sup>1</sup> These sensors also measure temperature, humidity, and pressure.

B.6.2. Microcontroller Units

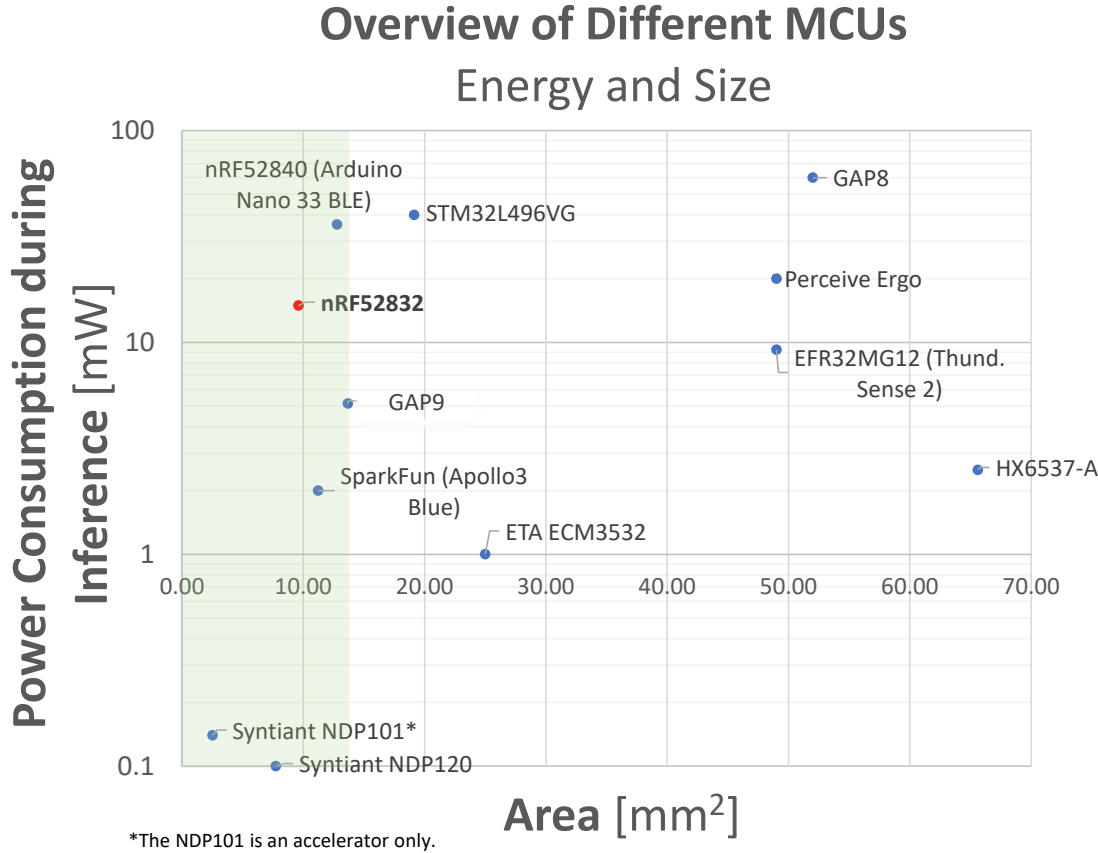


Figure B.1.: Power consumption and area of different microcontroller units. The green area represents the area footprint that fits on the sensor arm. The nRF52832 is the processor that is currently on the sensor platform.

## C. Measuring Volatile Organic Compounds in Liquid

### C.1. Previous Work

In his previous work, Zhaoyu Gong encapsulated an SGPC3 sensor with [PVDF](#), [PTFE](#), and [PDMS](#) respectively. The process of doing so can be seen in [Figure C.1](#). The sensors were subsequently submersed in 200 mL water, after which 20 mL of vodka (40% vol. ethanol) was added. The sensor was left in this solution until communication stopped, with no capability of restarting it. The lifetime of each coated sensor can be seen in [Table C.1](#).

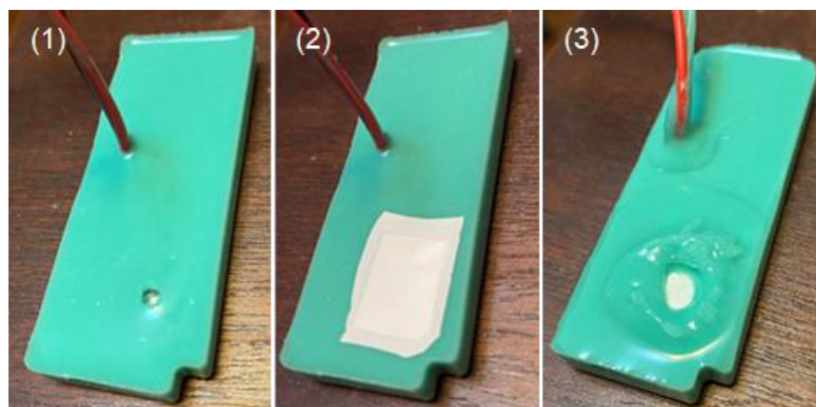


Figure C.1.: The encapsulation process using fast curing silicon around the electronics and [PVDF](#), [PTFE](#), and [PDMS](#) around the sensor membrane.

	<a href="#">PVDF</a>	<a href="#">PTFE</a>	<a href="#">PDMS</a>
Lifetime [Days]	2.76	1.77	0.54

Table C.1.: The lifetime of different [MOX](#) gas sensor encapsulations, given the process visualized in [Figure C.1](#).

## C.2. Sensor Packaging



(a) SGP40



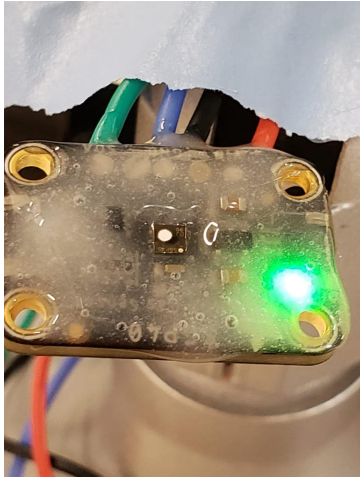
(b) BME688



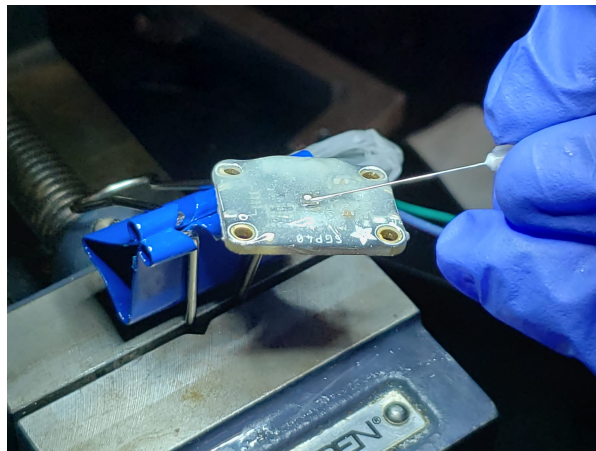
(c) CCS811

Figure C.2.: The packaging of the three sensors that were extensively tested in liquid. **a)** plastic packaging with large permeable membrane (SGP40, SGP30, STC31), **b)** metal casing with pinhole (BME688, BME680, ENS160, MiCS5524, ZMOD4410) and **c)** plastic packaging with large air inlets (CCS811, CCS801).

### C.3. Epoxy Protection



(a) Application process of epoxy



(b) The sensor breakout board after the epoxy is cured

Figure C.3.: Visualization of the SGP40 sensor breakout board **a)** during the application of epoxy, and **b)** the result after curing.

#### C.4. Microscope Analysis

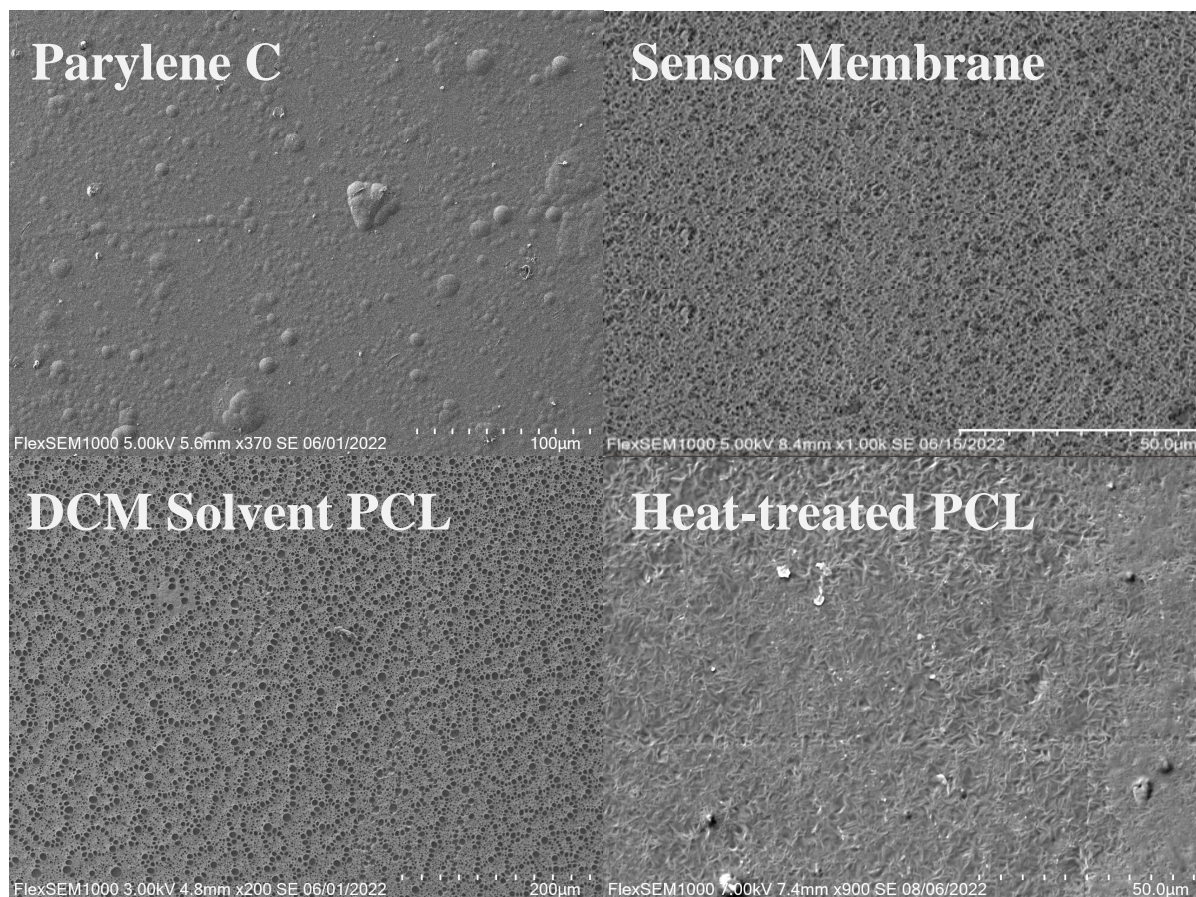
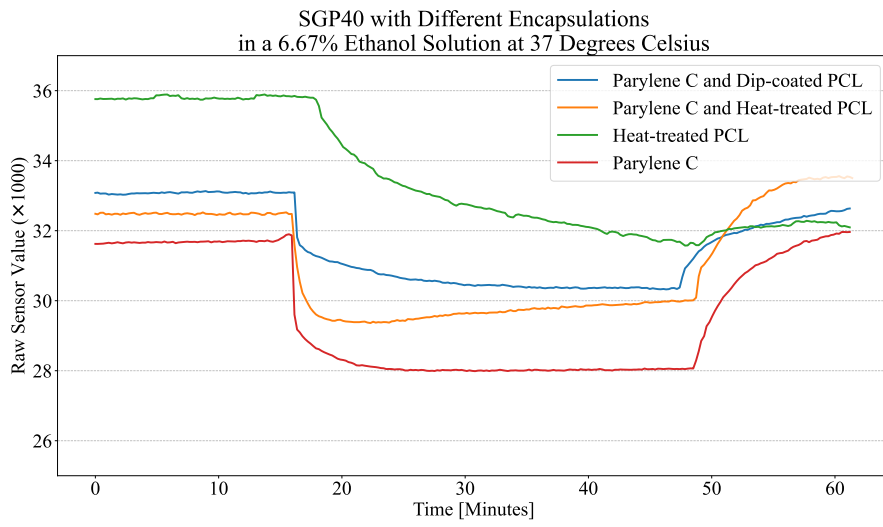
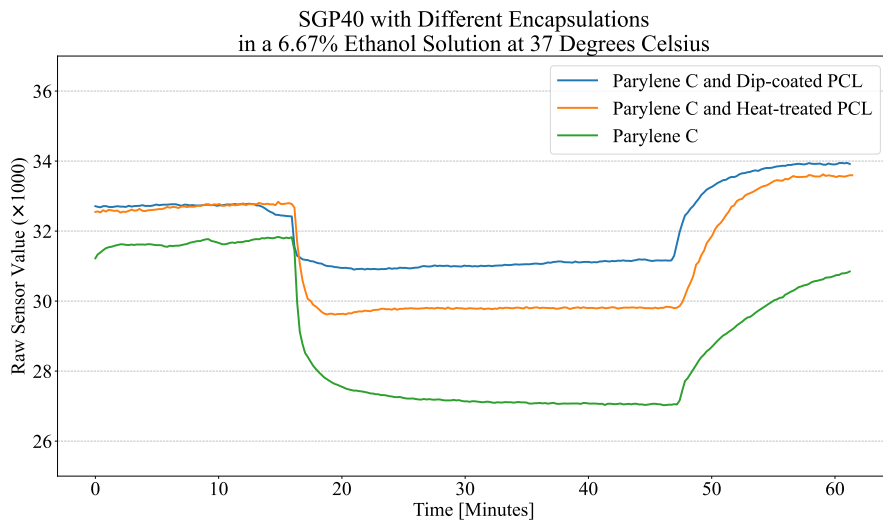


Figure C.4.: Visualization of the different encapsulation layers, including the intrinsic sensor membrane of the SGP40.

## C.5. Experimental Results



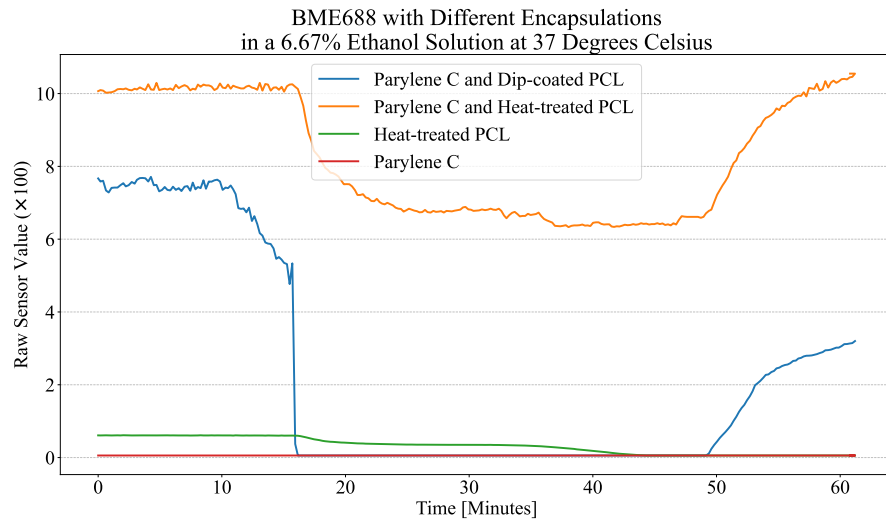
(a) Repetition 1



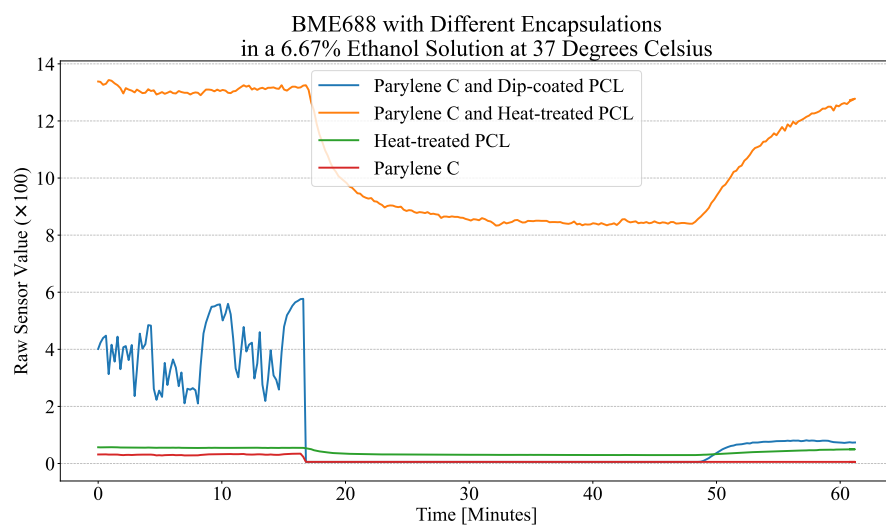
(b) Repetition 2

Figure C.5.: SGP40 with 4 different encapsulations submerged in a 6.67% vol. ethanol solution at 37 degrees Celsius for 30 minutes.

C. Measuring Volatile Organic Compounds in Liquid



(a) Repetition 1



(b) Repetition 2

Figure C.6.: BME688 with 4 different encapsulations submerged in a 6.67% vol. ethanol solution at 37 degrees Celsius for 30 minutes.



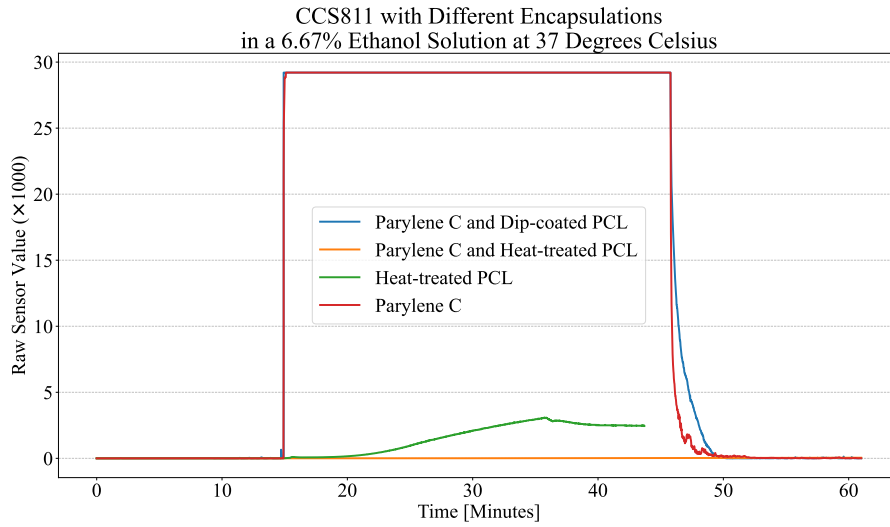


Figure C.7.: CCS811 with 4 different encapsulations submerged in a 6.67% vol. ethanol solution at 37 degrees Celsius for 30 minutes.

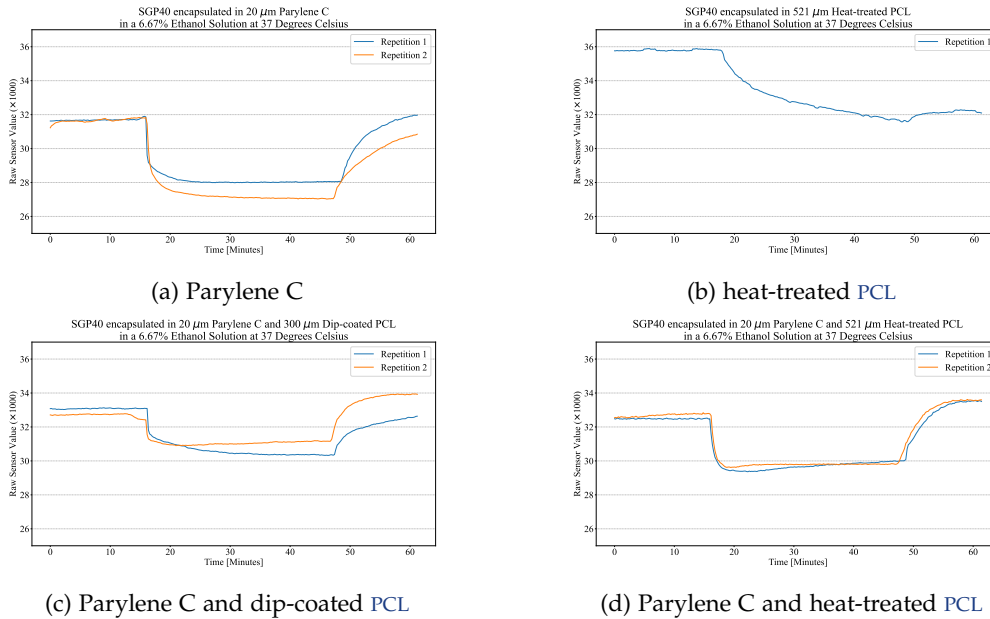
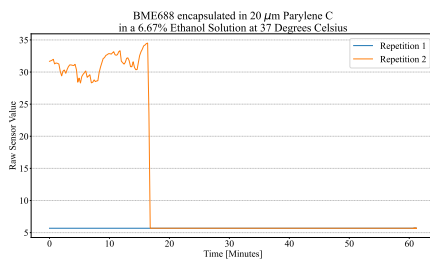
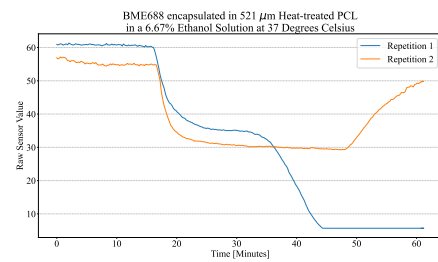


Figure C.8.: SGP40 with 4 different encapsulations submerged in a 6.67% vol. ethanol solution at 37 degrees Celsius for 30 minutes: a comparison of repetitions.

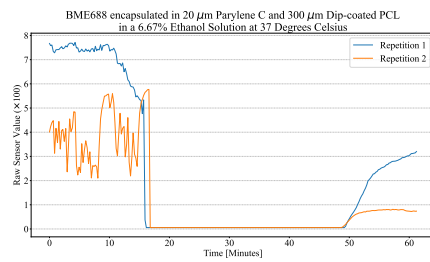
### C. Measuring Volatile Organic Compounds in Liquid



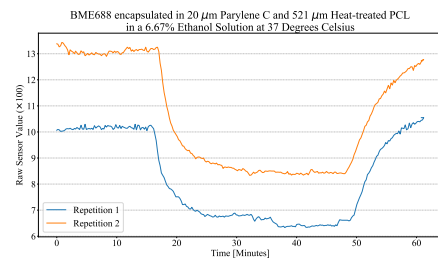
(a) Parylene C



(b) heat-treated PCL



(c) Parylene C and dip-coated PCL



(d) Parylene C and heat-treated PCL

Figure C.9.: BME688 with 4 different encapsulations submerged in a 6.67% vol. ethanol solution at 37 degrees Celsius for 30 minutes: a comparison of repetitions.

## C.5.1. Failed Experiments

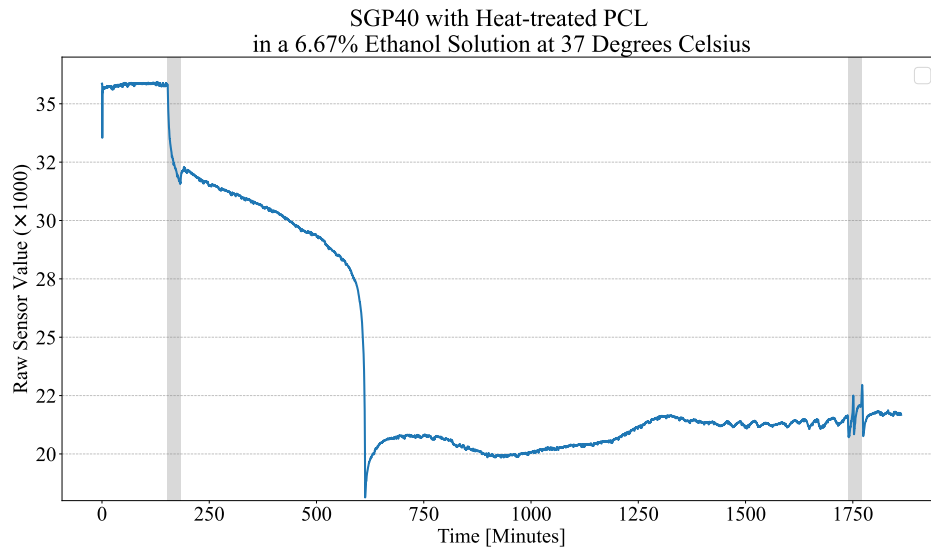


Figure C.10.: SGP40 encapsulated with heat-treated PCL submerged in a 6.67% vol. ethanol solution at 37 degrees Celsius for 30 minutes (see gray areas) over a period of more than 24 hours.

### C.5.2. Temperature Correlation Plots

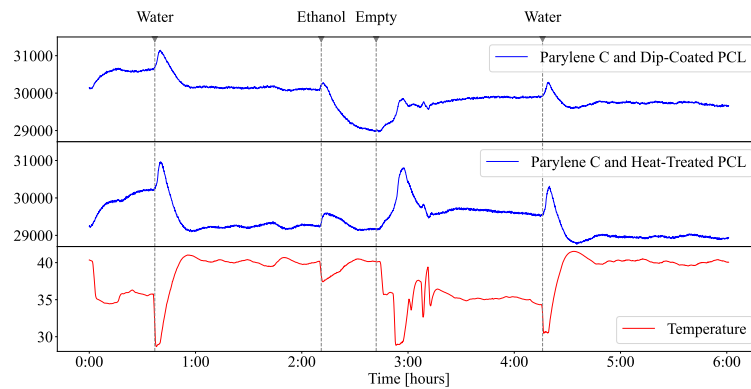
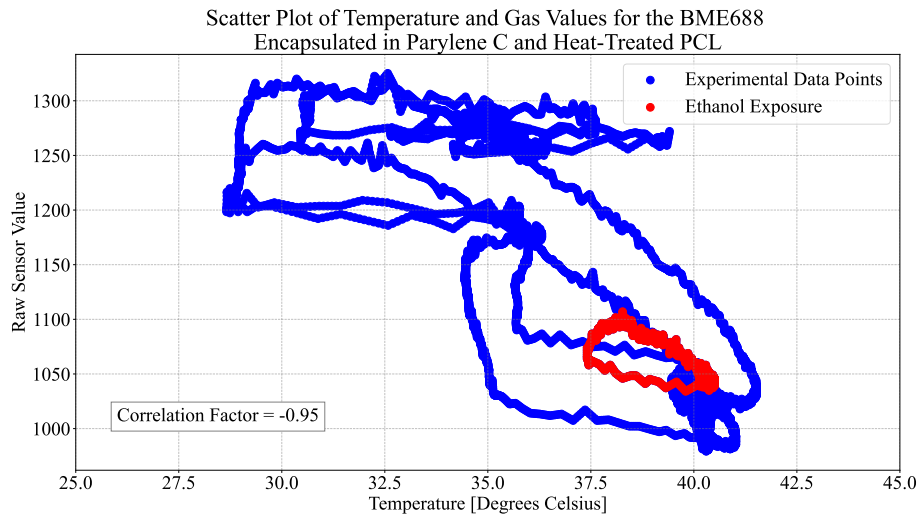
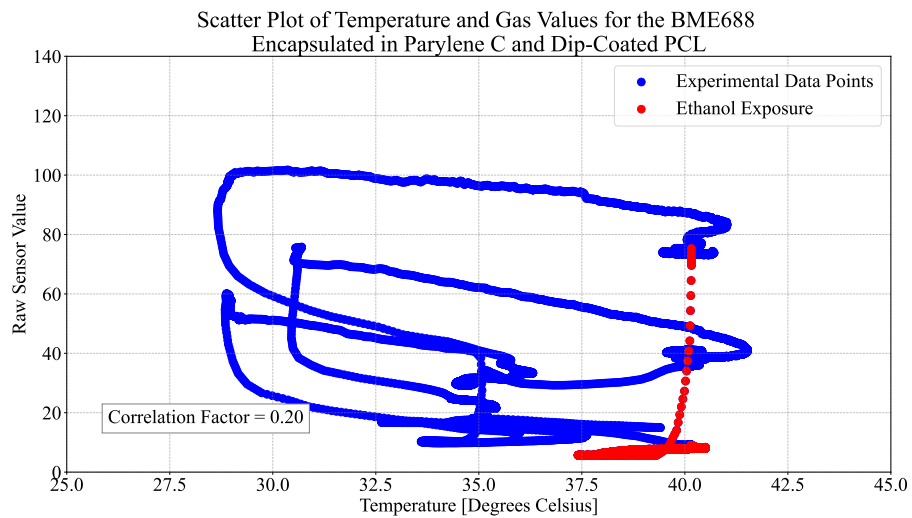


Figure C.11.: SGP40 with 2 different encapsulations exposed to a mixture of 50 mL Whiskey and 250 mL water (6.67% vol. ethanol) between the "Ethanol" and "Empty" mark. As can be seen, the sensor coated with parylene C and dip-coated PCL responds to ethanol, characterized by a clear dip in the sensor response. The sensor coated with parylene C and heat-treated PCL has an exactly opposite response to the temperature.



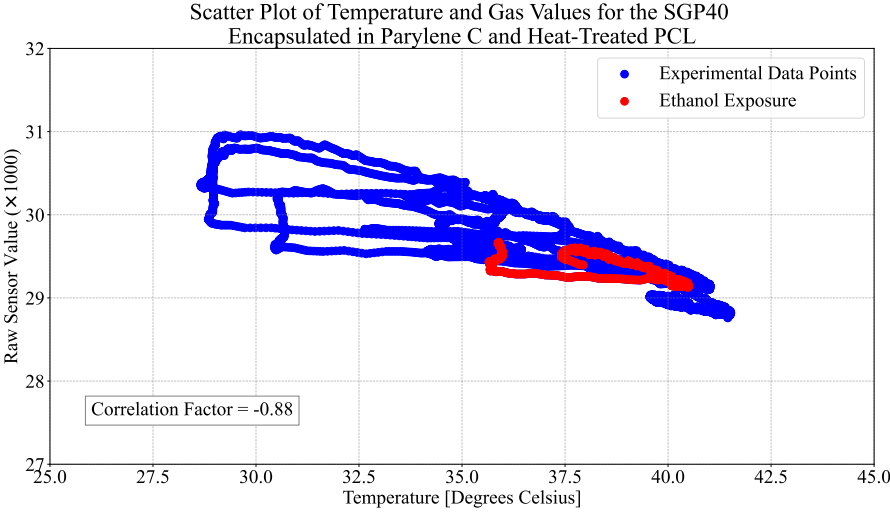
(a)



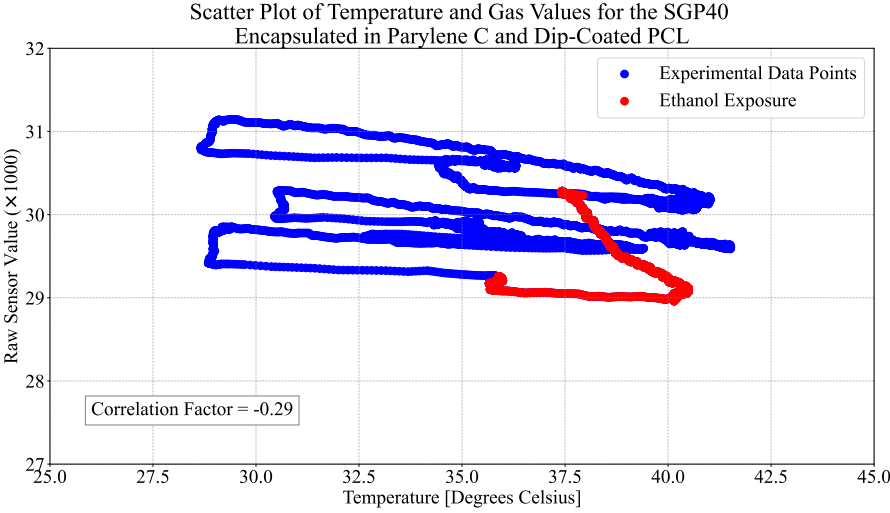
(b)

Figure C.12.: Scatter Plot of the BME688 in a long-term experiment, encapsulated with a) parylene C and heat-treated PCL and b) parylene C and dip-coated PCL. The red scatter are the data points corresponding with the exposure to ethanol. As can be seen, there is almost a perfect correlation between the sensor values and the temperature (correlation factor of -0.95).

C. Measuring Volatile Organic Compounds in Liquid



(a)



(b)

Figure C.13.: Scatter Plot of the SGP40 in a long-term experiment, encapsulated with a) parylene C and heat-treated PCL and b) parylene C and dip-coated PCL. The red scatter are the data points corresponding with the exposure to ethanol.

# D. Artificial Gastric Environment

## D.1. Lid Production

To produce the lid of the beaker that sealed the artificial gastric environment, two custom components were 3D printed. One was a mold for the silicone, and one is a holder for the beaker. The beaker is held upside down by the holder, and placed hanging into the mold with liquid silicone (Elite® Double 8 [117]). Once the silicone is cured, the beaker and lid are pulled out. The lid has holes for the sensor wires and the tubes for liquid inflow and outflow. The full process is visualized in Figure D.1, and real pictures of the components can be seen in Figure D.2.

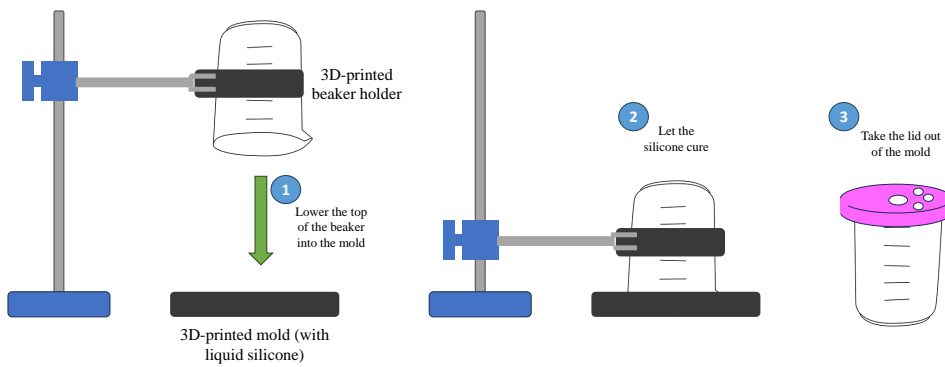


Figure D.1.: Schematic of the production process.

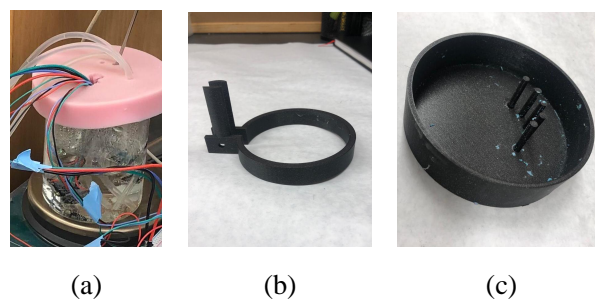


Figure D.2.: Pictures of **a)** the beaker with lid with wires and tubes, during a running experiment, **b)** the 3d-printed beaker holder and **c)** the 3d-printed mold for silicone.

## D.2. Schematics

### D.2.1. Sensor Readout

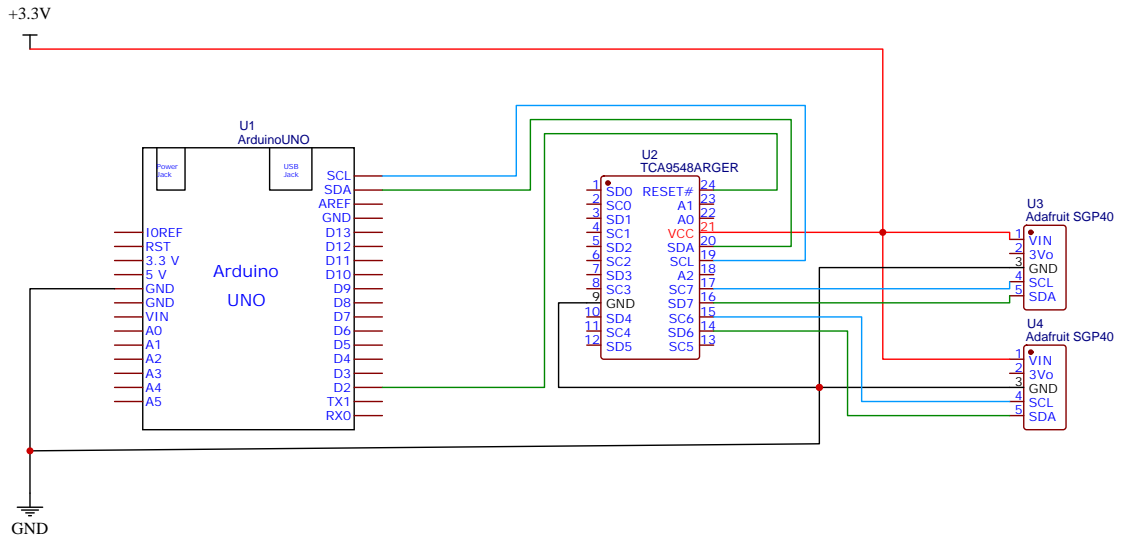


Figure D.3.: Sensor Readout Circuit Schematic.



### D.2.2. Motor Control

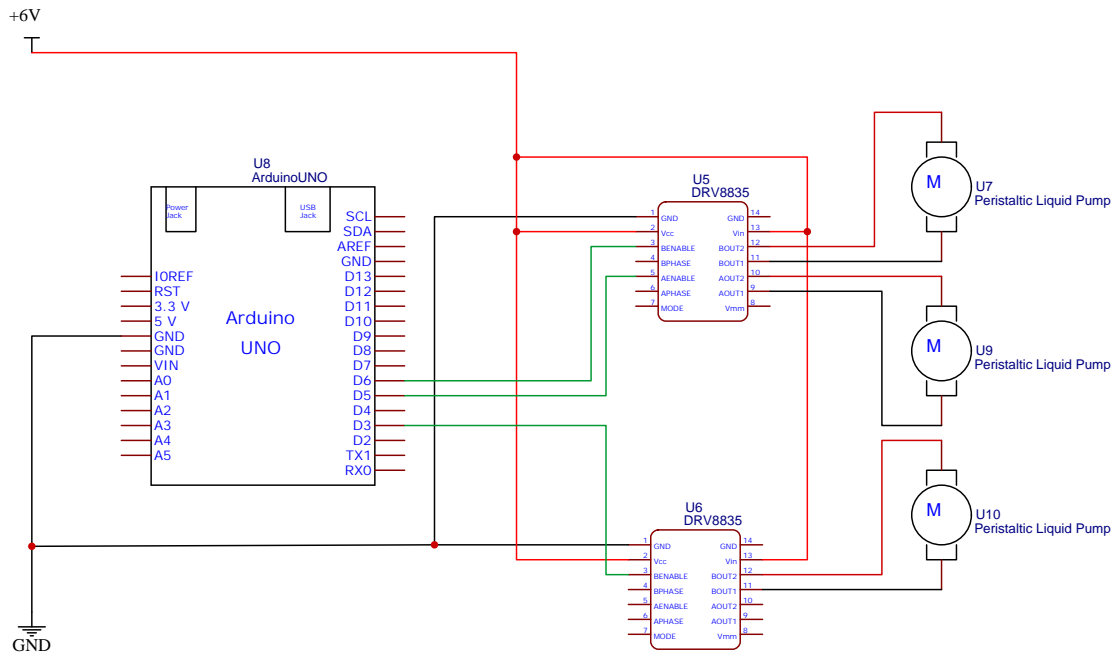


Figure D.4.: Motor Control Circuit Schematic.

### D.3. Finite State Machines

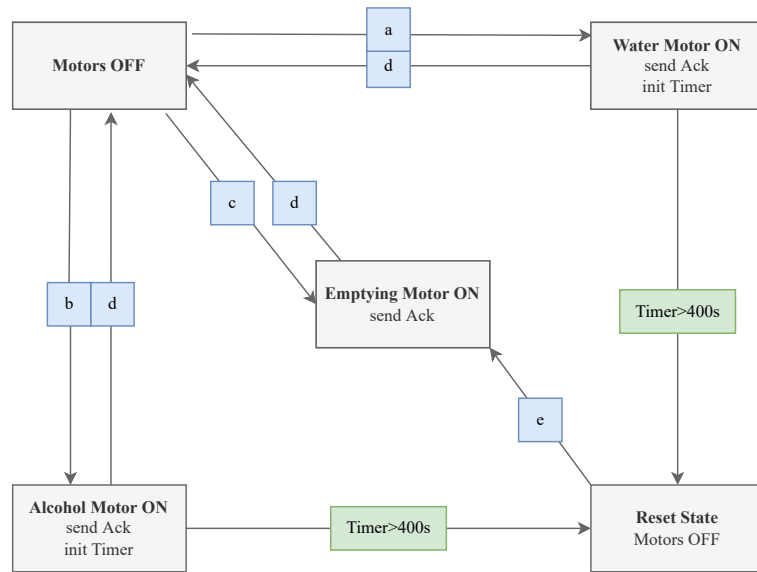


Figure D.5.: Motor Control - Arduino side. a,b,c,d and e are commands from the PC over the serial port.

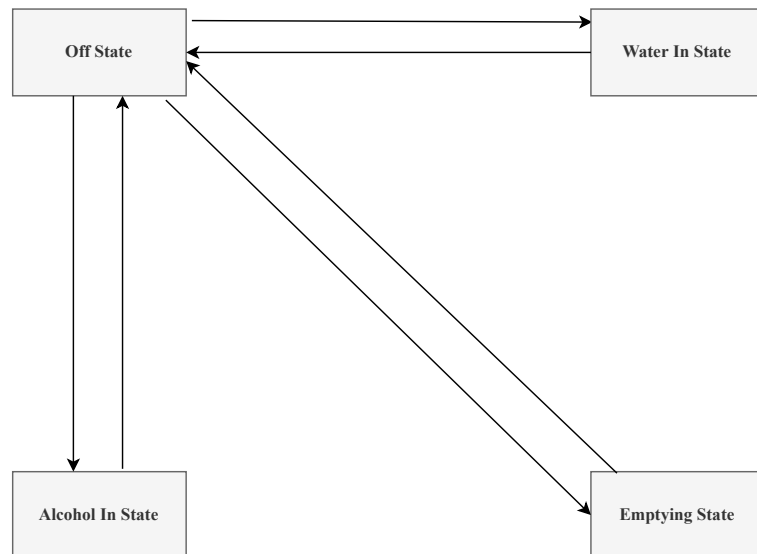


Figure D.6.: Motor Control - PC Side

## D.4. Communication Protocol

---

**Algorithm D.1:** Data Exchange Between Python and Arduino

---

```
1 while Python is connected to Arduino via COM port do
2   for PortNumber = 0 to 7 do
3     if PortNumber not on blacklist then
4       Request a MUX port using the code: "PortNumber";
5       RequestMuxPort (PortNumber);
6       Arduino samples from the sensor at the requested port number, and
7         sends back a response over the serial port.;
8       Response ← SampleSensor (PortNumber);
9       if Response is valid then
10        Extract the sensor type, data stream, and actual data from the
11          Response;
12        Process and log the data;
13      else
14        Reset Arduino using watchdog timer;
15        Add PortNumber to blacklist for 15 minutes;
```

---

### D.5. Experimental Procedure

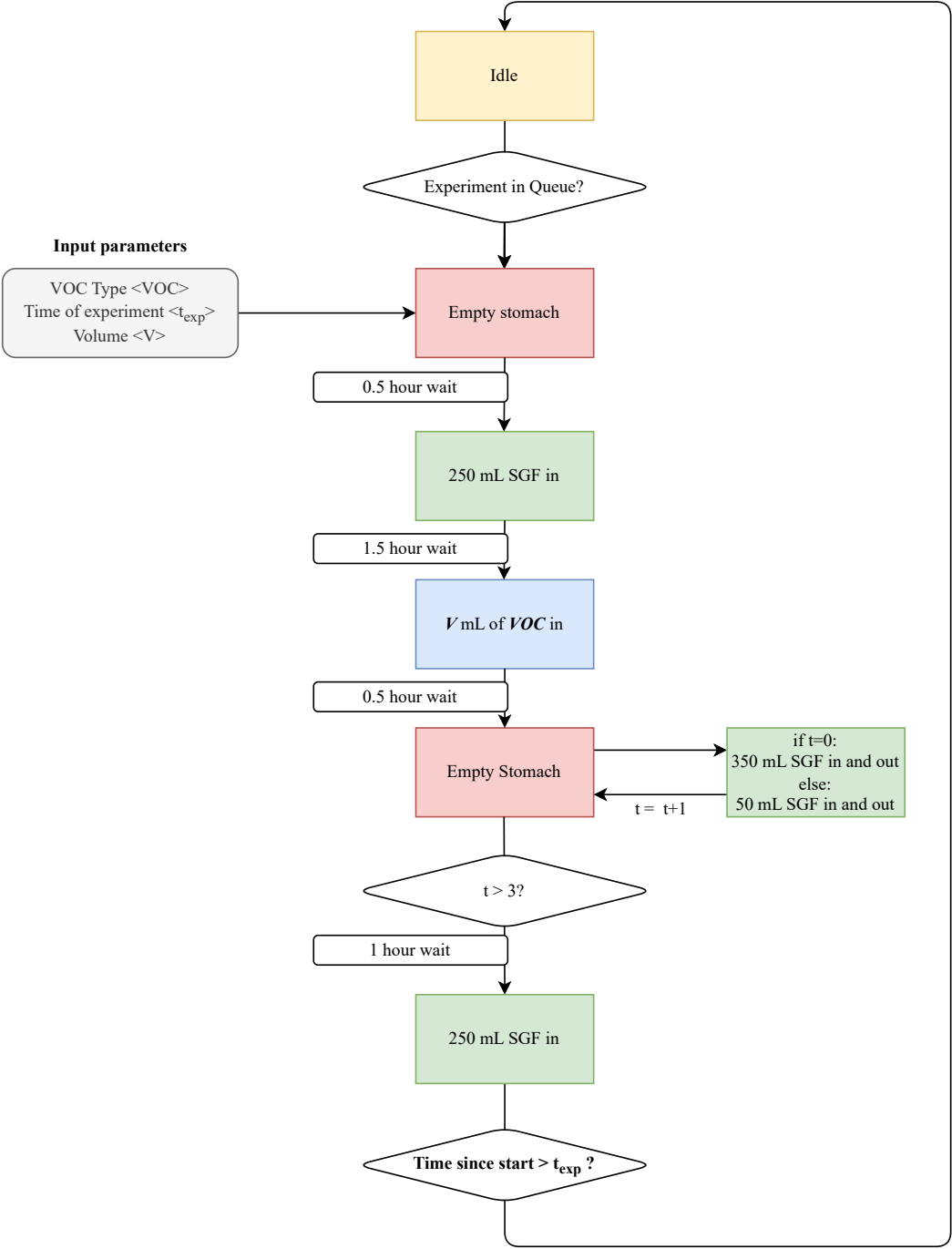


Figure D.7.: Experimental Process (SGF = Simulated Gastric Fluid)

## D.6. Experimental Results for Different Volumes of Ethanol

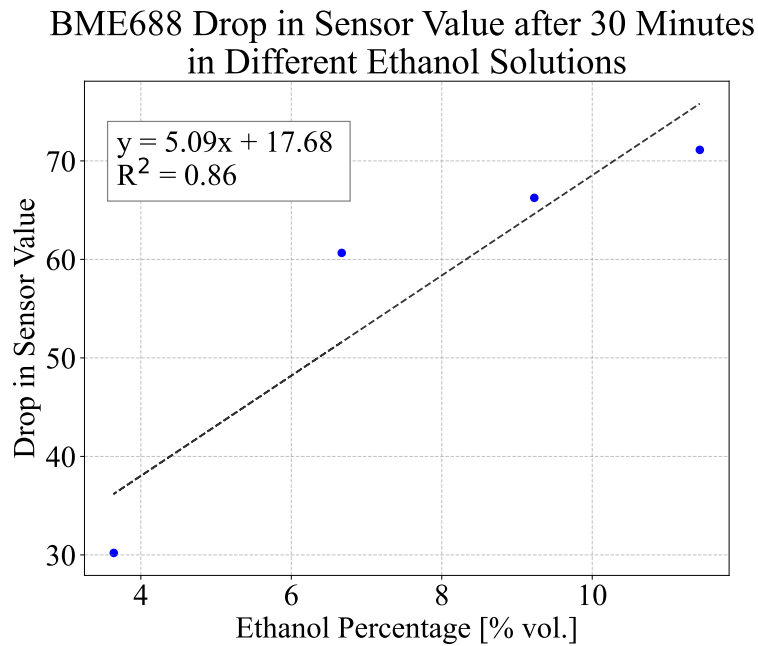
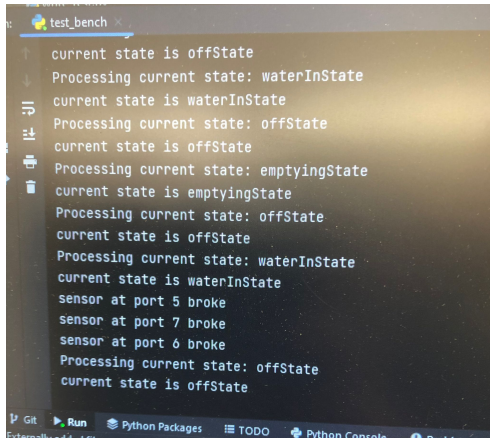


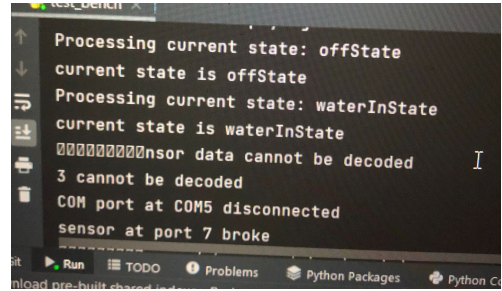
Figure D.8.: Experimental results of the BME688 encapsulated with parylene C and dip-coated PCL in the experimental environment. The graph shows the decrease in sensor value after 30 minutes of exposure to VOCs as a function of the percentage of ethanol in % vol. for 4 experiments.

## D.7. Sensor Failure Analysis



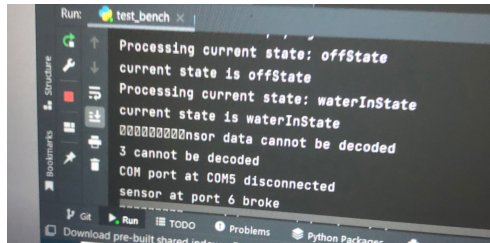
```
test_bench x
current state is offState
Processing current state: waterInState
current state is waterInState
Processing current state: offState
current state is offState
Processing current state: emptyingState
current state is emptyingState
Processing current state: offState
current state is offState
Processing current state: waterInState
current state is waterInState
sensor at port 5 broke
sensor at port 7 broke
sensor at port 6 broke
Processing current state: offState
current state is offState
```

(a)



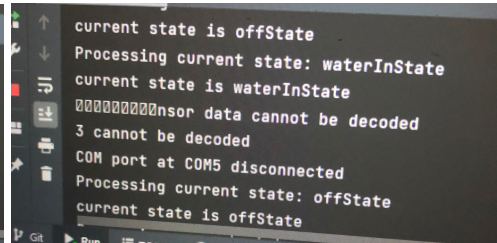
```
test_bench x
Processing current state: offState
current state is offState
Processing current state: waterInState
current state is waterInState
?????????sensor data cannot be decoded
3 cannot be decoded
COM port at COM5 disconnected
sensor at port 7 broke
```

(b)



```
Run: test_bench x
Processing current state: offState
current state is offState
Processing current state: waterInState
current state is waterInState
?????????sensor data cannot be decoded
3 cannot be decoded
COM port at COM5 disconnected
sensor at port 6 broke
```

(c)



```
Run: test_bench x
current state is offState
Processing current state: waterInState
current state is waterInState
?????????sensor data cannot be decoded
3 cannot be decoded
COM port at COM5 disconnected
Processing current state: offState
current state is offState
```

(d)

Figure D.9.: Four different captions of logging prints, in which can be seen that between “water in state” and “motor off state”, i.e. during the inflow of fresh water, the sensors fail, the COM port receives strange characters and the COM port connected to the sensors even disconnects. The microcontroller sends out a string called “sensor data” to specify that it is sending back sensor data. What the computer receives instead is an indecipherable string.

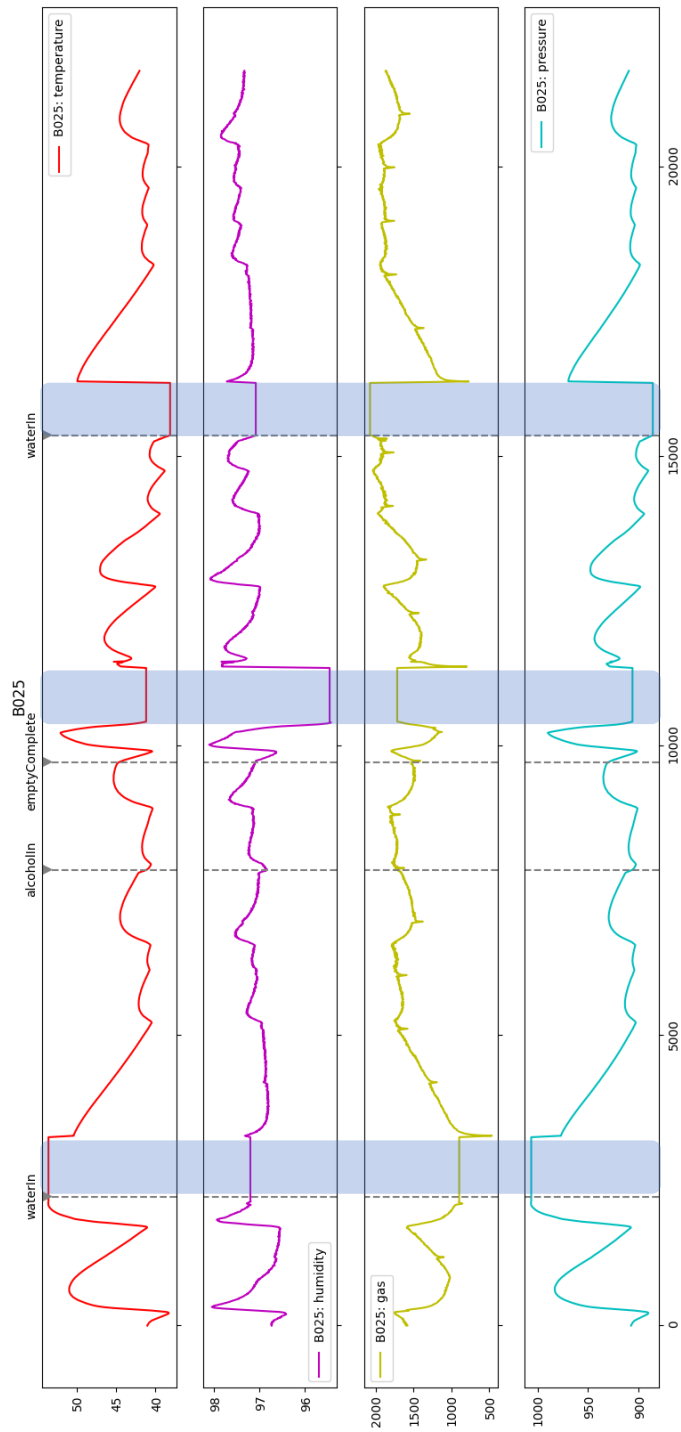


Figure D.10.: The different datastreams of the BME688 encapsulated in parylene C and heat-treated PCL during a single experiment. The periods at which more than 250 mL water is added to the experiment is marked in blue. As can be seen, the sensors break every time this happens.

## Bibliography

- [1] A. Beebe, K. Coulter, R. Lindsay, and E. Baker, "Equilibria in ethanol-water system at pressures less than atmospheric," *Industrial & Engineering Chemistry Industrial Edition*, vol. 34, no. 12, pp. 1501–1504, 1942.
- [2] G. J. Iddan, G. Meron, A. Glukhovsky, and P. Swain, "Wireless capsule endoscopy," *Nature*, vol. 405, no. 6785, p. 417, 2000.
- [3] L. Xin, Z. Liao, Y. P. Jiang, and Z. S. Li, "Indications, detectability, positive findings, total enteroscopy, and complications of diagnostic double-balloon endoscopy: a systematic review of data over the first decade of use," *Gastrointestinal Endoscopy*, vol. 74, no. 3, pp. 563–570, 2011.
- [4] B. Jacobson and R. Mackay, "A ph-endoradiosonde," *The Lancet*, vol. 269, no. 6981, p. 1224, 1957, originally published as Volume 1, Issue 6981. [Online]. Available: <https://www.sciencedirect.com/science/article/pii/S0140673657917920>
- [5] R. Mackay and B. Jacobson, "Endoradiosonde," *Nature*, vol. 179, no. 4567, pp. 1239–1240, 1957.
- [6] Y. Kim, G. Lee, S. Park, B. Kim, J.-O. Park, and et al., "Pressure monitoring system in gastro-intestinal tract," in *Proceedings of the 2005 IEEE International Conference on Robotics and Automation*. IEEE, 2005, pp. 1321–1326.
- [7] A. E. Ikolajczyk, S. Watson, B. L. Surma, and D. T. Rubin, "Assessment of tandem measurements of ph and total gut transit time in healthy volunteers," *Clinical and Translational Gastroenterology*, vol. 6, no. 9, p. e117, July 2015.
- [8] Y. L. Kong, X. Zou, C. A. McCandler, A. R. Kirtane, S. Ning, J. Zhou, A. Abid, M. Jafari, J. Rogner, D. Minahan, J. E. Collins, S. McDonnell, C. Cleveland, T. Bensele, S. Tamang, G. Arrick, A. Gimbel, T. Hua, U. Ghosh, V. Soares, N. Wang, A. Wahane, A. Hayward, S. Zhang, B. R. Smith, R. Langer, and G. Traverso, "3d-printed gastric resident electronics," *Advanced Materials Technologies*, vol. 4, no. 3, p. 1800490, 2019. [Online]. Available: <https://onlinelibrary.wiley.com/doi/abs/10.1002/admt.201800490>
- [9] R. J. Saad and W. L. Hasler, "A technical review and clinical assessment of the wireless motility capsule," *Gastroenterology & Hepatology*, vol. 7, no. 12, pp. 795–804, December 2011.
- [10] S. Yang, V. Sencadas, S. S. You, N.-Z.-X. Jia, S. S. Srinivasan, H. Huang, A. E. Ahmed, J. Liang, and G. Traverso, "Powering implantable and ingestible electronics," *Advanced Functional Materials*, vol. 31, p. 2009289, 2021.
- [11] C. J. Bettinger, "Materials advances for next-generation ingestible electronic medical devices," *Trends in Biotechnology*, vol. 33, no. 10, pp. 575–585, October 2015.



- [12] —, “Advances in materials and structures for ingestible electromechanical medical devices,” *Angewandte Chemie International Edition*, vol. 57, no. 52, pp. 16 946–16 958, December 2018.
- [13] C. Steiger, N. V. Phan, H.-W. Huang, H. Sun, J. N. Chu, D. Reker, D. Gwynne, J. Collins, S. Tamang, R. McManus *et al.*, “Dynamic monitoring of systemic biomarkers with gastric sensors,” *Advanced Science*, vol. 8, no. 24, p. 2102861, 2021.
- [14] A. Baranska, Z. Mujagic, A. Smolinska, J. Dallinga, D. M. Jonkers, E. Tigchelaar, J. Dekens, A. Zhernakova, T. Ludwig, A. A. Masclee, C. Wijmenga, and F.-J. van Schooten, “Volatile organic compounds in breath as markers for irritable bowel syndrome: a metabolomic approach,” *Aliment Pharmacol Ther*, vol. 44, no. 1, pp. 45–56, 2016.
- [15] L. Xiang, S. Wu, Q. Hua, C. Bao, and H. Liu, “Volatile organic compounds in human exhaled breath to diagnose gastrointestinal cancer: A meta-analysis,” *Front Oncol*, vol. 11, p. 606915, 2021.
- [16] A. Smolinska, E. M. Klaassen, J. W. Dallinga, K. D. van de Kant, Q. Jobsis, E. J. Moonen, O. C. van Schayck, E. Dompeling, and F.-J. van Schooten, “Profiling of volatile organic compounds in exhaled breath as a strategy to find early predictive signatures of asthma in children,” *PLoS One*, vol. 9, no. 4, p. e95668, 2014, erratum in: *PLoS One*. 2014;9(8):e105447.
- [17] N. Alkhoury, K. Eng, F. Cikach, N. Patel, C. Yan, A. Brindle, E. Rome, I. Hanouneh, D. Grove, R. Lopez, S. L. Hazen, and R. A. Dweik, “Breathprints of childhood obesity: changes in volatile organic compounds in obese children compared with lean controls,” *Pediatric Obesity*, vol. 10, no. 1, pp. 23–29, 2015. [Online]. Available: <https://onlinelibrary.wiley.com/doi/abs/10.1111/j.2047-6310.2014.221.x>
- [18] A. Ettema, M. Lenders, J. Vliegen, A. Slettenaar, M. Tjepkema-Cloostermans, and C. de Vos, “Detecting multiple sclerosis via breath analysis using an enose, a pilot study,” *Journal of breath research*, vol. 15, no. 2, p. 027101, 2021.
- [19] O. Herman-Saffar, Z. Boger, S. Libson, D. Lieberman, R. Gonen, and Y. Zeiri, “Early non-invasive detection of breast cancer using exhaled breath and urine analysis,” *Computers in biology and medicine*, vol. 96, pp. 227–232, 2018.
- [20] S. Kort, M. Brusse-Keizer, J.-W. Gerritsen, and J. van der Palen, “Data analysis of electronic nose technology in lung cancer: generating prediction models by means of aethena,” *Journal of Breath Research*, vol. 11, no. 2, p. 026006, 2017.
- [21] B. Schmekel, F. Winquist, and A. Vikström, “Analysis of breath samples for lung cancer survival,” *Analytica chimica acta*, vol. 840, pp. 82–86, 2014.
- [22] C. Steiger, A. Abramson, P. Nadeau, and *et al.*, “Ingestible electronics for diagnostics and therapy,” *Nature Reviews Materials*, vol. 4, no. 2, pp. 83–98, 2019.
- [23] M. B. Esser, G. Leung, A. Sherk, M. K. Bohm, Y. Liu, H. Lu, and T. S. Naimi, “Estimated deaths attributable to excessive alcohol use among us adults aged 20 to 64 years, 2015 to 2019,” *JAMA Network Open*, vol. 5, no. 11, p. e2239485, November 2022.
- [24] S. M. Alessi, N. P. Barnett, and N. M. Petry, “Objective continuous monitoring of alcohol consumption for three months among alcohol use disorder treatment outpatients,” *Alcohol*, vol. 81, pp. 131–138, December 2019.

## Bibliography

- [25] X. Liu, C. Steiger, S. Lin, G. A. Parada, J. Liu, H. F. Chan, H. Yuk, N. V. Phan, J. Collins, S. Tamang, G. Traverso, and X. Zhao, "Ingestible hydrogel device," *Nature Communications*, vol. 10, no. 1, p. 493, January 2019.
- [26] M. Rondanelli, F. Perdoni, V. Infantino, M. A. Faliva, G. Peroni, G. Iannello, M. Nichetti, T. A. Alalwan, S. Perna, and C. Cocuzza, "Volatile organic compounds as biomarkers of gastrointestinal diseases and nutritional status," *J Anal Methods Chem*, vol. 2019, p. 7247802, 2019.
- [27] J. J. Darrow, "Capsule endoscopy instead of colonoscopy? the FDA approves the PillCam COLON," *Harvard Law School Blog*, March 4 2014. [Online]. Available: <https://blog.petrieflom.law.harvard.edu/2014/03/04/capsule-endoscopy-instead-of-colonoscopy-the-fda-approves-the-pillcam-colon/>
- [28] O. Oluwoye, H. Reneau, J. Herron, K. C. Alcover, S. McPherson, J. Roll, and M. G. McDonell, "Pilot study of an integrated smartphone and breathalyzer contingency management intervention for alcohol use," *Journal of Addictive Medicine*, vol. 14, no. 3, pp. 193–198, 2020.
- [29] J. Wang, N. Nuñovero, Z. Lin, R. Nidetz, S. Buggaveeti, C. Zhan, K. Kurabayashi, W. Steinecker, and E. Zellers, "A wearable mems gas chromatograph for multi-vapor determinations," *Procedia Engineering*, vol. 168, pp. 1398–1401, 12 2016.
- [30] C. K. McGinn, Z. A. Lampion, and I. Kymissis, "Review of gravimetric sensing of volatile organic compounds," *ACS sensors*, vol. 5, no. 6, pp. 1514–1534, 2020.
- [31] A. H. Jalal, F. Alam, S. Roychoudhury, Y. Umasankar, N. Pala, and S. Bhansali, "Prospects and Challenges of Volatile Organic Compound Sensors in Human Healthcare," *ACS Sensors*, vol. 3, no. 7, pp. 1246–1263, Jul. 2018, publisher: American Chemical Society. [Online]. Available: <https://doi.org/10.1021/acssensors.8b00400>
- [32] F.-G. Banica, *Chemical Sensors and Biosensors: Fundamentals and Applications*. Chichester: John Wiley and Sons, 2012, print ISBN 978-0-470-71066-1; Web ISBN 0-470710-66-7; ISBN 978-1-118-35423-0. [Online]. Available: <https://doi.org/10.1002/9781118354230>
- [33] H.-J. Kim and J.-H. Lee, "Highly sensitive and selective gas sensors using p-type oxide semiconductors: Overview," *Sensors and Actuators B: Chemical*, vol. 192, pp. 607–627, 2014.
- [34] Bosch, "Bme680: Low power gas, pressure, temperature humidity sensor," 2022. [Online]. Available: <https://www.bosch-sensortec.com/media/boschsensortec/downloads/datasheets/bst-bme680-ds001.pdf>
- [35] Sensirion, "Preliminary datasheet sgp40," 2020. [Online]. Available: <https://docs.rs-online.com/1956/A700000007055193.pdf>
- [36] ScioSense, "Ccs811: Ultra-low power digital gas sensor for monitoring indoor air quality," 2021. [Online]. Available: <https://www.sciosense.com/wp-content/uploads/documents/SC-001232-DS-3-CCS811B-Datasheet-Revision-2.pdf>
- [37] S. Kulkarni, N. G. Kalayil, J. James, S. Parsewar, and R. Shriram, "Detection of parkinson's disease through smell signatures," in *2020 International Conference on Communication and Signal Processing (ICCSP)*, 2020, pp. 808–812.

- [38] D. M. Kita, H. Lin, A. Agarwal, K. Richardson, I. Luzinov, T. Gu, and J. Hu, "On-chip infrared spectroscopic sensing: redefining the benefits of scaling," *IEEE Journal of Selected Topics in Quantum Electronics*, vol. 23, no. 2, pp. 340–349, 2016.
- [39] L. Rodriguez-Saona, D. P. Aykas, K. R. Borba, and A. Urtubia, "Miniaturization of optical sensors and their potential for high-throughput screening of foods," *Current Opinion in Food Science*, vol. 31, pp. 136–150, 2020, food Chemistry and Biochemistry • Food Bioprocessing. [Online]. Available: <https://www.sciencedirect.com/science/article/pii/S2214799320300382>
- [40] Plantower, "Pmsa003i series data manual," 2018. [Online]. Available: [https://cdn-shop.adafruit.com/product-files/4505/4505\\_PMSA003I\\_series\\_data\\_manual\\_English\\_V2.6.pdf](https://cdn-shop.adafruit.com/product-files/4505/4505_PMSA003I_series_data_manual_English_V2.6.pdf)
- [41] J. Kim, I. Jeerapan, S. Imani, T. N. Cho, A. Bandodkar, S. Cinti, P. P. Mercier, and J. Wang, "Noninvasive alcohol monitoring using a wearable tattoo-based iontophoretic-biosensing system," *Acs Sensors*, vol. 1, no. 8, pp. 1011–1019, 2016.
- [42] R. M. Swift, C. S. Martin, L. Swette, A. LaConti, and N. Kackley, "Studies on a wearable, electronic, transdermal alcohol sensor," *Alcoholism: Clinical and Experimental Research*, vol. 16, no. 4, pp. 721–725, 1992.
- [43] E. Sense, "Easy gas sensor es1-ag1-1000 - all gas," 2016. [Online]. Available: <https://sensorsandpower.angst-pfister.com/fileadmin/products/datasheets/188/ES1-AG-1K.1620-21570-0009-E-0217.pdf>
- [44] Sensirion, "Datasheet stc31: Co2 sensor based on thermal conductivity," 2020. [Online]. Available: [https://www.tme.eu/Document/e665cbd4416f86845874670f19d2a9e9/TC\\_DS\\_STC31\\_D1%20%28002%29.pdf](https://www.tme.eu/Document/e665cbd4416f86845874670f19d2a9e9/TC_DS_STC31_D1%20%28002%29.pdf)
- [45] A. G. Dent, T. G. Sutedja, and P. V. Zimmerman, "Exhaled breath analysis for lung cancer," *Journal of thoracic disease*, vol. 5, no. Suppl 5, p. S540, 2013.
- [46] S.-I. Ohira and K. Toda, "Micro gas analyzers for environmental and medical applications," *Analytica Chimica Acta*, vol. 619, no. 2, pp. 143–156, 2008.
- [47] E. L. W. Gardner, J. W. Gardner, and F. Udrea, "Micromachined thermal gas sensors—a review," *Sensors*, vol. 23, no. 2, 2023. [Online]. Available: <https://www.mdpi.com/1424-8220/23/2/681>
- [48] J. Erfkamp, M. Guenther, and G. Gerlach, "Hydrogel-based sensors for ethanol detection in alcoholic beverages," *Sensors*, vol. 19, no. 5, 2019. [Online]. Available: <https://www.mdpi.com/1424-8220/19/5/1199>
- [49] A. Kumar and R. Prajesh, "The potential of acoustic wave devices for gas sensing applications," *Sensors and Actuators A: Physical*, p. 113498, 2022.
- [50] S.-J. Young and Z.-D. Lin, "Ethanol gas sensors based on multi-wall carbon nanotubes on oxidized si substrate," *Microsystem Technologies*, vol. 24, no. 1, pp. 55–58, 2018.
- [51] N. M. Shaalan, F. Ahmed, M. Rashad, O. Saber, S. Kumar, A. Aljaafari, A. Ashoabi, A. Z. Mahmoud, and M. Ezzeldien, "Low-temperature ethanol sensor via defective multiwalled carbon nanotubes," *Materials*, vol. 15, no. 13, 2022. [Online]. Available: <https://www.mdpi.com/1996-1944/15/13/4439>

## Bibliography

- [52] S. Maqbool, H. P. Parkman, and F. K. Friedenberg, "Wireless capsule motility: comparison of the smartpill® gi monitoring system with scintigraphy for measuring whole gut transit," *Digestive diseases and sciences*, vol. 54, no. 10, pp. 2167–2174, 2009.
- [53] P. Swain, "Wireless capsule endoscopy," *Gut*, vol. 52, no. suppl 4, pp. iv48–iv50, 2003.
- [54] K. Kalantar-Zadeh, K. J. Berean, N. Ha, and et al., "A human pilot trial of ingestible electronic capsules capable of sensing different gases in the gut," *Nature Electronics*, vol. 1, no. 2, pp. 79–87, 2018.
- [55] M. Inda, M. Jimenez, Q. Liu, N. Phan, J. Ahn, C. Steiger, A. Wentworth, A. Riaz, T. Ziritloglu, K. Wong *et al.*, "Ingestible capsule for detecting labile inflammatory biomarkers in situ," *bioRxiv*, pp. 2022–02, 2022.
- [56] H.-W. Huang, C. Ehmke, C. Steiger, I. Ballinger, M. Jimenez, N. Phan, H. Sun, K. Ishida, J. Kuosmanen, J. Jenkins *et al.*, "In situ detection of gastrointestinal inflammatory biomarkers using electrochemical gas sensors," in *2022 44th Annual International Conference of the IEEE Engineering in Medicine & Biology Society (EMBC)*. IEEE, 2022, pp. 2491–2494.
- [57] K. J. Berean, N. Ha, J. Z. Ou, A. F. Chrimes, D. Grando, C. K. Yao, J. G. Muir, S. A. Ward, R. E. Burgell, P. R. Gibson *et al.*, "The safety and sensitivity of a telemetric capsule to monitor gastrointestinal hydrogen production in vivo in healthy subjects: a pilot trial comparison to concurrent breath analysis," *Alimentary Pharmacology & Therapeutics*, vol. 48, no. 6, pp. 646–654, 2018.
- [58] M. Camilleri, N. K. Thorne, Y. Ringel, W. L. Hasler, B. Kuo, T. Esfandyari, A. Gupta, S. M. Scott, R. W. McCallum, H. P. Parkman, E. E. Soffer, G. E. Wilding, J. R. Semler, and S. S. C. Rao, "Wireless ph-motility capsule for colonic transit: prospective comparison with radiopaque markers in chronic constipation," *Neurogastroenterology & Motility*, vol. 22, no. 8, pp. 874–e233, 2010.
- [59] P. R. Chai, R. K. Rosen, and E. W. Boyer, "Ingestible biosensors for real-time medical adherence monitoring: Mytmed," in *Proceedings of the 2016 49th Hawaii International Conference on System Sciences*. IEEE, 2016, pp. 3416–3423.
- [60] P. R. Chai, C. Vaz, G. R. Goodman, H. Albrechta, H. Huang, R. K. Rosen, E. W. Boyer, K. H. Mayer, and C. O'Cleirigh, "Ingestible electronic sensors to measure instantaneous medication adherence: A narrative review," *Digital Health*, vol. 8, p. 20552076221083119, 2022.
- [61] M. Mimee, P. Nadeau, A. Hayward, S. Carim, S. Flanagan, L. Jerger, J. Collins, S. McDonnell, R. Swartwout, R. J. Citorik, V. Bulović, R. Langer, G. Traverso, A. P. Chandrakasan, and T. K. Lu, "An ingestible bacterial-electronic system to monitor gastrointestinal health," *Science*, vol. 360, no. 6391, pp. 915–918, 2018.
- [62] E. De la Paz, N. H. Maganti, A. Trifonov, and et al., "A self-powered ingestible wireless biosensing system for real-time in situ monitoring of gastrointestinal tract metabolites," *Nature Communications*, vol. 13, no. 1, p. 7405, 2022.
- [63] G. Traverso, G. Ciccarelli, S. Schwartz, T. Hughes, T. Boettcher, R. Barman, R. Langer, and A. Swiston, "Physiologic status monitoring via the gastrointestinal tract," *PLoS one*, vol. 10, no. 11, p. e0141666, 2015.

- [64] H. Cao, V. Landge, U. Tata, Y.-S. Seo, S. Rao, S.-J. Tang, H. F. Tibbals, S. Spechler, and J.-C. Chiao, "An implantable, batteryless, and wireless capsule with integrated impedance and pH sensors for gastroesophageal reflux monitoring," *IEEE Transactions on Biomedical Engineering*, vol. 59, no. 11, pp. 3131–3139, 2012.
- [65] S. Sharma, K. B. Ramadi, N. H. Poole, and et al., "Location-aware ingestible microdevices for wireless monitoring of gastrointestinal dynamics," *Nature Electronics*, vol. 6, no. 4, pp. 242–256, 2023.
- [66] A. Nemiroski, M. Ryou, C. C. Thompson, and R. M. Westervelt, "Swallowable fluorometric capsule for wireless triage of gastrointestinal bleeding," *Lab Chip*, vol. 15, pp. 4479–4487, 2015. [Online]. Available: <http://dx.doi.org/10.1039/C5LC00770D>
- [67] G. E. Banis, L. A. Beardslee, J. M. Stine, R. M. Sathyam, and R. Ghodssi, "Capacitive sensing of triglyceride film reactions: a proof-of-concept demonstration for sensing in simulated duodenal contents with gastrointestinal targeting capsule system," *Lab on a Chip*, vol. 20, no. 11, 2020.
- [68] N. Gluck, B. Shpak, R. Brun, T. Rösch, N. Arber, and M. Moshkowitz, "A novel prepless x-ray imaging capsule for colon cancer screening," *Gut*, vol. 65, no. 3, pp. 371–373, 2016.
- [69] X. Wang, V. Seetohul, R. Chen, Z. Zhang, M. Qian, Z. Shi, G. Yang, P. Mu, C. Wang, Z. Huang *et al.*, "Development of a mechanical scanning device with high-frequency ultrasound transducer for ultrasonic capsule endoscopy," *IEEE transactions on medical imaging*, vol. 36, no. 9, pp. 1922–1929, 2017.
- [70] C. Mc Caffrey, K. Twomey, and V. Ogurtsov, "Development of a wireless swallowable capsule with potentiostatic electrochemical sensor for gastrointestinal track investigation," *Sensors and Actuators B: Chemical*, vol. 218, pp. 8–15, 2015.
- [71] J. O'Grady, C. L. Murphy, L. Barry, F. Shanahan, and M. Buckley, "Defining gastrointestinal transit time using video capsule endoscopy: a study of healthy subjects," *Endoscopy International Open*, vol. 8, no. 3, pp. E396–E400, 2020.
- [72] R. Nakamura, S. Izumi, H. Kawaguchi, H. Ohta, and M. Yoshimoto, "Swallowable sensing device for long-term gastrointestinal tract monitoring," in *2016 38th Annual International Conference of the IEEE Engineering in Medicine and Biology Society (EMBC)*, 2016, pp. 3039–3042.
- [73] Y. Mori and T. Inaba, "Ethanol production from starch in a pervaporation membrane bioreactor using *Clostridium thermohydrosulfuricum*," *Biotechnology and Bioengineering*, vol. 36, no. 8, pp. 849–853, 1990.
- [74] G. S. Golubev, I. L. Borisov, and V. V. Volkov, "Performance of commercial and laboratory membranes for recovering bioethanol from fermentation broth by thermopervaporation," *Russian Journal of Applied Chemistry*, vol. 91, no. 8, pp. 1375–1381, 2018.
- [75] A. G. Nassif, S. S. Ibrahim, H. S. Majdi, and Q. F. Alsalhy, "Ethanol separation from an ethanol-water solution using vacuum membrane distillation," *Membranes*, vol. 12, no. 8, p. 807, 2022.
- [76] Advantec, "Membrane filters." [Online]. Available: <https://www.labtek.com.au/SuppliersData/Advantec/Membrane%20Filters.pdf>

## Bibliography

- [77] Z. Wu, C. Zhang, L. Peng, X. Wang, Q. Kong, and X. Gu, "Enhanced stability of mfi zeolite membranes for separation of ethanol/water by eliminating surface si-oh groups," *ACS applied materials & interfaces*, vol. 10, no. 4, pp. 3175–3180, 2018.
- [78] Q. Liu, X. Wang, Y. Guo, and et al., "Mechanism of ethanol/water reverse separation through a functional graphene membrane: a molecular simulation investigation," *Frontiers of Chemical Science and Engineering*, vol. 17, no. 3, pp. 347–357, 2023.
- [79] Bosch, "Bme688," 2022. [Online]. Available: <https://www.bosch-sensortec.com/media/boschsensortec/downloads/datasheets/bst-bme688-ds000.pdf>
- [80] Sensirion, "Datasheet sgp30 sensirion gas platform," 2017. [Online]. Available: [https://www.mouser.com/pdfdocs/Sensirion\\_Gas\\_Sensors\\_SGP30\\_Datasheet\\_EN-1148053.pdf](https://www.mouser.com/pdfdocs/Sensirion_Gas_Sensors_SGP30_Datasheet_EN-1148053.pdf)
- [81] Renesas, "Zmod4410," 2023. [Online]. Available: <https://www.renesas.com/eu/en/document/dst/zmod4410-datasheet>
- [82] Sciosense, "Ens160 digital metal oxide multi-gas sensor," 2020. [Online]. Available: [https://www.mouser.com/datasheet/2/1081/SC\\_001224\\_DS\\_1\\_ENS160\\_Datasheet\\_Rev\\_0\\_95-2258311.pdf](https://www.mouser.com/datasheet/2/1081/SC_001224_DS_1_ENS160_Datasheet_Rev_0_95-2258311.pdf)
- [83] ams, "Ccs801," 2016. [Online]. Available: [https://www.mouser.com/datasheet/2/588/CCS801\\_DS000457\\_2-00-1140362.pdf](https://www.mouser.com/datasheet/2/588/CCS801_DS000457_2-00-1140362.pdf)
- [84] S. Sensortech, "Mics5524." [Online]. Available: <https://cdn-shop.adafruit.com/product-files/3199/MiCS-5524.pdf>
- [85] "Diabetic ketoacidosis," Online, National Health Service, 2023, accessed on the 13th of June, 2023. [Online]. Available: <https://www.nhs.uk/conditions/diabetic-ketoacidosis/>
- [86] T. Liu, L. Guo, M. Wang, C. Su, D. Wang, H. Dong, J. Chen, and W. Wu, "Review on algorithm design in electronic noses: Challenges, status, and trends," *Intelligent Computing*, vol. 2, p. 0012, 2023.
- [87] J. Yan, X. Guo, S. Duan, P. Jia, L. Wang, C. Peng, and S. Zhang, "Electronic nose feature extraction methods: A review," *Sensors*, vol. 15, no. 11, pp. 27 804–27 831, 2015.
- [88] J. Yan, F. Tian, Q. He, Y. Shen, S. Xu, J. Feng, and K. Chaibou, "Feature extraction from sensor data for detection of wound pathogen based on electronic nose," *Sensors and Materials*, vol. 24, no. 2, pp. 57–73, 2012.
- [89] P. Shakya, E. Kennedy, C. Rose, and J. K. Rosenstein, "High-dimensional time series feature extraction for low-cost machine olfaction," *IEEE Sensors Journal*, vol. 21, no. 3, pp. 2495–2504, 2021.
- [90] I. Guyon and A. Elisseeff, "An introduction to variable and feature selection," *Journal of Machine Learning Research*, vol. 3, pp. 1157–1182, 3 2003, submitted 11/02; Published 3/03.
- [91] R. Chen, C. Dewi, S. Huang *et al.*, "Selecting critical features for data classification based on machine learning methods," *Journal of Big Data*, vol. 7, no. 1, p. 52, 2020.

- [92] M. J. Christoe, J. Yuan, A. Michael, and K. Kalantar-Zadeh, "Bluetooth signal attenuation analysis in human body tissue analogues," *IEEE Access*, vol. 9, pp. 85 144–85 150, 2021.
- [93] R. David, J. Duke, A. Jain, V. J. Reddi, N. Jeffries, J. Li, N. Kreeger, I. Nappier, M. Natraj, S. Regev, R. Rhodes, T. Wang, and P. Warden, "Tensorflow lite micro: Embedded machine learning on tinyml systems," 2021.
- [94] EloquentArduino, "micromlgen: A python library for microcontroller machine learning model code generation," 2022. [Online]. Available: <https://github.com/eloquentarduino/micromlgen>
- [95] J. Jongboom, "Introducing eon: Neural networks in up to 55% less ram and 35% less rom," 2022. [Online]. Available: <https://www.edgeimpulse.com/blog/introducing-eon>
- [96] L. Breiman, "Random forests," *Machine learning*, vol. 45, pp. 5–32, 2001.
- [97] S. Hymel, C. Banbury, D. Situnayake, A. Elium, C. Ward, M. Kelcey, M. Baaijens, M. Majchrzycki, J. Plunkett, D. Tischler, A. Grande, L. Moreau, D. Maslov, A. Beavis, J. Jongboom, and V. J. Reddi, "Edge impulse: An mlops platform for tiny machine learning," 2023.
- [98] M. Giordano, N. Baumann, M. Crabolu, R. Fischer, G. Bellusci, and M. Magno, "Design and performance evaluation of an ultralow-power smart iot device with embedded tinyml for asset activity monitoring," *IEEE Transactions on Instrumentation and Measurement*, vol. 71, p. 2510711, 2022.
- [99] M. Z. M. Shamim, "Tinyml model for classifying hazardous volatile organic compounds using low-power embedded edge sensors: Perfecting factory 5.0 using edge ai," *IEEE Sensors Letters*, vol. 6, no. 9, pp. 1–4, 2022.
- [100] S. O. Ooko, D. Mukanyiligira, J. P. Munyampundu, and J. Nsenga, "Edge ai-based respiratory disease recognition from exhaled breath signatures," in *2021 IEEE Jordan International Joint Conference on Electrical Engineering and Information Technology (JEEIT)*. IEEE, 2021, pp. 89–94.
- [101] S. V. Lahade, S. Namuduri, H. Upadhyay, and S. Bhansali, "Alcohol sensor calibration on the edge using tiny machine learning (tiny-ml) hardware," in *Electrochemical Society Meeting Abstracts 237*, no. 26. The Electrochemical Society, Inc., 2020, pp. 1848–1848.
- [102] "Elite Double 22 Fast Curing Silicone," <https://www.zhermack.com/en/product/elite-double-22/>, accessed 25th of June, 2023.
- [103] M. Sang, K.-I. Kim, J. Shin, and K. J. Yu, "Ultra-thin flexible encapsulating materials for soft bio-integrated electronics," *Advanced Science*, vol. 9, p. 2202980, 2022.
- [104] E. Malikmammadov, T. E. Tanir, A. Kiziltay, V. Hasirci, and N. Hasirci, "Pcl and pcl-based materials in biomedical applications," *Journal of Biomaterials Science, Polymer Edition*, vol. 29, no. 7-9, pp. 863–893, May 2018.
- [105] J. Hsu, L. Rieth, R. Normann, P. Tathireddy, and F. Solzbacher, "Encapsulation of an integrated neural interface device with parylene c," *IEEE Transactions on Biomedical Engineering*, vol. 56, no. 1, pp. 23–29, Jan 2009.

## Bibliography

- [106] “3M™ Scotch-Weld™ Epoxy Adhesive DP110 Translucent,” [https://www.3m.com/3M/en\\_US/p/d/b40066469/](https://www.3m.com/3M/en_US/p/d/b40066469/), accessed 25th of June, 2023.
- [107] S. C. Systems, *PDS 2010 LABCOTER™ 2 Parylene Deposition System Operator’s Manual*, December 2003.
- [108] Prusa I3 Mk3. Webpage. Accessed on 20th of July 2023. [Online]. Available: <https://libraries.uta.edu/services/technology/prusa-i3-mk3>
- [109] E. K. Ulleberg, I. Comi, H. Holm, E. B. Herud, M. Jacobsen, and G. E. Vegarud, “Human gastrointestinal juices intended for use in in vitro digestion models,” *Food Digestion*, vol. 2, no. 1-3, pp. 52–61, 2011. [Online]. Available: <https://doi.org/10.1007/s13228-011-0006-6>
- [110] M. Minekus, “The tno gastro-intestinal model (tim),” in *The Impact of Food Bioactives on Health: in vitro and ex vivo models*, K. Verhoeckx, P. Cotter, I. López-Expósito, C. Kleiveland, T. Lea, A. Mackie, T. Requena, D. Swiatecka, and H. Wichers, Eds. Cham (CH): Springer, 2015, ch. 5. [Online]. Available: [https://doi.org/10.1007/978-3-319-16104-6\\_5](https://doi.org/10.1007/978-3-319-16104-6_5)
- [111] E. C. Thuenemann, G. Mandalari, G. T. Rich *et al.*, “Dynamic gastric model (dgm),” in *The Impact of Food Bioactives on Health: in vitro and ex vivo models*, K. Verhoeckx, P. Cotter, I. López-Expósito, C. Kleiveland, T. Lea, A. Mackie, T. Requena, D. Swiatecka, and H. Wichers, Eds. Cham (CH): Springer, 2015, ch. 6. [Online]. Available: <https://www.ncbi.nlm.nih.gov/books/NBK500144/>
- [112] M. J. Ferrua and R. P. Singh, “Human gastric simulator (riddet model),” in *The Impact of Food Bioactives on Health: in vitro and ex vivo models*, K. Verhoeckx, P. Cotter, I. López-Expósito, C. Kleiveland, T. Lea, A. Mackie, T. Requena, D. Swiatecka, and H. Wichers, Eds. Cham (CH): Springer, 2015, ch. 7. [Online]. Available: [https://doi.org/10.1007/978-3-319-16104-4\\_7](https://doi.org/10.1007/978-3-319-16104-4_7)
- [113] O. Ménard, D. Picque, and D. Dupont, “The didgi® system,” in *The Impact of Food Bioactives on Health: in vitro and ex vivo models*, K. Verhoeckx, P. Cotter, I. López-Expósito, C. Kleiveland, T. Lea, A. Mackie, T. Requena, D. Swiatecka, and H. Wichers, Eds. Cham (CH): Springer, 2015, ch. 8. [Online]. Available: [https://doi.org/10.1007/978-3-319-16104-4\\_8](https://doi.org/10.1007/978-3-319-16104-4_8)
- [114] K. Verhoeckx, P. Cotter, I. López-Expósito, C. Kleiveland, T. Lea, A. Mackie, T. Requena, D. Swiatecka, and H. Wichers, Eds., *The Impact of Food Bioactives on Health: in vitro and ex vivo models*. Cham (CH): Springer, 2015. [Online]. Available: <https://doi.org/10.1007/978-3-319-16104-6>
- [115] J. B. Dressman, R. R. Berardi, L. C. Dermentzoglou, T. L. Russell, S. P. Schmaltz, J. L. Barnett, and K. M. Jarvenpaa, “Upper gastrointestinal (gi) ph in young, healthy men and women,” *Pharmaceutical Research*, vol. 7, no. 7, pp. 756–761, 1990. [Online]. Available: <https://doi.org/10.1023/A:1015852808834>
- [116] T. Okabe *et al.*, “Determinants of liquid gastric emptying: comparisons between milk and isocalorically adjusted clear fluids,” *BJA: British Journal of Anaesthesia*, vol. 114, no. 1, pp. 77–82, January 2015. [Online]. Available: <https://doi.org/10.1093/bja/aeu338>
- [117] “Elite Double 8 Fast Curing Silicone,” <https://www.zhermack.com/en/product/elite-double-8/>, accessed 25th of June, 2023.



## Colophon

This document was typeset using  $\text{\LaTeX}$ , using the KOMA-Script class `scrbook`. The main font is Palatino.



